June 2023

Environmental chemical analysis method optimization and application to northwest Cuban marine sediment

Thea R. Bartlett
University of South Florida

Environmental Chemical Analysis Method Optimization and Application to Northwest Cuban Marine Sediment

by

Thea R. Bartlett

A thesis submitted in partial fulfillment
of the requirements for the degree of
Master of Science
with a concentration in Chemical Oceanography
College of Marine Science
University of South Florida

Major Professor: Brad E. Rosenheim, Ph.D.
Isabel C. Romero, Ph.D.
David F. Naar, Ph.D.
Misael Díaz-Asencio, Ph.D.

Date of Approval:
May 22, 2023

Keywords: GC-MS/MS, Pollutants, Method Development, Mass Spectrometry, Cuba

ACKNOWLEDGMENTS

This research was made possible in part by grants from The Gulf of Mexico Research Initiative (GOMRI) including the Center for Integrated Modeling and Analysis of Gulf Ecosystems (C-IMAGE), and Resuspension, Redistribution and Deposition of Deepwater Horizon (DwH) Recalcitrant Hydrocarbons to offshore Depocenters (REDIRECT) and also in part by the Ann and Werner Von Rosenstiel Fellowship in Marine Science. The authors thank the captain and crew of the *R/V Weatherbird II*, for collection of field samples. The authors thank Ethan Goddard for endless support in the Marine Environmental Chemistry Laboratory (MECLab).

TABLE OF CONTENTS

LIST OF TABLES

LIST OF FIGURES

ABSTRACT

A method for gas chromatography tandem mass spectrometry (GC-MS/MS) in selected reaction monitoring (SRM) mode has been optimized to quantify 250 compounds of a variety of compound classes such as polycyclic aromatic hydrocarbons (PAHs), oxidized PAHs, organochlorinated pesticides, polychlorinated biphenyls, biomarkers (hopanes, steranes, tri-aromatic steroids, and fecal sterols), aliphatic hydrocarbons, and plastic additives. This method was validated based on available QA/QC standards using several environmental samples, both sediment and biota, and standard reference materials. This contaminant-focused method can be used as a forensic geochemistry tool to evaluate oil contamination and other contaminant histories in future research studies. When applied to sediment cores, this method can be used to construct a history of contamination events ranging from oil spills to non-point sources such as agricultural runoff. The method was tested in offshore sediments from Cuba for a preliminary assessment of the contamination history in the area. The third chapter of this thesis outlines the steps taken thus far and presents preliminary data results for Cuba that can be added to in future studies. The optimization of the method was achieved by maximizing usage of time windows and the power of SRM mode on the GC-MS/MS. The application of this method to Cuban sediment cores reveals distinct changes in contamination inputs that are related to land-use changes over time.

CHAPTER ONE:

INTRODUCTION AND BACKGROUND

Assessing contamination concentrations and input histories is important for protecting ecosystems. Reliable data about the historical inputs of contaminants in most geographic areas are not available because long-term monitoring or sampling programs have not been undertaken. Many organic contaminants, such as polychlorinated biphenyls (PCBs) and polycyclic aromatic hydrocarbons (PAHs), are well-preserved in sediments (Heim and Schwarzbauer, 2013). Thus, sediments can act as a record of contaminant inputs and can be used in place of, or as a compliment to, long-term monitoring programs. Dated sediment profiles of organic contaminants have been used to obtain reliable information about type and extent of contamination over time (Díaz-Asencio et al., 2009; Su et al., 1998; Zhang et al., 2009). Specific organic molecules from well-preserved classes can indicate specific sources of contamination. By measuring multiple types of organic contaminants in a dated sediment core, the historical record of contaminant inputs from specific sources can be reconstructed and understood in terms of industrial and societal development, which can then be used to assess the impact on the environment.

In previous research, sediment studies focused on only a few types of organic contaminants, thereby limiting the understanding of certain components to the total contamination puzzle (Audry et al., 2004; Farrington and Tripp, 1977; Mitra and Bianchi, 2003; Nowell, 2019; Pruell and Quinn, 1985; Sosa et al., 2019; Tolosa et al., 2010; Volkman et al., 1992). Whereas these studies are important, they do not give a complete picture of organic

contamination in the environment. In order to develop a more holistic understanding of contamination inputs over time, it is important to measure a multitude of compounds from many different sources.

There is a relationship between anthropogenic actions and effects on the environment that can be followed by analyzing organic compounds in the environment. Organic contaminants have a strong affinity for organic matter in the water column, and therefore attach to sinking particulates that accumulate on the seafloor. Over time, as sediment accumulates, the contaminants are buried and preserved (Canfield, 1994; Ingall and Van Cappellen, 1990). As contaminants are preserved in sediments, it is possible to reconstruct past contaminant inputs by analyzing sediment cores chronologically. This reconstruction can then be used to evaluate the anthropogenic activities in the past and to assess how those activities potentially impacted the environment and ecological conditions. For example, Alonso-Hernández et al. (2015) used a ^{210}Pb-dated sediment core to reconstruct land-based organochlorine pesticide (OCP) inputs in the Gulf of Batabanó, Cuba. This study determined that there was evidence of pesticide contamination beginning in the 1970s (Alonso-Hernández et al., 2015). In another example, Zhang et al. (2009) also used a ^{210}Pb-dated sediment core collected from the Yellow Sea in China to reconstruct releases of polycyclic aromatic hydrocarbons (PAH) and polychlorinated biphenyls (PCB) to the marine environment. They found that there were increased releases of PAHs during 1938-1944 and 1956-1962 related to production and usage of petro-chemicals in industrial activities and a large PCB peak in 1980-1992 related to improper disposal of PCB containing equipment (Zhang et al., 2009). The above examples show that viewing contamination in chronologically constrained sediment cores acts as a forensic geochemical tool to evaluate contamination inputs over time for a given area. However, the above examples only

show a few kinds of contamination, leaving other kinds of contamination out, something that could be reconciled with a more comprehensive method, which is the focus of this research.

Reconstructing the historical record of organic contaminant input into coastal marine sediments can be complicated by multiple land-based anthropogenic activities, such as deforestation and building of dams, that alter natural inputs of sediments and organic matter. Deforestation can increase physical erosion and chemical weathering, which leads to an increase in sedimentation rate, which could increase contaminant loads if the eroded soil contains contaminants (Roulet et al., 2000). Building dams that redirect river flow can decrease water flow to a region and potentially decrease sedimentation rates (Zamora et al., 2013). Additionally, fine grained clay-rich sediments tend to show an increase in concentrations of contaminants due to a larger surface area to mass ratio (Burban et al., 1989). Therefore, it is important to understand sedimentation accumulation rates and sediment composition alongside contaminant concentrations and sources in sedimentary records to have a clear understanding of how contamination events have varied over time.

When analyzing a sediment core to understand past organic contamination, different molecules can be used to understand different contamination sources. Some molecules are themselves considered contaminants, whereas others are not directly contaminants but can be indicators of specific contamination sources. As mentioned previously, a clear understanding of contamination events over time requires assessment of sedimentation rates and sediment composition. Moreover, this clear understanding must include a perspective for both natural and anthropogenic inputs of organic molecules. Natural inputs can be determined by measuring specific PAHs, aliphatic compounds, and biomarkers that originate from environmental sources, such as terrestrial soil. Anthropogenic inputs can be determined by OCPs, PCBs, other PAHs,

and fecal sterols. OCPs can indicate contamination from agricultural practices, fecal sterols can be used to detect wastewater inputs, and PCBs and PAHs can be used to measure releases from industrial activities. By using the method developed in this research it is possible to simultaneously measure all the types of anthropogenic inputs mentioned. The simultaneous measurement of many types of anthropogenic and natural inputs allows a researcher to better understand the complex relationship between human actions and environmental impacts which can be used to protect delicate ecosystems.

CHAPTER TWO:

GC-MS/MS-SRM METHOD OPTIMIZATION

Note: This chapter is concurrently being revised for submission to the journal Chemosphere, with the following title:

Simultaneous trace determination of 250 intermediate and semi-volatile organic chemicals in environmental samples via gas chromatography tandem mass spectrometry

by

Thea R. Bartlett and Isabel C. Romero, from the

University of South Florida, College of Marine Science, St. Petersburg, Florida, 33701

2.1 Introduction

There are hundreds of thousands of intermediate and semi-volatile organic chemicals (I/SVOCs) within chemical classes (e.g., from polar to non-polar) that co-exist in the marine environment. I/SVOCs are of interest, because they have multiple sources, are often bioavailable, have potential diverse health impacts, and can be transformed into more toxic compounds or persist in the environment. Source apportionment and quantification of natural and anthropogenic chemical markers are required to assess organic matter and contamination inputs. Anthropogenic I/SVOCs can affect ecosystems differently and often will interact decreasing environmental health (Coxon et al., 2019; Jones and De Voogt, 1999; Lohmann et al., 2007; Oberdörster et al., 1999; Safe, 1994). Any efforts to remediate diminished ecosystem function

must first accurately assess the levels and scope of contaminants involved. Understanding only one type of contamination at any given time is not sufficient to understand ecosystem health. High-throughput and cost-effective methods for sample analysis of multiple classes of I/SVOCs are necessary to improve monitoring programs and rapid assessment of impacted environmental areas.

Typically, targeted gas-chromatography mass-spectrometry (GC-MS) is used to study I/SVOCs. Previous works have needed in-depth extraction methods in order to accurately quantify compounds using GC-MS and were limited to a few selected compounds (Camino-Sánchez et al., 2011; Chen et al., 2013; He et al., 2017; Lehotay et al., 2010; Pérez-Carrera et al., 2007; Wang et al., 2012). With the addition of more capable technology, such as tandem mass spectrometry using a selective monitoring method, it has become possible to measure more compounds with simpler extraction methods (Adhikari et al., 2017; Andrási et al., 2013; Baroudi et al., 2020; Brooks et al., 2015; Jacquot et al., 1996; Koesukwiwat et al., 2011; Overholt et al., 2016; Romero et al., 2016; Romero et al., 2015; Romero et al., 2017; Saravanabhavan et al., 2009). However, even these more in-depth analyses only measure one or two types of compounds per sample, consequently, the samples need to be analyzed multiple times to be able to quantify a broader number of chemicals covering different contamination types. Moreover, small sample sizes and time constraints may therefore force researchers to only measure a limited number of compounds, thereby preventing a full understanding of a contamination event occurring in the environment. For example, a massive sedimentation event of oil-contaminated marine snow was observed in 2010 in the northern Gulf of Mexico (nGoM) as a consequence of the Deepwater Horizon oil spill (Daly et al., 2016). Only through the quantification of several compound groups via multiple analyses, for the first time it was possible to chemically

characterize the organic material deposited on the seafloor during this event (Romero et al., 2015; Romero et al., 2017). Results from these studies indicated which natural depositional mechanisms that transported the oil-contaminated marine snow to the seafloor within the large-scale impacted area (~0.8-1.8 million barrels of oil discharged in ~11,000 km^2 from coastal to deep-sea areas in the nGoM). Similarly, past accidental oil spill events have also included multiple analyses for understanding the impact to the environment (Al-Sarawi et al., 2015; Burns and Teal, 1979; Franco et al., 2006; Page et al., 2002).

Our objective was to generate a rapid quantitative method for the analysis of 250 I/SVOCs using enhanced resolution gas chromatography coupled with a triple quadrupole mass spectrometer in Selective Reaction Monitoring (SRM) mode (GC-MS/MS-SRM). This method combines several previously applied analytical methods (Diercks et al., 2021; Romero et al., 2021) and adds new compound types, targeting 250 different compounds. This comprehensive GC-MS/MS method maximizes the capabilities of the tandem mass-spectrometry technology by quantifying the targeted 250 I/SVOCs in complex samples (e.g., sediment, biota) in a single-run analysis. The targeted compounds correspond to seven compound classes with a wide range in molecular weight and hydrophobicity (Appendix A, Tables A1-A5): polycyclic aromatic hydrocarbons (PAHs; 2-6 ring including alkylated homologs, 66 total PAHs), oxidized-PAHs (34 total oxidized-PAHs), organochlorinated pesticides (OCPs; 33 total pesticides), polychlorinated biphenyls (PCBs; 32 total PCBs), biomarkers (C27–C35 hopanoids, C27–C29 steranes, C20–C28 tri-aromatic steroids, 4 fecal sterols, 45 total biomarkers), aliphatic hydrocarbons (C10-C37 *n*-alkanes and isoprenoid alkanes, 30 total aliphatics), and plastic additives (6 total phthalates). This comprehensive approach allows for rapid screening of multiple contamination sources in the environment. OCPs are indicators of agricultural and

urban sources. PCBs are indicators of industry and their legacy products. Ratios of fecal sterols can show contamination from both livestock production and human sewage, while other biomarkers can help track oil spills in the environment. Phthalates can indicate plastic leaching into the environment. Aliphatics are used to identify natural and anthropogenic carbon sources. PAHs are indicative of combustion and oil pollution, while their more toxic oxidation products indicate long-term biological and environmental impacts. Specifically, OCPs, PCBs, and PAHs and their oxidation products have been established as having toxic, mutagenic, and carcinogenic effects on organisms (Gómez-Gutiérrez et al., 2007; Halek et al., 2008; Honda and Suzuki, 2020; Long et al., 1995; Lundstedt et al., 2007; Nikolaou et al., 2009; Nowell et al., 2014; Sun et al., 2021; Zhao et al., 2010).

This comprehensive and rapid GC-MS/MS-SRM method was tested using reference standards and environmental samples from the nGoM. Samples from the nGoM, have not only been exposed to large amounts of spilled oil and other contaminants, but also to natural sources of I/SVOCs (e.g., oil seeps) via multiple inputs (Adhikari et al., 2015; Bianchi et al., 2007; MacDonald et al., 2002; McNutt et al., 2012; Mitra and Bianchi, 2003; Romero et al., 2021; Stout et al., 2016; Wang et al., 2006). As the first time applying a high-throughput quantitative GC-MS/MS-SRM method for 250 I/SVOCs in complex samples, this study demonstrates an analytical method that optimizes the assessment of natural and anthropogenic inputs to marine environments under acute and persistent impact events.

2.2 Methods

2.2.1 Materials and Chemicals

Solvents and reagents used were of the highest grade and purity available. Solvents used were a mixture of *n*-hexane (GC-Resolv, H3074, Fisher Scientific, Hampton, NH, USA) and methylene chloride (Optima, D1514, Fisher Scientific, Hampton, NH, USA). Deuterated and non-deuterated surrogate standards were obtained for PAHs (acenaphthene-d10, benz[a]anthracene d12, benzo[a]pyrene d12, dibenz[a,h]anthracene d14, fluoranthene d10, and phenanthrene d10; ISM-750-1, Ultra Scientific-Agilent, Santa Clara, CA, USA), oxidized-PAHs (2-naphthol d8, 1-nitronaphthalene d7, and 9-fluorenone d8; D-5648, D-5797, D-5442, CDN Isotopes, Pointe-Claire, QC, Canada), biomarkers (5α-Cholestane-2,2,4,4 d4; D-6099, CDN Isotopes, Pointe-Claire, QC, Canada), PCBs and OCPs (tetrachloro-m-xylene; Cat# 32027, Restek, Bellafonte, PA, USA; and biphenyl d10; Cat# 72058, Absolute Standards, Hamden, CT, USA), aliphatics (*n*-pentacosane d32, D-3915, CDN Isotopes, Pointe-Claire, QC, Canada; tetracosane d50, IST-730-1, Ultra Scientific-Agilent, Santa Clara, CA, USA; *n*-dotriacontane d66, D-0973, CDN Isotopes, Pointe-Claire, QC, Canada) and phthalates (di-n-butyl phthalate D4 and di-n-octyl phthalate D4; PHTH-D4-002S, PHTH-D4-008S, Accustandard, New Haven, CT, USA).

Reference standards used were standard reference material 2779 Gulf of Mexico Crude Oil (NIST, Gaithersburg, MD, USA), PAH standard mix (US-106-N-1, Agilent, Santa Clara, CA, USA), M-508.1-X1 and M-508.1-X2 (Accustandard, New Haven, CT, USA), oxidized-PAH reference standards (anthrone 319899, xanthone X600, 9,10-phenanthrenequinone 275034, 1-naphthol N1000, 2-naphthol 185507, 9-hydroxyfluorene H31204, 2-naphthaldehyde N206, 9-fluorenone F1506, 1,4-naphthoquinone 152757, 1-nitronaphthalene 103594, and 9-

hydroxyphenanthene 21128 from Sigma Aldrich, St. Louis, MO, USA; and 9-nitrophenanthrene R-020N from Accustandard, New Haven, CT, USA); PCB Congener Mix #6 (C-CSA-06, Accustandard, New Haven, CT, USA), fecal sterol reference standards (epi-coprostanol C2882, and cholestanol 47129, Sigma Aldrich, St. Louis, MO, USA, and coprostanol/cholesterol, 92266, Absolute Standards, Hamden, CT, USA), and phthalate reference standard mix (EPA Phthalate Esters Mix: dimethyl phthalate, diethyl phthalate, di-n-butyl phthalate, benzyl butyl phthalate, di-2-ethylhexyl phthalate, and di-n-octyl phthalate, 48231, Sigma Aldrich, St. Louis, MO, USA).

2.2.2 Sample Information for Method Validation

For the validation of the optimized method and to compare to previous analyses, several samples of different matrices were analyzed using the described GC-MS/MS-SRM method. We followed modified EPA methods and QA/QC protocols (protocols 8270D and 8015C). The samples included three standard reference materials with certified values: NIST 1941b (Organics in marine sediment), NIST 2779 (MC252 crude oil), and IAEA 408 (estuarine sediment). All samples were analyzed in triplicate.

2.2.3 Extractions of Samples

Samples were extracted using a ThermoFisher Scientific Dionex ASE 350 Accelerated Solvent Extractor (ASE) under high temperature (100°C) and pressure (1500 psi) with a solvent mixture of 70% hexane and 30% methylene chloride (Diercks et al., 2021; Romero, 2018; Romero et al., 2020). The extraction method consisted of 0 min preheat, 6 min heat, 5 min static time, 60% flush volume, 60 sec purge, and 3 cycles at 100°C and 1500 psi. Samples were packed into stainless steel 10 ml extraction cells with combusted glass fiber filters, combusted,

deactivated (2% MQ water) silica gel, and combusted sand. Each cell contained, 3 g Si gel, 1 g of sediment or 20 mg squid mantle homogenized sample, and sand with combusted filters between each layer. This protocol using ASE cells with a predetermined packing allows for a single-step lipid extraction and purification procedure, significantly decreasing sample preparation time, solvent use, and sample loss (Romero et al., 2020; Romero et al., 2015; Romero et al., 2018) (Figure 1).

Prior to extraction, samples were spiked with deuterated and non-deuterated standards (see Materials and chemicals section) to correct for matrix effects and sample loss during extraction. Following extraction, granular copper was added to sediment samples and shaken for a minimum of 4 hours to remove any sulfur present. Extracts were concentrated using a RapidVap (Labconco RapidVap Vertex Evaporator) and a gentle nitrogen stream. Extraction blanks were added to each set of samples.

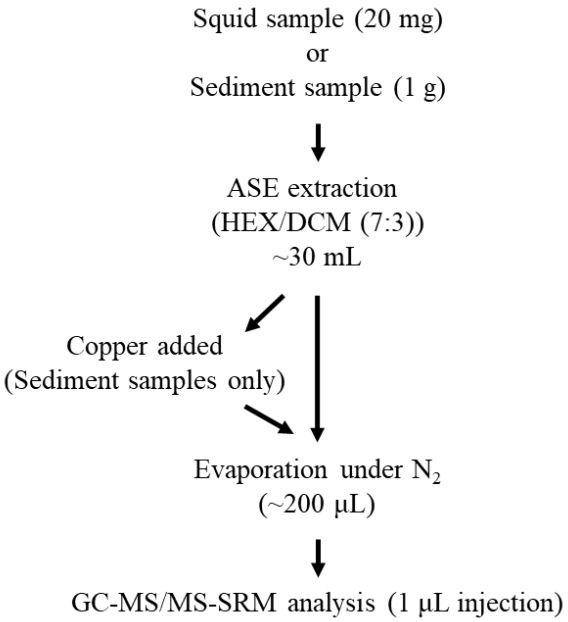

Figure 1: Analytical method scheme.

2.2.4 GC-MS/MS Parameters

Samples were analyzed on an Agilent 7890B gas chromatograph 7010 triple quadrupole mass spectrometer. One microliter of sample was injected into the multi-mode inlet in split-less mode. Inlet temperature held at 325°C. A 30m fused silica column (Rxi 5Sil MS with Integra-Guard, 30 m x 0.25 mm x 0.25 µm, Cat# 13623-124, Restek, Bellafonte, PA, USA) was used with the following oven parameters: initial temperature 60°C, hold time 2 min; ramp 1 rate 8°C/min to 200°C, hold time 0 min; ramp 2 rate 4°C/min to 300°C, hold time 0 min, ramp 3 rate 10°C/min to 350°C, hold time 5 min. Helium was used for carrier flow at a rate of 1 ml/min and Nitrogen gas was used for collision cell gas. The transfer line between the GC oven and the MS was held at 320°C, the ion source was held at 270°C, and both quadrupoles were held at 150°C.

For accuracy and precision of sample sets, the instrument was tuned daily with PFTBA (perfluorotributylamine), and samples were checked with certified standards. Sample batches were re-analyzed when replicated standards exceeded ±20% of relative standard deviation (RSD), and/or when recoveries were low. Recoveries ranged within QA/QC criteria of 50–120%.

2.2.5 Selection of SRM Transitions

The selection of SRM transitions consists of three main steps: identification of the precursor ion, selection of the product ion, and selection of the collision energy (Adhikari et al., 2017; Fernández-González et al., 2008; John et al., 2014). The standards listed above (see 2.2.1 Materials and Chemicals) were used to determine the transitions (combination of precursor and product ions with specific collision energy) for each compound of interest. The standards were run a minimum of two times to establish the transitions. The standards used were in the range 5-10 ng/µl concentration.

To identify the best precursor ion for each compound, the standards were run in full scan mode, which sets the first quadrupole to scan for all mass fragments from 50 to 500 amu in 0.1 amu increments with a threshold of 100 abundance and a scan time of 300 ms. During this step, the collision cell energy is set to zero and the second quadrupole is effectively turned off allowing the detector to analyze all the fragments of the compound. The best precursor ion was selected based on which mass peak had the most abundance. Therefore, the full scans showed the most abundant ion (precursor ion) and its retention time. Due to the nature of the full scan data, it is entirely possible to use mixture standards to establish multiple compounds simultaneously, as long as there is retention time separation between the compounds.

Once the precursor ion is identified, the product ion is selected by product ion scan (PIS). This is established by setting the first quadrupole to the selected precursor ion, having the second quadrupole complete a scan from 50 amu to 15 more amu than the precursor ion, and varying the collision energy from 0 to 60 eV. The selected collision energy produces the largest abundance of the product ion and a small abundance of the precursor ion. If the collision energy is too low, the precursor ion will not be fragmented enough and the abundance of the product ion will be low, or if the collision energy is too high the product ion can also be fragmented, then its abundance will not be as high as it could be. The PIS was run for a minimum of four collision energies. The most abundant product ion from the spectra was selected for the quantifier transition and the second most abundant product ion was selected for the qualifier transition. By creating two transitions for each compound, we can ensure correct peak identification in environmental samples. Once the transitions were selected, multiple collision energies were tested again to ensure the best fragmentation was achieved.

2.2.6 Calculation of Compound Concentrations

The steps listed above were completed on both target compounds and standards to produce chromatographic peaks. The areas of those peaks were then used to calculate concentrations. The areas of target compounds were normalized by the area of the corresponding surrogate compounds (standards added pre-extraction). The normalized area then had a relative response factor (RRF) applied to account for changes in instrument response. The formula for RRF is:

RRF= (area compound) * (amount surrogate) / (area surrogate) * (amount compound)

The RRFs were established based on 5-point calibration curves of the certified standards. The normalized and RRF corrected areas were then converted to concentrations by multiplying by the amount of surrogate standard added pre-extraction and dividing by the mass of sample.

2.2.7 Completed Method Optimization

Given the large number of compounds in this method, it is expected that many compounds will have very close retention times. To improve separation of compounds we created time segments/windows that contain a selected number of compounds (SRM transitions). To ensure that compounds are analyzed similarly in all time segments, the same scan time (amount of time the instrument scans through all SRM transitions) and cycles/s (number of times per second the instrument scans SRM transitions) were set for each time window. But, because some time segments have more SRM transitions than others, we added “dummy compounds” to each time segment (SRM transitions that do not elute in a specific time segment). By ensuring each time segment has the same number of SRM transitions, scan time, and cycles/s we

guaranteed that each compound was analyzed similarly regardless of the time segment it occurs within (Kochman et al., 2002; Koesukwiwat et al., 2011; Wong et al., 2010).

2.3 Results and Discussion

2.3.1 Collision Energy Optimization

Precursor ions were selected based on which mass peak was most abundant when analyzed in full scan mode with collision energy set to zero eV (Appendix B, Figure B1). All PAHs have precursor ions that are the same as their molecular ions. Similarly, the oxid-PAHs also have precursor ions equal to their molecular ions with the exception of the nitronaphthalenes (MI = 173, precursor ion = 127), the hydroxyphenanthrenes (MI = 210, precursor ion = 165), the nitrofluorenes (MI = 211, precursor ion = 165), the nitrofluoranthene-pyrenes (MI = 247, precursor ion = 200), and the nitrochrysenes (MI = 273, precursor ion = 226). Most OCPs have some fragmentation during ionization and therefore have precursor ions smaller than their molecular ions, with the exception of hexachlorobenzene (Alder et al., 2006; Lee et al., 2020). Generally, PCBs have precursor ions close to their molecular ions within 2 amu (Laušević et al., 1996; Lee et al., 2020; Ruddy et al., 2008). Each group of biomarkers (hopanes, steranes, TAS, fecal sterols) behave similarly and have the same precursor ion (smaller than the molecular ion due to some fragmentation during ionization) (Adhikari et al., 2017; Aeppli et al., 2014b; Stevens et al., 2013; Volkman et al., 1992). Phthalates fragment during ionization and all have precursor ions that are smaller than their molecular weight (Crawford et al., 2014; Giri et al., 2017).

After precursor ions were selected for all compounds, the selection of product ions was done by analyzing the fragments produced when running PIS with the selected precursor ions at

collision energy varied from 0 to 60 eV. Generally, precursor ion abundance drops rapidly at collision energies higher than 10-15 eV (Figure 2). By identifying the most abundant product ions produced at a specific collision energy, with the highest signal-to-noise (S/N) ratios, we were able to select the optimized SRM transitions for each compound (Tables 1-5). The collision energy at which the most abundant product ion is produced varies greatly by compound type. PAHs tend to have increasing collision energy with increasing molecular weight, unlike PCBs, which tend to have optimal collision energy at 30 eV regardless of molecular weight. This different behavior is due to the variable structures of PAHs being more difficult to fragment and the structure of the PCBs being the same apart from the addition of chlorines making fragmentation consistent for all molecular weights (Kalachova et al., 2013; Sørensen et al., 2016) (Figure 2). Biomarkers of similar structure (hopanes, steranes, TAS, or fecal sterols) fragment in similar patterns; but varied transitions are used to better separate peaks that have close retention times (Tables 1 and 2). Hopanes are all quantified with the same transition (191.2 → 95 CE 10), however the qualifier transitions are varied based on the molecular weight, different among C27-C29 hopanes but the same for C30-C35 hopanes. Steranes transitions are varied based on molecular weight, all C27 steranes have the same transitions, but they are different from the C28 steranes and so on. TAS have good separation of retention times and therefore all have the same transitions. Phthalates fragment in similar patterns and have very similar transitions to each other. Similar structured OCPs have the same transitions (e.g., Endosulfan I and II; a, b, g, and d HCH; cis and trans permethrin), but the rest have varied structures and therefore have unique transitions.

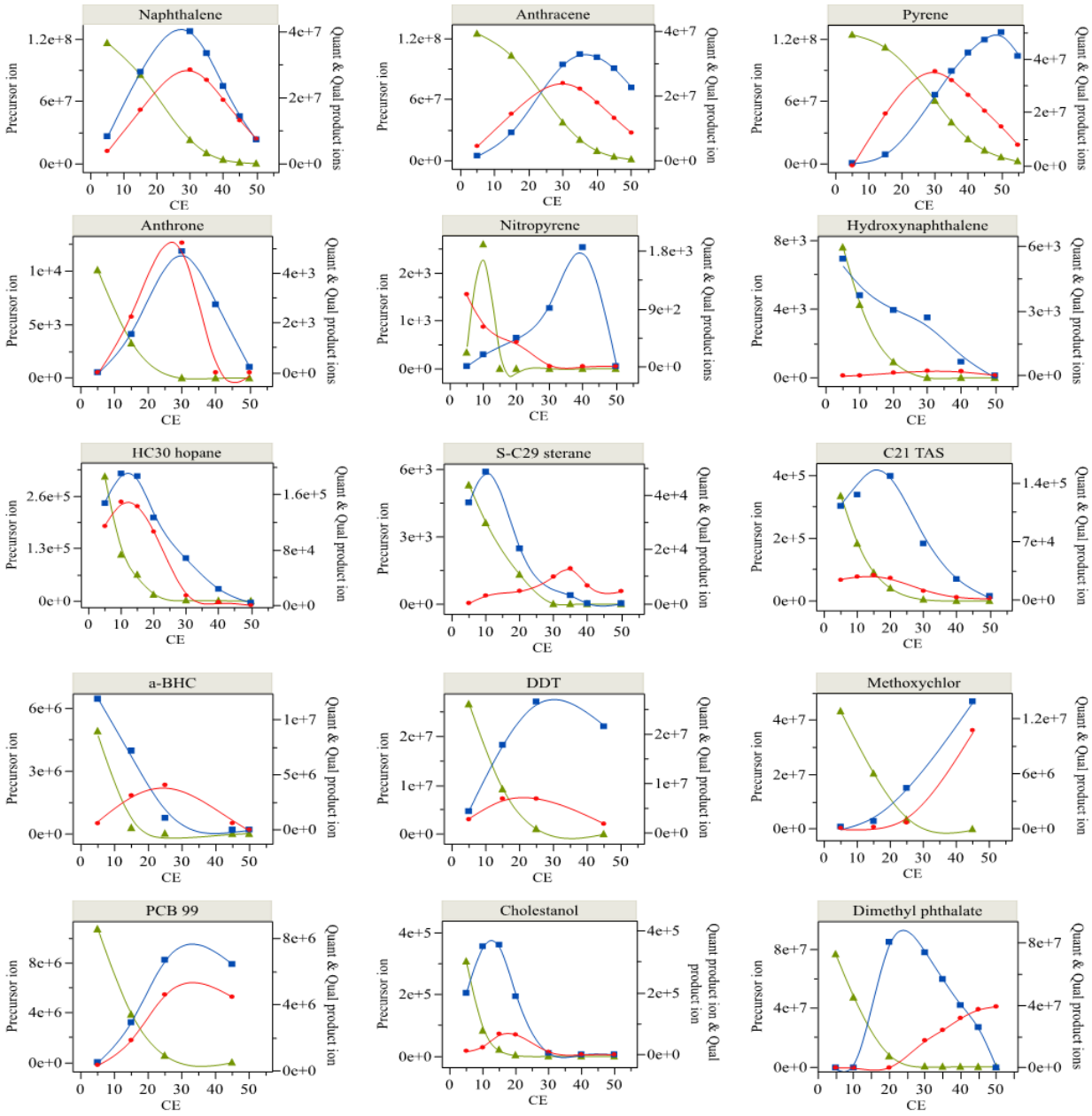

Figure 2: Collision Energy Optimization for SRM Transitions. Each plot depicts precursor ion abundance (shown in green), quantitation ion abundance (shown in blue), and qualifier ion abundance (shown in red) at varied collision energies (eV) for compounds from different compound groups. These plots are used for the selection of the best quantitation and qualifier SRMs for each compound.

Table 1: Empirically determined optimized quantitation (Quant) and qualification (Qual) transitions, retention time (RT, in minutes), and peak width (in minutes) for alkanes, fecal sterols, and phthalates (including surrogate standards).

Compounds	Quant Transition	Qual Transition	RT	Peak width
nC10	57 -> 57 CE 0	n/a	7.0	6.90 - 7.20
nC11	57 -> 57 CE 0	n/a	8.9	8.80 - 9.05
nC12	57 -> 57 CE 0	n/a	10.8	10.70 - 10.90
nC13	57 -> 57 CE 0	n/a	12.5	12.45 - 12.65
nC14	57 -> 57 CE 0	n/a	14.2	14.15 - 14.30
DMP	162.8 -> 77 CE 20	162.8 -> 51.1 CE 50	15.2	14.70 - 16.20
nC15-d32	66 -> 66 CE 0	n/a	15.5	15.00 - 16.00
nC15	57 -> 57 CE 0	n/a	15.8	15.75 - 15.90
nC16	57 -> 57 CE 0	n/a	17.3	17.25 - 17.35
DEP	149 -> 65.1 CE 30	149 -> 93 CE 20	17.3	16.95 - 17.95
nC17	57 -> 57 CE 0	n/a	18.7	18.65 - 18.75
Pr	57 -> 57 CE 0	n/a	18.8	18.75 - 18.85
P-d10	188 -> 184 CE 40	188 -> 158 CE 45	20.0	19.50 - 20.50
nC18	57 -> 57 CE 0	n/a	20.1	20.05 - 20.15
Py	57 -> 57 CE 0	n/a	20.2	20.15 - 20.25
nC19	57 -> 57 CE 0	n/a	21.5	21.45 - 21.60
DBP-d4	153 -> 69 CE 25	153 -> 97 CE 20	22.3	21.35 - 23.25
DBP	149 -> 65.1 CE 30	149 -> 93 CE 20	22.6	22.10 - 23.70
nC20	57 -> 57 CE 0	n/a	23.1	23.00 - 23.15
nC21	57 -> 57 CE 0	n/a	24.7	24.65 - 24.80
nC22	57 -> 57 CE 0	n/a	26.4	26.35 -26.50
nC23	57 -> 57 CE 0	n/a	28.2	28.10 - 28.25
nC24-d50	66 -> 66 CE 0	n/a	29.2	28.07 - 29.70
BBP	149 -> 65.1 CE 30	149 -> 93 CE 20	29.4	28.80 - 30.45
nC24	57 -> 57 CE 0	n/a	30.0	29.85 - 30.05
nC25	57 -> 57 CE 0	n/a	31.7	31.65 - 31.80
DEHP	149 -> 65.1 CE 30	149 -> 93 CE 20	32.6	31.85 - 34.00
nC26	57 -> 57 CE 0	n/a	33.5	33.40 - 33.60
nC27	57 -> 57 CE 0	n/a	35.2	35.15 - 35.35
DnOP-d4	153 -> 69 CE 25	153 -> 97 CE 20	35.5	34.00 - 36.45
DnOP	149 -> 65.1 CE 30	149 -> 93 CE 20	36.5	35.50 - 38.30
nC28	57 -> 57 CE 0	n/a	36.9	36.85 - 37.05
nC29	57 -> 57 CE 0	n/a	38.6	38.50 - 38.70
nC30	57 -> 57 CE 0	n/a	40.2	40.15 - 40.35
CP+epi-CP	233 -> 215 CE 5	233 -> 91 CE 45	41.4	41.05 - 41.75
nC31	57 -> 57 CE 0	n/a	41.8	41.70 - 41.90
CSE	145 -> 105 CE 20	145 -> 115 CE 30	42.0	41.65 - 42.15
CSA	233 -> 215 CE 5	233 -> 91 CE 45	42.1	41.85 - 42.65
nC32-d66	66 -> 66 CE 0	n/a	42.5	42.00 - 43.00
nC32	57 -> 57 CE 0	n/a	43.3	43.25 - 43.50
nC33	57 -> 57 CE 0	n/a	44.8	44.70 - 44.95
nC34	57 -> 57 CE 0	n/a	46.1	46.00 - 46.30
nC35	57 -> 57 CE 0	n/a	47.1	47.05 - 47.30
nC36	57 -> 57 CE 0	n/a	48.1	48.05 - 48.25
nC37	57 -> 57 CE 0	n/a	49.3	49.20 - 49.40

Table 2: Empirically determined optimized quantitation (Quant) and qualification (Qual) transitions, retention time (RT, in minutes), and peak width (in minutes) for hopanes, steranes, and tri-aromatic steroids (including surrogate standard).

Compounds	Quant Transition	Qual Transition	RT	Peak width
C20 TAS	231 -> 215 CE 40	231 -> 216 CE 20	30.6	30.50 - 30.65
C21 TAS	231 -> 215 CE 40	231 -> 216 CE 20	32.2	32.15 - 32.30
DiaC27βα S	372.7 -> 217 CE 10	372.7 -> 121 CE 10	34.4	34.35 - 34.50
DiaC27βα R	372.7 -> 217 CE 10	372.7 -> 121 CE 10	35.0	34.90 - 35.05
DiaC28βα S	386.7 -> 217 CE 10	386.7 -> 121 CE 10	35.9	35.80 - 36.05
DiaC28βα R	386.7 -> 217 CE 10	386.7 -> 121 CE 10	36.6	36.40 - 36.60
C27ααα S	372.7 -> 217 CE 10	372.7 -> 121 CE 10	37.0	37.00 - 37.10
C27αββ R	372.7 -> 217 CE 10	372.7 -> 121 CE 10	37.2	37.10 - 37.25
DiaC29βα S	400.7 -> 217 CE 10	400.7 -> 121 CE 10	37.2	37.10 - 37.30
C27αββ S	372.7 -> 217 CE 10	372.7 -> 121 CE 10	37.4	37.30 - 37.45
Cholestane-d4	221 -> 121 CE 15	376.7 -> 221 CE 10	37.6	37.1 - 38.10
C27ααα R	372.7 -> 217 CE 10	372.7 -> 121 CE 10	37.7	37.60 - 37.75
DiaC29βα R	400.7 -> 217 CE 10	400.7 -> 121 CE 10	37.8	37.70 - 37.95
Ts	191.2 -> 95 CE 10	370.5 -> 191.2 CE 10	38.2	38.15 - 38.30
C28ααα S	386.7 -> 217 CE 10	386.7 -> 121 CE 10	38.7	38.55 - 38.75
S-C26 TAS	231 -> 215 CE 40	231 -> 216 CE 20	38.8	38.70 - 38.90
C28αββ R	386.7 -> 217 CE 10	386.7 -> 121 CE 10	38.8	38.75 - 38.90
Tm	191.2 -> 95 CE 10	370.5 -> 191.2 CE 10	38.9	38.80 - 38.95
C28αββ S	386.7 -> 217 CE 10	386.7 -> 121 CE 10	39.0	38.85 - 39.05
C28ααα R	386.7 -> 217 CE 10	386.7 -> 121 CE 10	39.4	39.30 - 39.50
R-C26+S-C7 TAS	231 -> 215 CE 40	231 -> 216 CE 20	39.9	39.75 - 40.05
C29ααα S	400.7 -> 217 CE 10	400.7 -> 121 CE 10	39.9	39.80 - 40.05
C29αββ R	400.7 -> 217 CE 10	400.7 -> 121 CE 10	40.2	40.05 - 40.25
C29αββ S	400.7 -> 217 CE 10	400.7 -> 121 CE 10	40.3	40.25 - 40.40
BNH	191.2 -> 95 CE 10	384.5 -> 191.2 CE 10	40.3	40.25 - 40.40
S-C28 TAS	231 -> 215 CE 40	231 -> 216 CE 20	40.8	40.70 - 40.95
C29ααα R	400.7 -> 217 CE 10	400.7 -> 121 CE 10	40.8	40.75 - 40.90
NH + NNH	191.2 -> 95 CE 10	398.5 -> 191.2 CE 10	41.0	40.90 - 41.15
R-C27 TAS	231 -> 215 CE 40	231 -> 216 CE 20	41.3	41.20 - 41.40
NM	191.2 -> 95 CE 10	398.5 -> 191.2 CE 10	41.8	41.70 - 41.85
H	191.2 -> 95 CE 10	191.2 -> 121 CE 10	42.3	42.25 - 42.45
R-C28 TAS	231 -> 215 CE 40	231 -> 216 CE 20	42.4	42.30 - 42.50
M	191.2 -> 95 CE 10	191.2 -> 121 CE 10	43.0	42.85 - 43.05
HH-S	191.2 -> 95 CE 10	191.2 -> 121 CE 10	43.9	43.75 - 43.95
HH-R	191.2 -> 95 CE 10	191.2 -> 121 CE 10	44.0	43.95 - 44.15
HM	191.2 -> 95 CE 10	191.2 -> 121 CE 10	44.6	44.50 - 44.65
BHH-S	191.2 -> 95 CE 10	191.2 -> 121 CE 10	45.0	44.95 - 45.15
BHH-R	191.2 -> 95 CE 10	191.2 -> 121 CE 10	45.3	45.15 - 45.35
THH-S	191.2 -> 95 CE 10	191.2 -> 121 CE 10	46.3	46.20 - 46.35
THH-R	191.2 -> 95 CE 10	191.2 -> 121 CE 10	46.5	46.45 - 46.60
TkHH-S	191.2 -> 95 CE 10	191.2 -> 121 CE 10	47.4	47.30 - 47.50
TkHH-R	191.2 -> 95 CE 10	191.2 -> 121 CE 10	47.7	47.60 - 47.80
PHH-S	191.2 -> 95 CE 10	191.2 -> 121 CE 10	48.6	48.45 - 48.65
PHH-R	191.2 -> 95 CE 10	191.2 -> 121 CE 10	49.0	48.90 - 49.05

Table 3: Empirically determined optimized quantitation (Quant) and qualification (Qual) transitions, retention time (RT, in minutes), and peak width (in minutes) for polycyclic aromatic hydrocarbons (PAHs) and their oxidation products (including surrogate standards).

Compounds	Quant Transition	Qual Transition	RT	Peak width
N	128 -> 102 CE 30	128 -> 78 CE 30	10.6	10.50 - 10.70
2-me-N	142 -> 115 CE 40	142 -> 141 CE 15	12.6	12.50 - 12.80
N1	142 -> 115 CE 40	142 -> 141 CE 15	12.7	12.45 - 13.10
1-me-N	142 -> 115 CE 40	142 -> 141 CE 15	12.9	12.80 - 13.00
2,6-dme-N	156 -> 115 CE 40	156 -> 141 CE 15	14.5	14.35 - 14.45
1,4-NQ	158 -> 102 CE 20	158 -> 130 CE 5	14.6	14.55 - 14.70
N2	156 -> 115 CE 40	156 -> 141 CE 15	14.7	14.00 - 15.40
1,6-dme-N	156 -> 115 CE 40	156 -> 141 CE 15	14.7	14.70 - 14.85
NQ	158 -> 102 CE 20	158 -> 130 CE 5	15.2	14.50 - 15.80
1,2-dme-N	156 -> 115 CE 40	156 -> 141 CE 15	15.2	15.15 - 15.35
ACL	152 -> 151 CE 30	152 -> 150 CE 40	15.2	15.15 - 15.30
ACE-d10	164 -> 162 CE 20	164 -> 160 CE 30	15.6	15.10 - 16.10
ACE	154 -> 153 CE 15	154 -> 152 CE 40	15.7	15.60 - 15.75
1-NH	156 -> 127 CE 30	156 -> 77 CE 50	16.0	15.95 - 16.00
1-HN	144 -> 115 CE 30	144 -> 116 CE 10	16.1	16.00 - 16.15
2-NH	156 -> 127 CE 30	156 -> 77 CE 50	16.1	16.00 - 16.15
2-HN	144 -> 115 CE 30	144 -> 116 CE 10	16.3	16.15 - 16.30
HN	144 -> 115 CE 30	144 -> 116 CE 10	16.4	14.75 - 17.60
NH	156 -> 127 CE 30	156 -> 77 CE 50	16.5	15.60 - 17.45
N3	170 -> 155 CE 20	170 -> 127 CE 30	16.6	15.75 - 17.60
1-NN	127 -> 77 CE 20	127 -> 51 CE 40	17.0	16.80 - 17.20
F	166 -> 165 CE 30	166 -> 164 CE 45	17.3	17.15 - 17.35
2-NN	127 -> 77 CE 20	127 -> 51 CE 40	17.5	17.40 - 17.80
NN-d7	180 -> 122 CE 30	180 -> 94 CE 50	17.5	17.00 - 18.00
NN	127 -> 77 CE 20	127 -> 51 CE 40	17.6	16.35 - 18.80
N4	184 -> 169 CE 20	184 -> 154 CE 40	17.9	16.55 - 19.40
F1	180 -> 165 CE 20	180 -> 178 CE 20	19.0	18.60 - 19.40
FLO	180 -> 152 CE 20	180 -> 151 CE 30	19.2	18.10 - 20.65
9-FLO	180 -> 152 CE 20	180 -> 151 CE 30	19.4	19.35 - 19.45
FLO-d8	188 -> 160 CE 30	188 -> 132 CE 50	19.4	18.90 - 19.90
D	184 -> 152 CE 30	184 -> 139 CE 40	19.7	19.60 - 19.85
P-d10	188 -> 184 CE 40	188 -> 158 CE 45	20.0	19.50 - 20.50
P	178 -> 176 CE 35	178 -> 152 CE 30	20.1	20.00 - 20.15
AN	178 -> 176 CE 35	178 -> 152 CE 30	20.2	20.15 - 20.25
F2	194 -> 179 CE 20	194 -> 178 CE 20	20.6	20.15 - 21.30
4-me-D	198 -> 197 CE 15	198 ->165 CE 40	21.1	20.95 - 21.25
D1	198 -> 197 CE 15	198 ->165 CE 40	21.3	20.90 - 21.90
2/3-me-D	198 -> 197 CE 15	198 ->165 CE 40	21.4	21.30 - 21.50
1-me-D	198 -> 197 CE 15	198 ->165 CE 40	21.7	21.60 - 21.85
1-me-P	192 -> 191 CE 20	192 -> 189 CE 40	21.7	21.60 - 21.75
2-me-P	192 -> 191 CE 20	192 -> 189 CE 40	21.8	21.75 - 21.90
1-me-AN	192 -> 191 CE 20	192 -> 189 CE 40	21.9	21.90 - 22.00
P/AN1	192 -> 191 CE 20	192 -> 189 CE 40	22.0	21.50 - 22.50
3-me-P	192 -> 191 CE 20	192 -> 189 CE 40	22.1	22.00 - 22.10
9-me-P	192 -> 191 CE 20	192 -> 189 CE 40	22.1	22.10 - 22.25
ANT	194 -> 165 CE 30	194 -> 164 CE 50	22.2	21.10 - 23.90
F3	208 -> 178 CE 40	208 -> 193 CE 40	22.4	21.60 - 23.30
9,10-ANT	194 -> 165 CE 30	194 -> 164 CE 50	22.5	22.35 - 22.55
D2	212 -> 197 CE 20	212 -> 178 CE 20	23.1	22.30 - 24.00
P/AN2	206 -> 191 CE 20	206 -> 189 CE 40	23.9	23.00 - 24.90
1,2-dme-P	206 -> 191 CE 20	206 -> 189 CE 40	24.2	24.05 - 24.30
FL-d10	212 -> 208 CE 45	212 -> 210 CE 20	24.3	23.80 - 24.80
FL	202 -> 200 CE 50	202 -> 201 CE 30	24.4	24.25 - 24.40
D3	226 -> 211 CE 40	226 -> 225 CE 40	24.6	23.80 - 25.60

Compounds	Quant Transition	Qual Transition	RT	Peak width
XA	196.2 -> 139 CE 50	196.2 -> 168 CE 30	25.0	24.10 - 25.70
2-NF	211 -> 165 CE 10	211 -> 164 CE 30	25.1	24.95 - 25.15
NF	211 -> 165 CE 10	211 -> 164 CE 30	25.1	24.20 - 26.10
PY	202 -> 200 CE 50	202 -> 201 CE 30	25.2	25.15 - 25.25
2,3-HP	194 -> 165 CE 30	194 -> 139 CE 40	25.4	25.30 - 25.45
HP	194 -> 165 CE 30	194 -> 139 CE 40	25.5	24.30 - 26.90
9-NAN	223.2 -> 165 CE 30	223.2 -> 139 CE 50	25.5	25.40 - 25.65
9-XA	196.2 -> 139 CE 50	196.2 -> 168 CE 30	25.6	25.55 - 25.65
P/AN3	220 -> 189 CE 40	220 -> 205 CE 30	25.8	24.55 - 27.25
9,10-PQ	208 -> 180 CE 10	208 -> 152 CE 30	26.0	25.90 - 26.10
PQ	208 -> 180 CE 10	208 -> 152 CE 30	26.1	24.60 - 27.40
4,9-HP	194 -> 165 CE 30	194 -> 139 CE 40	26.2	26.10 - 26.30
NAN/NP	223.2 -> 165 CE 30	223.2 -> 139 CE 50	26.4	25.10 - 26.80
D4	240 -> 225 CE 40	240 -> 211 CE 40	26.7	25.25 - 28.00
Re	234 -> 219 CE 10	234 -> 204 CE 20	26.8	26.70 - 26.85
2-me-FL	216 -> 215 CE 30	216 -> 213 CE 40	26.8	26.75 - 26.95
9-NP	223.2 -> 165 CE 30	223.2 -> 139 CE 50	27.0	26.80 - 27.00
FL/PY1	216 -> 215 CE 30	216 -> 213 CE 40	27.1	26.20 - 28.05
P/AN4	234 -> 219 CE 10	234 -> 204 CE 20	27.4	25.55 - 29.15
1-me-PY	216 -> 215 CE 30	216 -> 213 CE 40	27.7	27.55 - 27.75
4-me-PY	216 -> 215 CE 30	216 -> 213 CE 40	27.8	27.75 - 27.90
FL/PY2	230 -> 215 CE 20	230 -> 229 CE 40	29.5	28.70 - 30.50
BAA-d12	240 -> 236 CE 40	240 -> 208 CE 60	30.9	30.50 - 31.14
BAA	228 -> 226 CE 40	228 -> 224 CE 60	31.0	30.95 - 31.05
CHR	228 -> 226 CE 40	228 -> 224 CE 60	31.1	31.05 - 31.25
FL/PY3	244 -> 228 CE 40	244 -> 229 CE 40	31.5	30.80 - 32.15
3-NFL	200 -> 199 CE 30	200 -> 198 CE 40	32.8	32.70 - 32.95
NFL/NPY	200 -> 199 CE 30	200 -> 198 CE 40	33.0	31.75 - 34.45
3-me-CHR	242 -> 239 CE 40	242 -> 241 CE 40	33.3	33.30 - 33.50
BAA/CHR1	242 -> 239 CE 40	242 -> 241 CE 40	33.4	32.75 - 34.25
1-NPY	200 -> 199 CE 30	200 -> 198 CE 40	33.5	33.30 - 33.65
6-me-CHR	242 -> 239 CE 40	242 -> 241 CE 40	33.6	33.50 - 33.60
FL/PY4	258 -> 243 CE 20	258 -> 228 CE 40	33.7	32.75 - 34.65
1-me-CHR	242 -> 239 CE 40	242 -> 241 CE 40	33.8	33.70 - 34.00
BAA/CHR2	256 -> 239 CE 40	256 -> 255 CE 20	35.8	35.00 - 37.00
BBFL	252 -> 250 CE 45	252 -> 224 CE 60	36.4	36.30 - 36.60
BKFL	252 -> 250 CE 45	252 -> 224 CE 60	36.6	36.60 - 36.70
BAA/CHR3	270 -> 239 CE 50	270 -> 255 CE 20	37.5	36.50 - 38.50
BEPY	252 -> 250 CE 45	252 -> 224 CE 60	37.6	37.55 - 37.80
BAPY-d12	264 -> 260 CE 50	264 -> 232 CE 60	37.8	37.30 - 38.03
NCHR	226 -> 224 CE 40	226 -> 225 CE 20	37.9	36.95 - 39.00
BAPY	252 -> 250 CE 45	252 -> 224 CE 60	37.9	37.80 - 37.95
Pe	252 -> 250 CE 45	252 -> 224 CE 60	38.3	38.20 - 38.40
6-NCHR	226 -> 224 CE 40	226 -> 225 CE 20	38.3	38.30 - 38.45
BAA/CHR4	284 -> 239 CE 50	284 -> 282 CE 50	39.0	37.65 - 39.85
BP/PER1	266 -> 265 CE 10	266 -> 264 CE 50	39.6	38.25 - 41.10
BP/PER2	280 -> 279 CE 10	280 -> 278 CE 50	41.8	40.30 - 42.70
DA-d14	292 -> 288 CE 45	292 -> 284 CE 60	43.1	42.06 - 43.60
DA	278 -> 276 CE 40	278 -> 274 CE 60	43.1	42.90 - 43.20
ID	276 -> 274 CE 50	276 -> 275 CE 30	43.2	43.00 - 43.25
6-NBAPY	297 -> 239 CE 40	297 -> 267 CE 10	43.3	43.15 - 43.40
NBAPY	297 -> 239 CE 40	297 -> 267 CE 10	43.4	42.00 - 44.90
BP/PER3	294 -> 293 CE 10	294 -> 292 CE 50	43.6	42.30 - 44.50
BGP	276 -> 274 CE 50	276 -> 275 CE 30	43.9	43.75 - 44.00

Table 4: Empirically determined optimized quantitation (Quant) and qualification (Qual) transitions, retention time (RT, in minutes), and peak width (in minutes) for organochlorinated pesticides (OCPs) (including surrogate standards).

Compounds	Quant Transition	Qual Transition	RT	Peak width
HCCPD	237 -> 119 CE 30	237 -> 143 CE 30	13.1	12.95 - 13.45
Biph-d10	164 -> 162 CE 20	164 -> 160 CE 30	14.2	13.70 - 14.70
ETR	183 -> 140 CE 20	183 -> 108 CE 50	15.1	14.90 - 15.45
CNB	191 -> 53 CE 40	191 -> 113 CE 20	15.9	15.75 - 16.35
PPC	120 -> 77 CE 20	120 -> 51 CE 40	17.4	17.25 - 17.75
TCMX	244 -> 209 CE 20	207 -> 136 CE 20	17.6	17.01 - 18.65
TRI	306 -> 264 CE 5	306 -> 206 CE 10	18.2	18.10 - 18.55
a-HCH	219 -> 183 CE 5	219 -> 147 CE 20	18.7	18.60 - 18.95
BHC	284 -> 214 CE 40	284 -> 249 CE 20	18.9	18.75 - 19.20
SMZ	201 -> 186 CE 5	201 -> 68 CE 50	19.3	19.15 - 19.65
b-HCH	219 -> 183 CE 5	219 -> 147 CE 20	19.4	19.30 - 19.50
ATA	200 -> 68 CE 40	200 -> 104 CE 20	19.4	19.25 - 19.75
g-HCH	219 -> 183 CE 5	219 -> 147 CE 20	19.6	19.50 - 19.80
CTN	266 -> 133 CE 50	266 -> 231 CE 20	20.1	19.95 - 20.50
d-HCH	219 -> 183 CE 5	219 -> 147 CE 20	20.3	20.20 - 20.55
MEB	198 -> 82 CE 20	198 -> 55 CE 35	21.2	21.05 - 21.45
ALA	188 -> 160 CE 10	188 -> 130 CE 40	21.5	21.30 - 21.65
HEP	272 -> 237 CE 15	272 -> 235 CE 15	21.7	21.50 - 21.85
MOAC	238 -> 162 CE 10	238 -> 133 CE 30	22.6	22.45 - 22.85
CYA	225 -> 169 CE 20	225 -> 132 CE 55	22.8	22.60 - 23.15
ALD	263 -> 193 CE 35	263 -> 191 CE 35	22.8	22.60 - 22.95
DCPA	301 -> 167 CE 55	301 -> 223 CE 30	22.8	22.65 - 23.10
HEP-epox	353 -> 263 CE 15	353 -> 217 CE 50	24.0	23.85 - 24.20
g-CHL	373 -> 266 CE 35	373 -> 264 CE 35	24.8	24.65 - 24.95
EDS-I	241 -> 206 CE 20	241 -> 170 CE 30	25.3	25.10 - 25.45
a-CHL	373 -> 266 CE 35	373 -> 264 CE 35	25.3	25.10 - 25.45
DDE	246 -> 176 CE 35	246 -> 175 CE 40	26.1	25.90 - 26.30
DLD	263 -> 193 CE 35	263 -> 191 CE 35	26.2	26.05 - 26.40
END	263 -> 193 CE 35	263 -> 191 CE 35	27.0	26.80 - 27.15
CBL	251 -> 139 CE 20	251 -> 111 CE 40	27.3	27.10 - 27.60
EDS-II	241 -> 206 CE 20	241 -> 170 CE 30	27.3	27.20 - 27.55
DDD	235 -> 165 CE 25	235 -> 199 CE 20	27.6	27.40 - 27.90
END-AL	250 -> 215 CE 30	250 -> 142 CE 55	27.9	27.70 - 28.10
EDS-sul	387 -> 206 CE 45	387 -> 219 CE 40	28.8	28.65 - 29.00
DDT	235 -> 165 CE 25	235 -> 199 CE 20	29.0	28.90 - 29.30
MOXC	227 -> 141 CE 40	227 -> 115 CE 55	31.3	31.10 - 31.65
cis-PERM	183 -> 168 CE 10	183 -> 77 CE 30	35.1	34.90 - 35.25
trans-PERM	183 -> 168 CE 10	183 -> 77 CE 30	35.4	35.25 - 35.75

Table 5: Empirically determined optimized quantitation (Quant) and qualification (Qual) transitions, retention time (RT, in minutes), and peak width (in minutes) for polychlorinated biphenyls (PCBs) (including surrogate standards).

Compounds	Quant Transition	Qual Transition	RT	Peak width
Biph-d10	164 -> 162 CE 20	164 -> 160 CE 30	14.2	13.70 - 14.70
TCMX	244 -> 209 CE 20	207 -> 136 CE 20	17.6	17.01 - 18.65
PCB 8	222 -> 152 CE 30	222 -> 151 CE 55	18.9	18.75 - 19.15
PCB 28	256 -> 186 CE 30	256 -> 151 CE 50	21.3	21.15 - 21.55
PCB 52	292 -> 222 CE 25	292 -> 220 CE 25	22.3	22.15 - 22.35
PCB 44	292 -> 222 CE 25	292 -> 220 CE 25	22.4	22.35 - 22.55
PCB 49	292 -> 222 CE 25	292 -> 220 CE 25	22.9	22.75 - 23.10
PCB 37	256 -> 186 CE 30	256 -> 151 CE 50	23.1	23.00 - 23.50
PCB 77	292 -> 222 CE 25	292 -> 220 CE 25	24.1	23.95 - 24.15
PCB 74	292 -> 222 CE 25	292 -> 220 CE 25	24.2	24.15 - 24.25
PCB 70	292 -> 222 CE 25	292 -> 220 CE 25	24.3	24.25 - 24.50
PCB 66	292 -> 222 CE 25	292 -> 220 CE 25	24.9	24.70 - 25.05
PCB 126	326 -> 256 CE 30	326 -> 254 CE 30	25.1	24.95 - 25.15
PCB 87	326 -> 256 CE 30	326 -> 254 CE 30	25.2	25.15 - 25.45
PCB 99	326 -> 256 CE 30	326 -> 254 CE 30	26.0	25.80 - 26.20
PCB 60	292 -> 222 CE 25	292 -> 220 CE 25	26.4	26.30 - 26.60
PCB 101	326 -> 256 CE 30	326 -> 254 CE 30	26.7	26.50 - 26.90
PCB 114	326 -> 256 CE 30	326 -> 254 CE 30	27.3	27.10 - 27.50
PCB 118	326 -> 256 CE 30	326 -> 254 CE 30	27.7	27.50 - 27.95
PCB 156	360 -> 290 CE 35	360 -> 288 CE 30	28.1	27.95 - 28.40
PCB 82	326 -> 256 CE 30	326 -> 254 CE 30	28.2	28.05 - 28.40
PCB 183	394 -> 324 CE 30	394 -> 322 CE 30	28.5	28.40 - 28.80
PCB 128	360 -> 290 CE 35	360 -> 288 CE 30	29.1	28.95 - 29.10
PCB 153	360 -> 290 CE 35	360 -> 288 CE 30	29.2	29.10 - 29.35
PCB 105	326 -> 256 CE 30	326 -> 254 CE 30	29.6	29.45 - 19.60
PCB 169	360 -> 290 CE 35	360 -> 288 CE 30	29.6	29.50 - 29.80
PCB 179	394 -> 324 CE 30	394 -> 322 CE 30	29.7	29.55 - 29.80
PCB 180	394 -> 324 CE 30	394 -> 322 CE 30	29.9	29.80 - 30.20
PCB 158	360 -> 290 CE 35	360 -> 288 CE 30	30.1	30.00 - 30.35
PCB 138	360 -> 290 CE 35	360 -> 288 CE 30	31.1	30.95 - 31.50
PCB 170	394 -> 324 CE 30	394 -> 322 CE 30	31.7	31.55 - 32.05
PCB 166	360 -> 290 CE 35	360 -> 288 CE 30	32.7	32.45 - 32.75
PCB 187	394 -> 324 CE 30	394 -> 322 CE 30	32.8	32.65 - 33.20
PCB 189	394 -> 324 CE 30	394 -> 322 CE 30	34.1	33.90 - 34.50

2.3.2 Chromatographic Resolution

The oven ramp parameters included in this method (for only 52 minutes) in combination with the selected SRM transitions produce great chromatographic resolution with high S/N ratios for the 250 targeted compounds in the respective transitions, even though most compounds are not baseline resolved in the total ion chromatogram (TIC) (Appendix B, Figure B1). Furthermore, several compounds from different groups have very similar retention times, yet the method is able to accurately quantify the compounds due to the different SRM transitions. For example, dimethyl phthalate and 1,2-dimethyl naphthalene both have the same retention time at 15.2 minutes and PCB 126 and 2-nitrofluorene both have a retention time of 25.1 minutes, yet each of these four compounds have high chromatographic resolution in their respective SRM transitions (Figure 3). However, other compounds such as R-C26 and S-C27 TAS, norhopane and norneohopane, and coprostanol and epi-coprostanol, have similar retention times and transitions. Therefore, these paired compounds co-elute, and their concentrations are calculated together. Lengthening the oven ramp program could separate these compounds, but this was not done to avoid potential drawbacks such as peak shouldering and peak widening for all compounds included in our method (Koesukwiwat et al., 2011; Tsochatzis et al., 2021; Wong et al., 2010).

Overall, we found that the applied SRM method allows us to chromatographically separate most of the target compounds and also to quantify them over a range of concentrations (Appendix C, Tables C1-C6). The power of tandem mass spectrometry has been suggested to eradicate the need for chromatographic separation (Bolaños et al., 2007; Garrido Frenich et al., 2005). However, within compound groups, chromatographic separation is still vital, particularly when creating and optimizing SRM transitions (Figure 3).

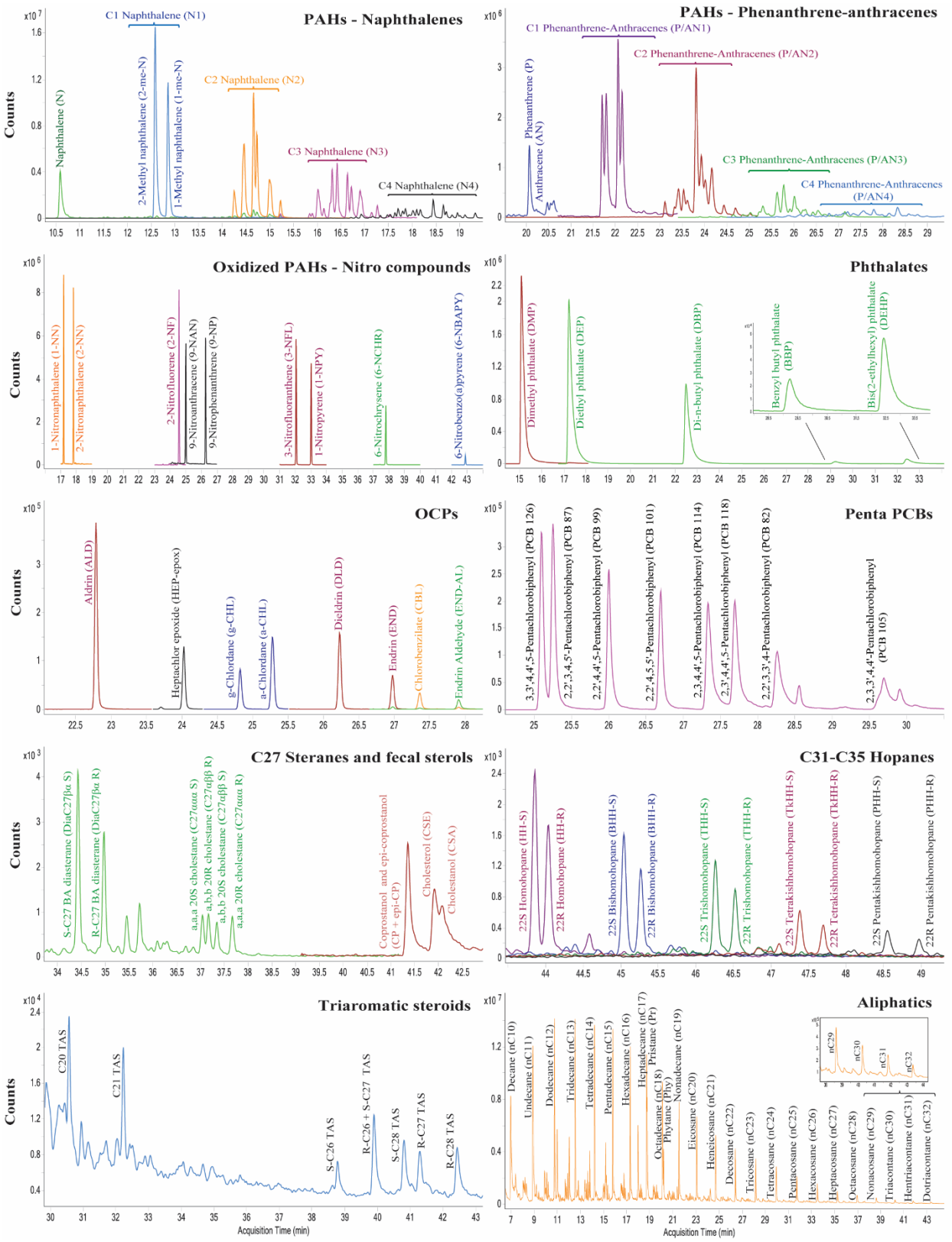

Figure 3: Chromatographic resolution of individual peaks within diverse compound groups, exemplifying the wide range of compound classes separated effectively.

2.3.3 Percentage Recovery

ASE extraction methods are well documented as having incomplete extractions, however the extractions have been found to have very consistent, measurable patterns of extraction, or recovery, for individual compounds (Alexandrou et al., 2001; Heemken et al., 1997; Kinross et al., 2020; Subedi et al., 2011). We found the individual percentage recovery for each of our compounds through our extraction method. This makes it possible to account for the individual compound loss and accurately calculate concentrations for each of the compounds in this method. For our reported extraction method using 30% dichloromethane and 70% *n*-hexane, all but four of the compounds have recoveries within QA/QC criteria (Appendix C, Tables C1-C6). The four compounds that fall below QA/QC criteria (ALA, ATA, MOAC, and PPC) are included in this report because they can meet the QA/QC criteria if a second extraction of 100% dichloromethane is completed using the same ASE method and the extracts are combined. As a small aside, we originally included three additional OCPs (cyanazine, metribuzin, and simazine), however these compounds were eventually removed due to inefficient extraction, even including the secondary extraction with 100% DCM. By determining the recovery for each compound, we are able account for losses throughout the extraction process and calculate accurate concentrations.

2.3.4 Method Validation Samples

The described method was validated by comparison to two extracted standard reference materials that were analyzed in triplicate and another standard reference material that was diluted and analyzed directly. The calculated concentrations of the standard reference materials are compared to their certified concentrations. Certified concentrations reported by NIST and IAEA

were used as a comparison for extracted concentrations of 1941b and IAEA-408, respectively. Calculated concentrations for NIST 2779 were also analyzed and compared to the concentrations reported by NIST. Reported concentrations and uncertainties were then compared to calculated concentrations and uncertainties for the extracted standard reference materials. We found that most of our calculated concentrations were close to the certified concentrations with a few exceptions (Appendix D, Figures D1-D9).

For PCBs, a pattern of some compounds having concentrations higher in the published values and some compounds having concentrations higher in our extracts was seen in both the 1941b and IAEA-408 values. In 1941b, 43% of the measured values for PCBs fall within the envelope of the published values, 26% were higher in the extracts, and 30% were higher in the published values. In IAEA-408, 38% of the measured values for PCBs fall within the envelope of the published values, 23% were higher in the extracts, and 38% were higher in the published values. There are five PCBs that have higher values for the published values: PCB 101, PCB 118, PCB 138, PCB 153, and PCB 180. These five PCBs are called the 'indicator PCBs' and are often used as an overall indicator of PCB concentrations (Abella et al., 2015). Given this information, it seems that the methods used to calculate the concentrations in the reference materials were calibrated for sensitivity of those main congeners, whereas our method is not honed specifically for those PCBs. This is further supported by the other PCBs (PCB 128, PCB 170, and PCB 156) which are calculated as being higher in our extracts. Additionally, the reference values only included values for 23 and 13 individual PCBs in 1941b and IAEA-408 respectively, whereas our method quantifies (with strong R^2 and recovery values and low LODs) 32 PCBs.

There are very few reported values for OCPs in the standard reference materials we used, six in 1941b and eleven in IAEA-408. Given such low numbers to begin with, even a few compounds being off will represent a large portion of the overall compounds for this group. In 1941b, 33% of measured values for OCPs fall within the envelope of published values, all the remaining values (n=4, 67%) were higher in the published values. In IAEA-408, 36% of measured values for OCPs fall within the envelope of published values, and similar to 1941b, the remaining values (n=7, 64%) were higher in the published values. Many of the compounds that we calculated as having lower concentrations for (e.g., DDE, ALD, g-CHL) are more polar than others. Our extraction method is not the best for highly polar compounds, therefore, even with our RRFs taking into account relative recoveries, it is possible we may not be getting all of these compounds and the extraction methods used to calculate concentrations in the standard reference materials have higher recoveries for more polar compounds. Again though, we quantify many more OCPs (n=33) and our method is optimized for all of them, not just a select few.

PAHs also had similar patterns between 1941b and IAEA-408. 79% of our values fell in the envelope of the published values for 1941b and 68% for IAEA-408. Of the compounds that did not fall in the envelope, 12% and 9% were higher in the extracts and 9% and 23% were higher in the published values for 1941b and IAEA-408 respectively. Our calculated concentrations for PY and BGP were higher than the published values and our calculated concentrations for AN, Pe, and ID were lower than the published values for both 1941b and IAEA-408. These compounds are all fairly difficult to integrate, even with optimized chromatography.

NIST 2779 was heavily used in the development of the methods this optimized method stems from. Due to this, it was ensured that major compounds of interest (aliphatics, biomarkers,

and PAHs) were not only easily quantifiable, but also optimized to ensure the highest possible number of the compounds present in 2779 could be identified and quantified. All analyzed PAHs, aliphatic hydrocarbons, and biomarkers fell in the envelope of the published values for NIST 2779.

2.4 Conclusion

This optimized method for the rapid analysis of 250 I/SVOCs using GC-MS/MS-SRM represents a significant advancement in the field of environmental analytical chemistry. One of the key strengths of our method is the ability to measure a wide variety of compound classes, including PAHs, oxid-PAHs, OCPs, PCBs, biomarkers, aliphatic hydrocarbons, and plastic additives, in a single analysis. This is in contrast to other methods that only focus on a limited number of compound types. The utilization of tandem mass spectrometry technology, individualized SRM transitions, and RRF corrections allows for accurate quantification of diverse compound classes without compromising chromatographic separation or data quality. The ability to simultaneously analyze multiple compound classes provides a more comprehensive and holistic view of the environmental samples, enabling a deeper understanding of the complex composition of I/SVOCs from both natural and anthropogenic sources. This enhanced capability of our method sets it apart from other methods and makes it a valuable tool for environmental monitoring and risk assessment studies. This method offers a robust, efficient, and comprehensive approach for the analysis of I/SVOCs, and its expanded capabilities in measuring diverse compound classes make it superior to other methods in the field. There is great potential for this method in addressing current and emerging challenges in environmental

analysis and can contribute to a better understanding of the fate, transport, and impact of I/SVOCs in environmental systems.

CHAPTER THREE:

NORTHWEST CUBAN MARINE SEDIMENT ANALYSIS

3.1 Background Information

Cuba is an archipelago made up of more than 3,000 islands and cays located between the Gulf of Mexico (northwest), the Atlantic Ocean (northeast), and the Caribbean Sea (south). (Figure 4).

Figure 4: Map of Cuba showing Havana (red), the Island of Youth (white), and the Gulf of Batabanó

The climate is subtropical to tropical with two annual seasons: summer and winter (Dierksmeier, 1996). The summer season is the rainy season and typically when hurricanes occur, generally one every two years (Dierksmeier, 1996; Suárez et al., 2012). The island of Cuba is long to the east and west and narrow to the north and south made from mountains that are part of the Greater Antillean Ridge (Pardo, 1975). Rivers on Cuba flow down the mountains,

generally to the north and south, causing them to be typically short (Dierksmeier, 1996). Due to the short river lengths sedimentation rates depend heavily on rainfall (Dierksmeier, 1996). As noted in Díaz-Asencio et al. (2011), an anomaly from heavier than average rainfall cause by a strong ENSO event in 1982 was recorded in sediment cores collected in Havana Bay.

Political changes within Cuba caused changes in infrastructure, agricultural practices, and industrial development. Cuba has spent much of the last two centuries either being controlled by or depending heavily on other countries, namely Spain, the United States, and the USSR. During each country's time of influence, the imports into Cuba would come from the respective country. This is particularly important for contaminants as the different countries each followed their own policies and protocols for chemical handling, development, and usage. Agriculture in Cuba has focused on the monoculture of sugarcane for most of the last two centuries; records indicate that sugarcane monoculture was fully established as far back as the late 1700s (Gott, 2005). The production of sugarcane and the environmental toll of monocultures only increased with the introduction of pesticides in the 1950s because monocultures of crops tend to be destructive to the environment and require large amounts of water and pesticides to maintain (Gliessman, 1985). Cuba's agriculture focused heavily on sugarcane because the export of sugarcane was the main source of trade and commerce both for Cuba and the various countries that occupied it (Castellanos and Alvarez, 1996). In the late 19th century, Spain occupied Cuba and imported supplies to the island (Staten, 2005). In 1898, Cuba was briefly occupied by the United States, an occupation which lasted until 1902 when Cuba became a republic (Pérez, 1983; Staten, 2005). Throughout this time, most imports came from the United States and the monoculture of sugarcane continued. The 1953-1959 revolution in Cuba resulted in the accession of a Marxist regime under Fidel Castro which re-oriented the economy and attempted to diversify agriculture

by decreasing the sugarcane monoculture (Gleijeses, 2002; Oppenheim, 2001). Following the revolution, Cuba became more dependent on the USSR than the United States. Due to Cuba's new ties to communism, tensions grew with the United States and the United States placed a trade embargo on Cuba in 1961 (Gorsuch, 2015). As a result, Cuban agriculture turned back to sugarcane as a means of boosting the economy (Oppenheim, 2001).

In 1968, Cuba further aligned with the USSR as a means of importing necessary food and oil in exchange for exporting large amounts of sugar to the Soviet Union (Oppenheim, 2001). Following Cuba's alignment with the USSR, priorities and funding shifted from building and maintaining infrastructure to maximizing sugar output (Oppenheim, 2001). As a result, much of the infrastructure, particularly water resources (water treatment plants, etc.), has, to this day, suffered from lack of good maintenance (Powell, 2004). However, energy production was developed significantly, particularly after the alignment with the USSR due to the fact that Cuba entered into a sugar-for-oil agreement and the mass production of sugar required updated energy infrastructure (Suárez et al., 2012). To meet their obligations with the USSR, Cuba needed to devote roughly 75% of all agricultural lands to sugar production (Castellanos and Alvarez, 1996). Prior to the ramp up of production of sugar cane, in 1955 Cuba was producing approximately half its potential capacity (Summers, 1955). From 1968 to 1991, the production of sugarcane was heavily industrialized; any means to increase production was used, which included heavy use of fertilizers, pesticides, and irrigation (Oppenheim, 2001). In general, the production of sugar relied very heavily on machines and chemicals. During this period, the sediment records may indicate heavy use of pesticides and significant sedimentation due to erosion caused by clear-cutting to increase sugarcane fields (Dierksmeier, 1996).

The collapse of the Soviet Union in 1991 caused significant and widespread changes to agriculture, infrastructure, and the economy in Cuba, which in turn caused changes in contaminant releases in the surrounding environments. The Cuban economy crashed due to its heavy reliance on imports from the USSR (Bronfman, 2010). Sugar monoculture was no longer possible due to the loss of demand for export and the loss of supplies from import (Castellanos and Alvarez, 1996). This resulted in a major famine with extreme food shortages and electrical blackouts (Withheld, 2008). Beginning in the late 1990s, out of necessity, Cuba's agriculture shifted to organic, sustainable, polyculture, which it still maintains today (Bronfman, 2010). Since the famine and loss of support from the USSR, Cuba has largely been isolated, with support coming mostly from Venezuela (Dosal, 2006). Currently, Cuba remains generally isolated, with only small, intermittent, amounts of trade with the United States (Staten, 2005). Without support from the USSR and the extreme decrease in agricultural activity, the sediment records would be expected to show a steep decrease in contaminant concentrations after 1991.

Between 1992 and 2003, Cuba began producing enough oil to generate electricity using oil-fired power plants, but the oil contained high levels of sulfur resulting in damage to the power plants (Suárez et al., 2012). The damage to the plants caused blackouts in 2004-2005 (Suárez et al., 2012). The use of oil-fired power plants would be expected to be reflected in the sediment record as an increase in pyrogenic PAH contaminants. As of 2009, approximately 60% of energy production in Cuba continues to be from oil-fired power plants, approximately 25% comes from various types of generators, and only about 4% comes from renewable energy sources (Suárez et al., 2012). The sediment records are expected to show a continued input of pyrogenic contaminants from approximately 1992 to present.

The water resources infrastructure throughout Cuba is in a constant state of disrepair. As of 2004, only five water sanitation plants existed in Cuba, all of which were nearly 70 years old (Powell, 2004). Due to the low number of wastewater treatment plants and the low efficiency of the existing plants, raw sewage is discharged into waterways on all sides of Cuba. The lack of wastewater treatment plants in Cuba may be observed in the sediment records by sewage contamination.

Over the past several decades, there have been few studies tracking contaminants in the Caribbean (Fernandez et al., 2007). Specifically, Cuba, which has had limited access, has not been an area extensively studied for organic contaminants. Cuba has experienced many changes in its history, especially related to agricultural and petro-chemical industrialization. Recently, there have been a few select studies that measured contaminants in specific areas of Cuba, such as Cienfuegos Bay (Tolosa et al., 2009, 2010; Tolosa et al., 2014), the Gulf of Batabanó (Alonso-Hernandez et al., 2014; Alonso-Hernández et al., 2015) and Havana Bay (Díaz-Asencio et al., 2011; Martins et al., 2018). However, a transect of marine sediments from the north-west coast of Cuba has not been analyzed for organic compounds. This region is characterized by a diversity of land-use types including a nature preserve (Gulf of Guanahacabibes), several port and industrial cities (Mariel, Havana City, and Santa Lucia) and a region of heavy tobacco production (Pinar del Rio) (Baker, 2018; Gott, 2005). Information regarding the status of organic compounds, contaminants particularly, in many Caribbean coastal areas is in short supply. This study would expand on a small pool of data that exists for contaminants in coastal tropical regions. Additionally, results from this research can be compared to results from other environments, e.g., Persian Gulf in Iran (Jafarabadi et al., 2017), and the Mississippi River in the USA (Wang et al., 2012).

3.2 Methods

3.2.1 Sample Collection

In May of 2017, during a research cruise aboard the R/V Weatherbird II, sediment cores were collected from the north-west coast of Cuba (see Table 6 and Figure 5 for locations of sites). The sediment cores were collected using an Ocean Instruments MC-800 multi-corer, which retrieves up to eight 10 cm diameter cores without disturbing the sediment-water interface. At each site, each of the eight cores were used for various analyses. One core was used to establish chronology using methods described in Larson et al. (2018), Díaz-Asencio et al. (2020), and Schwing et al. (2017). Another core was used for analysis of organic compounds and stable isotope analysis. The organic cores were subsampled in 2 and 5 mm increments using a calibrated threaded rod as described in Schwing et al. (2016). During extrusion, subsamples were placed in combusted (450˚C for 4 hours) glass jars. After extrusion, samples in jars were frozen, freeze-dried, and homogenized via mortar and pestle.

Table 6: Sampling sites and nearest important landmark

Site name	Nearest landmark	Latitude	Longitude	Water depth (m)	Rough distance from coast
44-150	Nearshore city of Havana	23° 9'23.28"N	82°22'7.92"W	316	~1 km N
44-750	Offshore from city of Havana	23°14'16.38"N	82°20'39.90"W	1475	<10 km N
43-750	Offshore from city of Mariel	23° 7'44.64"N	82°43'54.66"W	1512	10 km N
40-750	Offshore from city of Puerto Esperanza	23° 0'14.40"N	83°40'50.22"W	1590	20 km N
39-750	Offshore from city of Santa Lucia	22°48'14.88"N	84° 6'29.16"W	1250	20 km N-NW
37-250	On western edge of Gulf of Guanahacabibes Nature Preserve	22° 9'4.08"N	84°49'34.74"W	530	40 km W

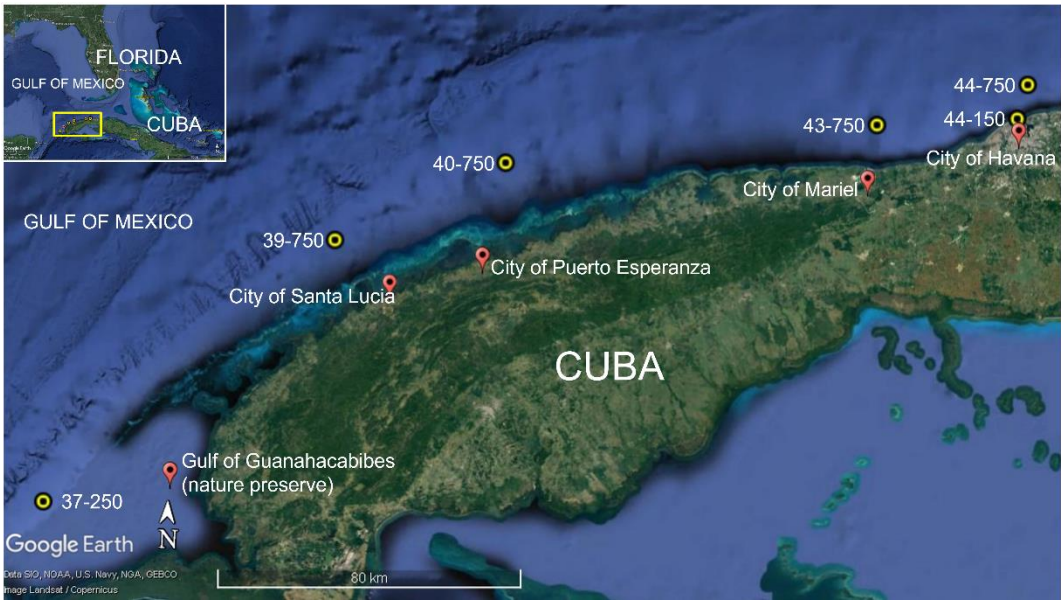

Figure 5: Map of sampling sites

3.2.2 Stable Isotope Analysis

A subsample of selected depths was taken from the organic cores for analysis of stable isotopes. The subsamples were weighed, acidified with 10% HCl to remove carbonates, dried at low temperature (~60°C) to remove any moisture, and weighed again. Each sample (8-10mg) was weighed on a Mettler-Toledo precision micro-balance, encapsulated in tin foil, and loaded into a Costech Technologies Zero-Blank Autosampler prior to combustion at 1050°C and reduction at 650°C in a Carlo-Erba NA2500 Series-II Elemental Analyzer (EA) coupled in continuous-flow mode to a Finnigan Delta Plus XL isotope ratio mass spectrometer (IRMS). Measurements were normalized using NIST 8573 and NIST 8574 *L*-glutamic acid standard reference materials. Reference material NIST 2702 marine sediment was used as a quality control standard. Samples were run in duplicate and if a pair of samples had a range greater than the standard error, the sample was run again, and the value of the triplicate sample was used as a qualifier.

3.2.3 Organic Compound Analysis

Samples were extracted using an accelerated solvent extraction system (ASE 350, Thermo-Scientific Dionex) with a solvent mix of 30% dichloromethane and 70% hexane. Prior to extraction, each sample had a suite of deuterated and non-deuterated standards added to correct for differences in extraction efficiency. Samples were analyzed on an Agilent 7890B gas chromatograph 7010 triple quadrupole mass spectrometer (GC-MS/MS) in selected reaction monitoring (SRM) mode. The analysis method on the GC-MS/MS is described in Chapter 2. The cores were prepared for analysis by the methods outlined in Chapter 2.

3.3.3 ^{210}Pb Geochronology

As described in Larson et al. (2018), Díaz-Asencio et al. (2020), and Schwing et al. (2017), the sediment cores were dated using the following methods. Excess ^{210}Pb and excess ^{234}Th activities in sediment samples were determined for age dating using short-lived radionuclide geochronology. Samples were counted for 48 hours on a Canberra Series HPGe (High-Purity Germanium) Coaxial Planar Photon Detector to obtain raw activities. To account for the short half-life (24.1 days) of ^{234}Th, samples were counted within 120 days of collection. Raw activities were corrected for counting time, detector efficiency, and the fraction of the total radioisotope measured, resulting in activity values expressed in disintegrations per minute per gram (dpm/g). Age dates were assigned to each sample analyzed using the Constant Rate of Supply (CRS) Model, following the approach described in previous methods (Appleby and Oldfieldz, 1983; Binford, 1990; Díaz-Asencio et al., 2020; Larson et al., 2018; Schwing et al., 2017; Schwing et al., 2015).

3.3 Results and Discussion

3.3.1 Bulk $\delta^{15}N$ and $\delta^{13}C$ Measurements

Stable isotope analyses were performed on 86 samples from the six sites listed in Table 6. The overall range for $\delta^{13}C$ values from all sites was -25.79 to -14.62 ‰ (Figure 6). The most depleted samples were the recently deposited samples from 44-750 and the entire core for 44-150. From there, as sampling moves to the west, the samples become enriched, with the highest values found at 37-250. The trends seen in the $\delta^{13}C$ values could be due to several factors, such as fossil fuel burning, freshwater input supplying signal from terrestrial plants, or mixing of terrestrial and marine sources, however it is impossible to make these conclusions based solely on the $\delta^{13}C$ values (Craig, 1953; Degens, 1969; Sharp, 2017).

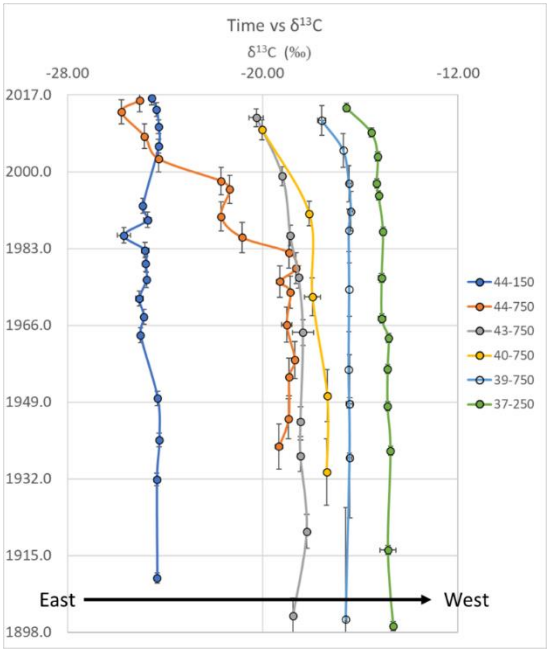

Figure 6: $\delta^{13}C$ depth profiles of all sites. Note the enrichment moving from east to west. Error bars represent standard deviation about the mean.

By plotting $\delta^{13}C$ vs the carbon to nitrogen ratio (C:N), it becomes possible to understand more of the interactions that are occurring in the environment to produce the patterns we see in

the sediment record. The $\delta^{13}C$ vs C:N plot (Figure 7) further shows the distinct difference between recent 44-750 deposits and the western sites. This could indicate the greater terrestrial influence found at the sites off of Havana Bay and greater marine influence for the rest of the sites, particularly 37-250 (Sharp, 2017).

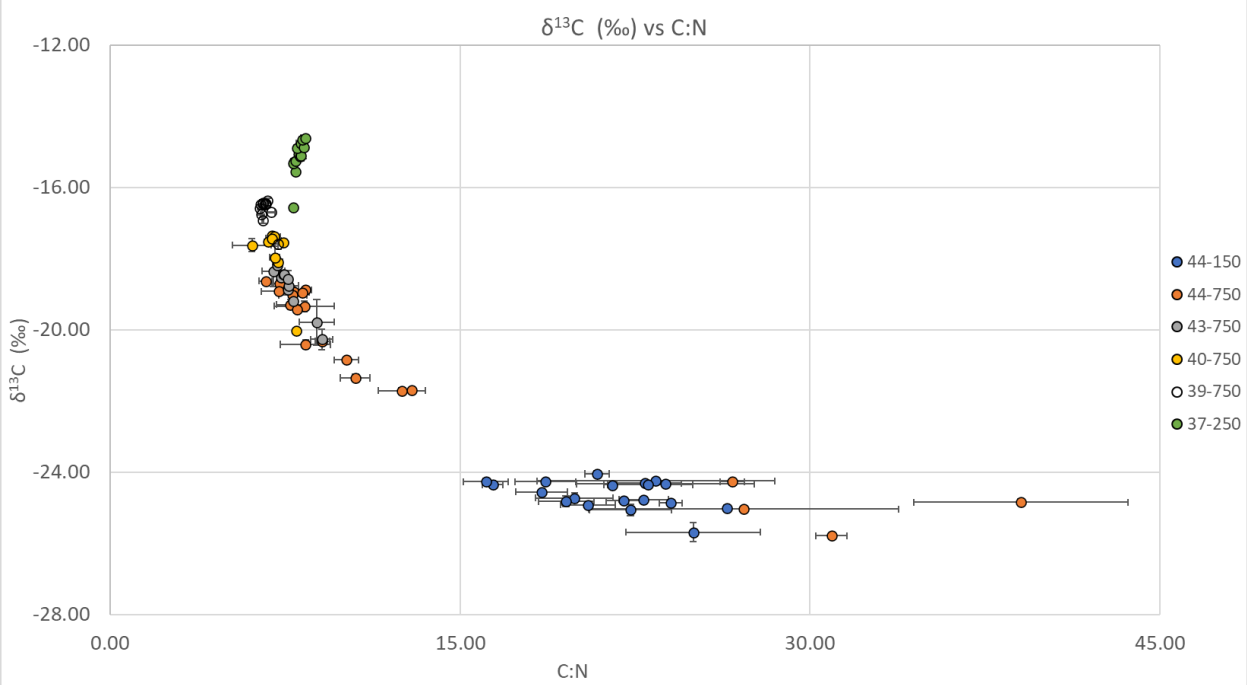

Figure 7: $\delta^{13}C$ vs C:N for all plots. Error bars represent standard deviation about the mean.

The values for $\delta^{15}N$ ranged from 1.35 to 5.90 ‰ for all sites, with the most depleted values found at 37-250 (Figure 8). Most of the $\delta^{15}N$ values, for all sites excluding 37-250, were around 4-5 ‰ and 37-250 was around 1.5 ‰. Typically, a more depleted $\delta^{15}N$ signal indicates greater terrestrial input (Peterson and Fry, 1987; Sharp, 2017), however this does not match the interpretations for the rest of the data and again, it is near impossible to draw such conclusions from a single set of values.

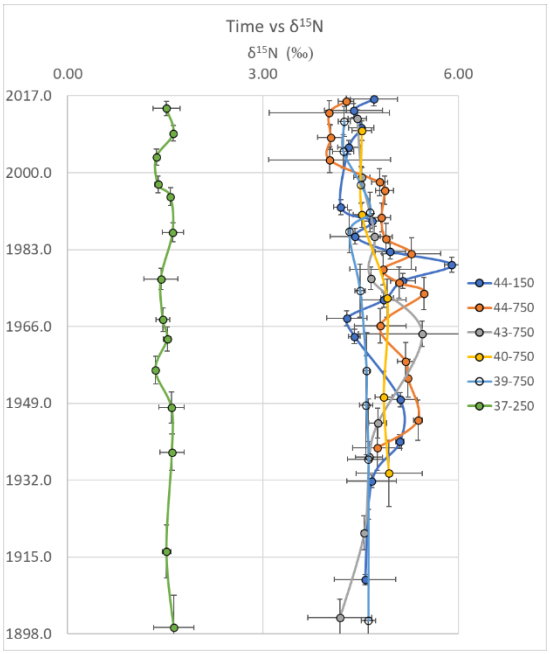

Figure 8: $\delta^{15}N$ depth profiles of all sites. Error bars represent standard deviation about the mean.

When $\delta^{13}C$ and $\delta^{15}N$ are plotted against each other, 3 distinct groups can be seen (Figure 9). The blue box in this figure can be thought of as the 'urban' influenced sediment samples, which include 44-150 and more recent deposits of 44-750. The green box in this figure can be thought of as the 'marine' or 'seagrass' influenced samples, grouping the samples The 37-250 core, collected near the nature preserve, Guanahacabibes Gulf. Lastly, the yellow box is somewhere between 'urban' and 'marine' and contains the older sediment samples from 44-750 and all samples from cores 43-750, 40-750, and 39-750. None of the samples fall completely within the reference areas, which can be explained by each site having some influence from more than one source. Particularly interesting is the apparent shift in influence for 44-750 in the recent samples. Again, this could be due to fossil fuel, changes in freshwater input, or mixing of terrestrial and marine sources (Craig, 1953; Degens, 1969; Sharp, 2017). This is a very useful way to view these data because it helps us see where we can expect the most similarities and differences when the samples are analyzed for organic compounds. The samples that have very

similar results in the $\delta^{13}C$ vs $\delta^{15}N$ plot (similar compositions of the organic matter present) could be expected to have similar organic compounds. Figure 9 also shows which different sources may be contributing more to the signal at each site, ranging from marine particulate organic carbon (POC) to urban wastes to fertilizer components (nitrogen, phosphorus, potassium [NPK]), which each have a distinct value (Alonso-Hernández et al., 2020; Ishikawa et al., 2017; Moncreiff and Sullivan, 2001). By using the differences seen between the sites in this plot (Figure 9), it will be easier to pinpoint which samples/sites to analyze for organics to understand what else is different in the distinct groups.

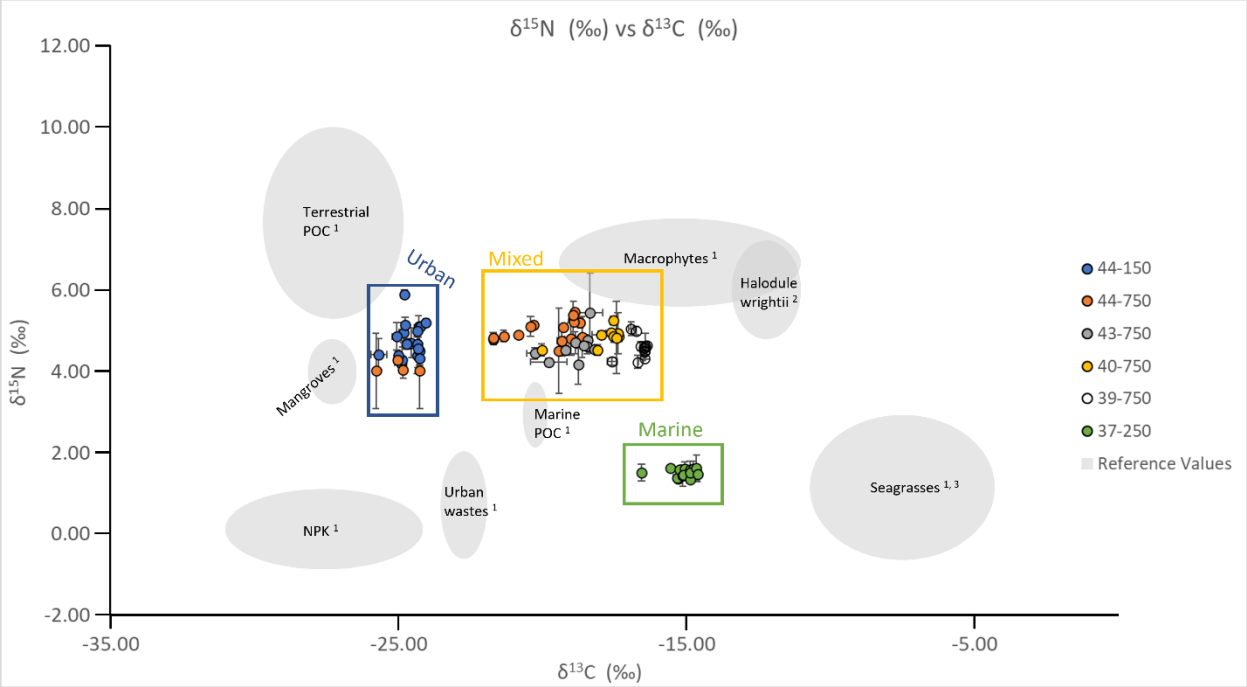

Figure 9: $\delta^{13}C$ vs $\delta^{15}N$ for all plots. Error bars represent standard deviation about the mean. Reference values: 1 = Alonso-Hernández et al. (2020), 2 = Moncreiff and Sullivan (2001), 3 = Ishikawa et al. (2017). POC = particulate organic carbon. NPK = denotes signature from fertilizers containing nitrogen, phosphorus, and potassium. Colored boxes represent distinct groups that the samples fall into: blue = urban, yellow = between urban and marine, green = marine.

Another set of parameters, %TOC and %N, show that 37-250 is very different than the rest of the samples (Figures 10 and 11). The percentage of organic carbon (%TOC) of the sites, excluding 37-250, was between 1-7%, typical of other Caribbean sediments (Alonso-Hernández et al., 2020; Alonso-Hernández et al., 2017; Franco et al., 2021), however 37-250 was significantly higher ~20-22%. Given that the samples were acidified before being measured for stable isotopes and 37-250 had the greatest mass loss, it appears that the non-carbonate organic matter present at 37-250 is highly carbon rich. This is most likely due to the setting of 37-250: carbonate sediments with influence from surrounding mangroves (Kennedy et al., 2004; Marchand et al., 2008; Resmi et al., 2016).

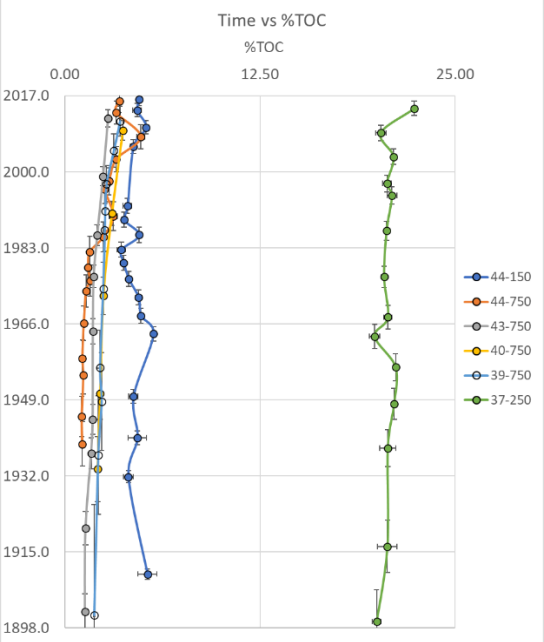

Figure 10: Percent organic carbon (%TOC) depth profiles for all sites. Error bars represent standard deviation about the mean.

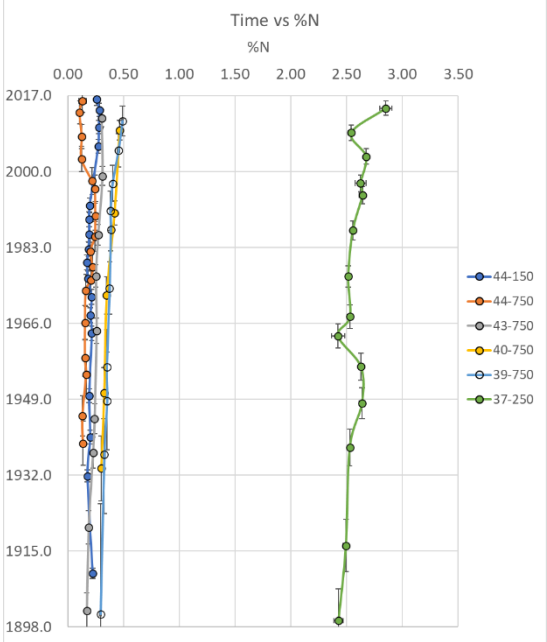

Figure 11: Percent nitrogen (%N) depth profiles for all sites. Error bars represent standard deviation about the mean.

3.3.2 Preliminary Organic Compound Analysis

The organic compound analysis has been successfully completed on the deep Havana core, core 44-750, which serves as a proof of concept for the optimized method, as described in Chapter 2. This core was specifically chosen for analysis as it was expected to exhibit significant organic compound changes over time, validating the efficacy of the developed organic compound analysis method in conjunction with geochronology, and producing valuable results.

The organic compound analysis trends fit nicely with the trend seen in the $\delta^{13}C$ data; the recent samples are very different from the rest of the core and after ~1980 the samples are very similar (Figure 12). A possible reason for the change in $\delta^{13}C$ values is that the source of carbon changed, which fits with the change seen in the organic compounds and contaminants. The source of carbon changed from a more marine source to a more terrestrial source around based on the pattern seen in Figure 9. The %TOC is also higher in the recent samples (~3-5% after 1980 and ~1-2% before 1980). The organic compound analysis shows that the increased TOC is made up of many PAHs as well as increased values for the rest of the compounds.

Compared to previous studies, the results of the organic compound analysis for 44-750 are quite different. In heavily contaminated sediments, concentrations of total aliphatic hydrocarbons (AHs) can range from 337 to as high as 1800 μg/g; the concentration of AHs in 44-750 is very low, similar to non-contaminated sediments (1-5 μg/g) (Farrington and Tripp, 1977; Romero et al., 2015). In a previous study that looked at sediments closer to shore near Havana (Martins et al., 2018), the AH concentrations were much higher than what was measured in 44-750. Due to this, it can be expected that 44-150 will have higher concentrations of AHs than 44-750, when it is measured in the future. In the same study (Martins et al., 2018), fecal sterol concentrations were found to be much lower near Havana than what was measured at 44-750.

In comparison to post oil spill contaminated sediment (14 µg/g) (Romero et al., 2015) and sediment collected near industrial effluents in Spain (49 µg/g) (Antizar-Ladislao, 2009), the total PAH concentrations measured in the surface samples of 44-750 were extremely high, reaching levels as high as 216 µg/g.

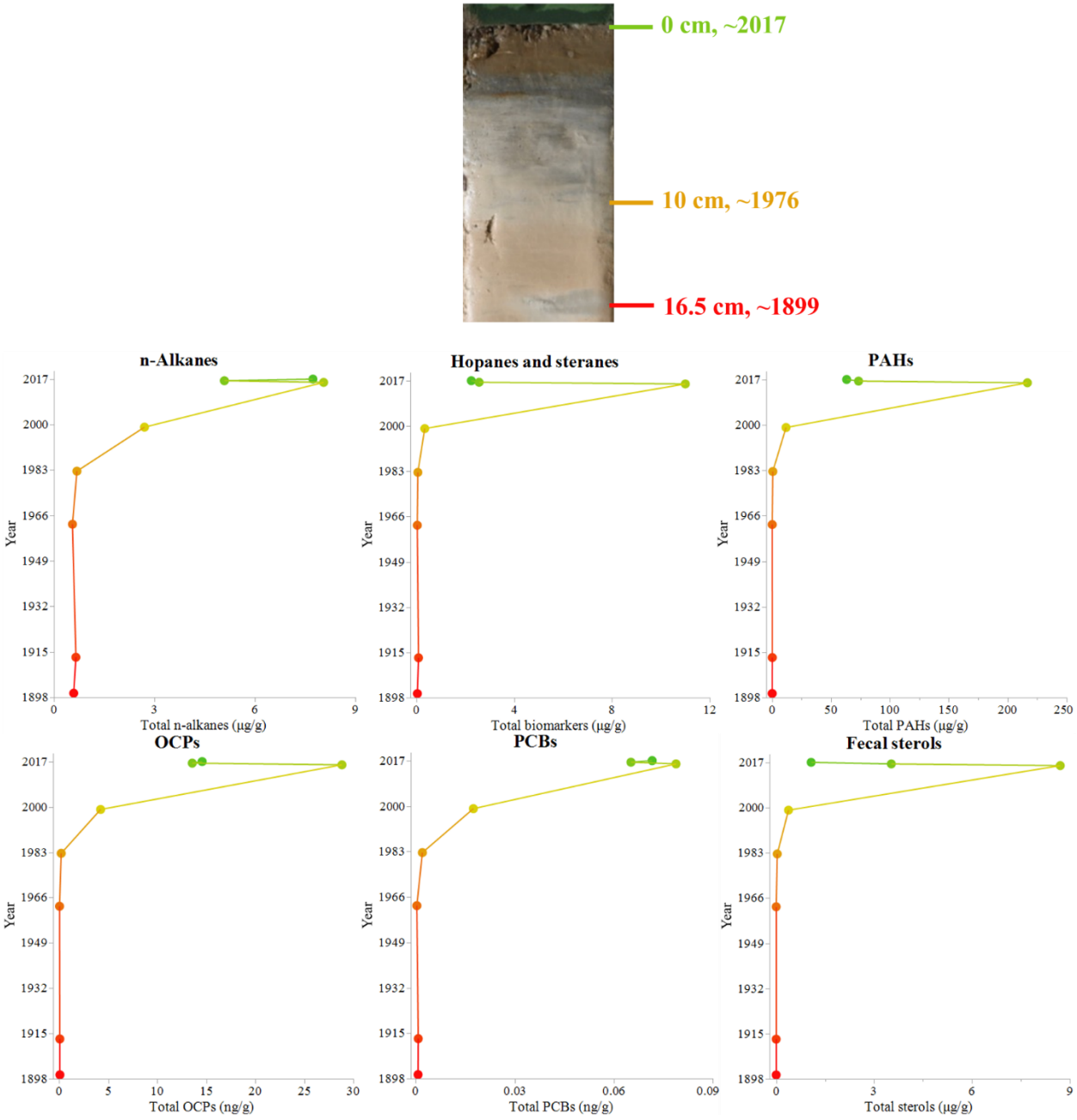

Figure 12: 44-750 total concentrations of organic compound groups over time. Note that surface/recent samples are green and deep/old samples are red.

Often, ratios of specific organic compounds can be used to understand changes in sources of carbon. Specifically, certain PAHs as a ratio to total PAHs can indicate sources of carbon as either anthropogenic or natural and differentiate between terrestrial and marine sources. Perylene and retene are two PAHs that have mainly natural sources; both are thought to be products of diagenesis of biogenic materials (Abrajano et al., 2003; Ramdahl, 1983; Romero et al., 2021; Venkatesan, 1988). An increase in these natural PAHs could come from an increase of terrestrial inputs. In Figure 13 a and d, retene and perylene are higher in recent samples and lower in older samples. This is most likely due to a change in the carbon source, which was also seen in the $\delta^{13}C$ profile.

In contrast to naturally occurring PAHs like retene and perylene, there exists another category of PAHs predominantly derived from human activities such as the combustion of fossil fuels. These PAHs, collectively known as the carcinogenic PAHs (BAA, CHR, BBFL, BKFL, ID, and DA), pose significant risks to both human health and the environment. (Bravo-Linares et al., 2012; Guo et al., 2010; Sanders et al., 2002; Wang et al., 1999). The percentage of carcinogenic PAHs out of the total PAHs can be seen as an indication of anthropogenic input. In more recent samples, the total PAH concentrations increased, therefore the carcinogenic PAHs also increased. As seen in Figure 13 c, in approximately 1999, there is a peak for carcinogenic PAH concentration, which does not directly match the overall total PAH concentration and therefore is indicative of an increase in anthropogenic contaminants. Further downcore, the overall PAH concentration decreases and therefore the concentration of the carcinogenic PAHs also decreases, however this is not reflected in the plot since the plot is percent carcinogenic PAHs.

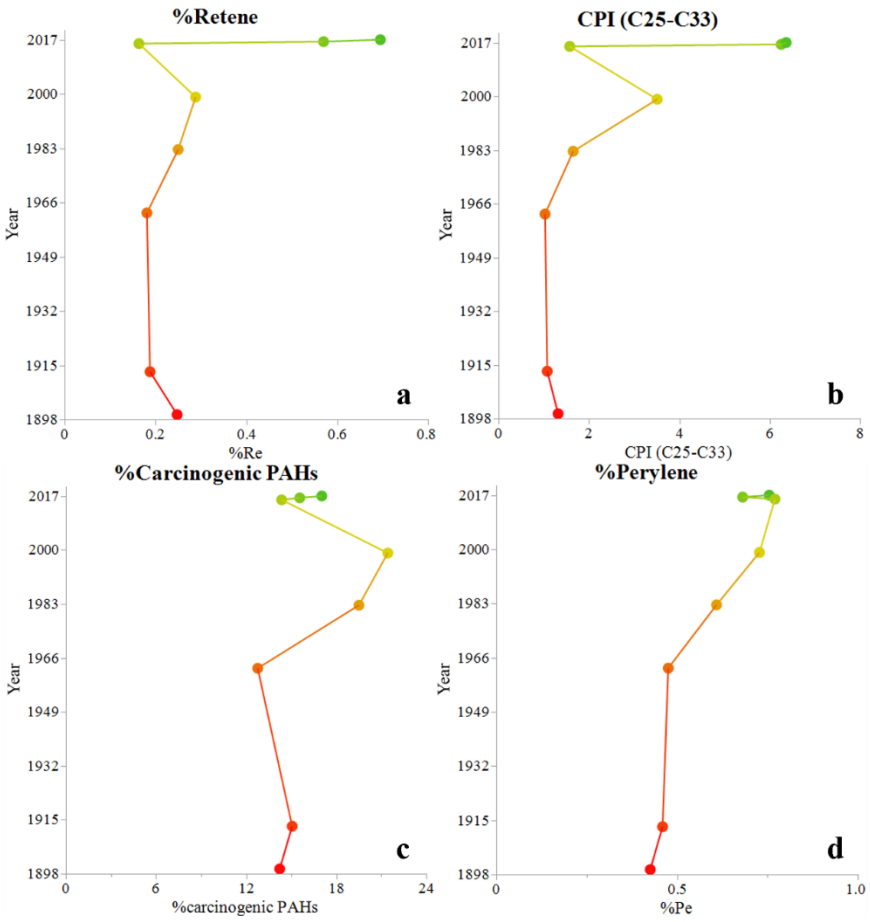

Figure 13: 44-750 diagnostic ratios; a) the percentage of retene over time ([retene]/Σ[PAHs]), b) the Carbon Preference Index (CPI) over time (1/2 (Σ[odd C25-C33]/ Σ[even C25-C33])) *n*-alkanes, c) the percentage of carcinogenic PAHs over time (Σ[BAA, CHR, BBFL, BKFL, ID, DA]/ Σ[PAHs]), d) percentage of perylene over time ([perylene]/Σ[PAHs]).

The carbon preference index (CPI) has long been used as an indicator of biogenic and anthropogenic inputs (Aeppli et al., 2014b; Ahad et al., 2011; Bray and Evans, 1961; El Nemr et al., 2013; Reddy et al., 2000; Romero et al., 2015; Xing et al., 2011). Typically, a CPI of 1 can be used to indicate presence of petroleum hydrocarbons (Aeppli et al., 2014a; Romero et al., 2015) or recent microbial degradation (Herrera-Herrera et al., 2020). The profile for 44-750 (Figure 13 b) most likely shows that there was mainly microbial degradation contributing to the CPI prior to the 1980s and there was a distinct increase after that period. A very high CPI can be

indicative of terrestrial plant matter, such as leaf waxes (Yan et al., 2021). Similar to the indication from the retene and perylene profiles (Figure 13 a and d) the increase in CPI beginning in the 1980s (Figure 13 b) shows there has been an increase in terrestrial input to this site beginning in the 1980s.

3.4 Conclusion

Overall, the stable isotope analysis data and the organic compound analysis data show that there was a change in the carbon source beginning in the 1980s, changing towards potentially an increase in terrestrial input. Around this time, Cuba significantly increased sugarcane production, which possibly led to an increase in deforestation and erosion. The increase in deforestation and erosion can be seen as an increase in terrestrial organic compounds found in the offshore marine sediments.

3.5 Future Work

Future projects related to this work should involve complete analysis of the cores described in this chapter. By applying the described organic compound analysis method to all collected sediment cores, more details about the historical input of contamination across Cuba throughout the past century may be uncovered. Special emphasis should be placed on depths/years that show large changes in the stable isotope analysis and large differences between sites. Additionally, adding an analysis of satellite data for the years of large changes in the stable isotope analysis could lend more insight into the causes of the increased terrestrial input seen in 44-750.

CHAPTER FOUR:

CONCLUSION

This thesis focuses on the development of an optimized method for the rapid analysis of 250 individual and semi-volatile organic compounds (I/SVOCs) using gas chromatography-tandem mass spectrometry in selected reaction monitoring mode (GC-MS/MS-SRM) in environmental samples, with a specific focus on sediment cores from Cuba. The research is conducted in the field of environmental analytical chemistry, with the aim of addressing the challenges associated with the comprehensive analysis of diverse compound classes in environmental matrices and using stable isotope data and geochronology to guide sample selection for contamination history analysis.

Chapter 1 provides an introduction to the importance of analyzing I/SVOCs in environmental samples, including their potential impacts on human health and the environment. The limitations of existing methods for I/SVOC analysis are discussed, and the research objectives, including the development of an optimized method for I/SVOC analysis and the application of stable isotope data and geochronology for sample selection, are outlined, with a specific focus on Cuba.

Chapter 2 presents the optimized method for the rapid analysis of 250 I/SVOCs using GC-MS/MS-SRM. The method's strengths, such as the comprehensive coverage of compound classes and the utilization of tandem mass spectrometry technology with individualized SRM transitions and response factor correction, are highlighted. The method's ability to provide a

holistic view of environmental samples allows for a deeper understanding of the complex composition of I/SVOCs from both natural and anthropogenic sources. The method is compared to other existing methods and is found to be superior in terms of its expanded capabilities and robustness.

Chapter 3 discusses the application of stable isotope data and geochronology as a guide for sample selection in the analysis of contamination history using the optimized method, with a specific focus on sediment cores from Cuba. The value of stable isotope data in providing insights into carbon sources and influences, and the need for a comprehensive organic compound analysis approach, is emphasized. The potential of the optimized method to uncover the historical input of contamination across Cuba throughout the past century, utilizing the information obtained from stable isotope data to inform sample selection, is discussed. Future work related to the analysis of sediment cores from Cuba using the optimized method is proposed, including a focus on depths/years that show significant changes in the overall trend of the core and the potential for analyzing new ratios of organic compounds to further understand ecosystem health in the context of Cuba's environmental history.

In summary, the optimized method for the rapid analysis of 250 I/SVOCs using GC-MS/MS-SRM presented in this thesis represents a significant advancement in the field of environmental analytical chemistry, with a specific focus on its application to analyze sediment cores from Cuba. The method's ability to measure diverse compound classes in a single analysis, combined with the application of stable isotope data and geochronology for sample selection, provides a comprehensive approach for analyzing I/SVOCs in sediment cores and understanding the contamination history of Cuba's environmental systems. Further research and application of this method have the potential to contribute to a better understanding of the fate, transport, and

impact of I/SVOCs in Cuba's environmental systems and can aid in environmental monitoring, risk assessment, and ecosystem health assessment studies in the context of Cuba's unique environmental history.

REFERENCES

Abella, V., Santoro, A., Scotece, M., Conde, J., López-López, V., Lazzaro, V., Gómez-Reino, J.J., Meli, R., and Gualillo, O. (2015) Non-dioxin-like polychlorinated biphenyls (PCB 101, PCB 153 and PCB 180) induce chondrocyte cell death through multiple pathways. Toxicology Letters 234, 13-19.

Abrajano, T.A., Jr., Yan, B., and O'Malley, V. (2003) High Molecular Weight Petrogenic and Pyrogenic Hydrocarbons in Aquatic Environments. Treatise on Geochemistry 9, 612.

Adhikari, P.L., Maiti, K., and Overton, E.B. (2015) Vertical fluxes of polycyclic aromatic hydrocarbons in the northern Gulf of Mexico. Marine Chemistry 168, 60-68.

Adhikari, P.L., Wong, R.L., and Overton, E.B. (2017) Application of enhanced gas chromatography/triple quadrupole mass spectrometry for monitoring petroleum weathering and forensic source fingerprinting in samples impacted by the Deepwater Horizon oil spill. Chemosphere 184, 939-950.

Aeppli, C., Nelson, R.K., Carmichael, C.A., Valentine, D.L., and Reddy, C.M. (2014a) Biotic and abiotic oil degradation after the Deepwater Horizon disaster leads to formation of recalcitrant oxygenated hydrocarbons: new insights using GC× GC, International Oil Spill Conference Proceedings. American Petroleum Institute, pp. 1087-1098.

Aeppli, C., Nelson, R.K., Radovic, J.R., Carmichael, C.A., Valentine, D.L., and Reddy, C.M. (2014b) Recalcitrance and degradation of petroleum biomarkers upon abiotic and biotic natural weathering of Deepwater Horizon oil. Environmental science & technology 48, 6726-6734.

Ahad, J.M.E., Ganeshram, R.S., Bryant, C.L., Cisneros-Dozal, L.M., Ascough, P.L., Fallick, A.E., and Slater, G.F. (2011) Sources of n-alkanes in an urbanized estuary: Insights from molecular distributions and compound-specific stable and radiocarbon isotopes. Marine Chemistry 126, 239-249.

Al-Sarawi, H.A., Jha, A.N., Al-Sarawi, M.A., and Lyons, B.P. (2015) Historic and contemporary contamination in the marine environment of Kuwait: An overview. Marine Pollution Bulletin 100, 621-628.

Alder, L., Greulich, K., Kempe, G., and Vieth, B. (2006) Residue analysis of 500 high priority pesticides: Better by GC–MS or LC–MS/MS? Mass Spectrometry Reviews 25, 838-865.

Alexandrou, N., Smith, M., Park, R., Lumb, K., and Brice, K. (2001) The Extraction of Polycyclic Aromatic Hydrocarbons from Atmospheric Particulate Matter Samples by Accelerated Solvent Extraction (ASE). International Journal of Environmental Analytical Chemistry 81, 257-280.

Alonso-Hernandez, C., Mesa-Albernas, M., and Tolosa, I. (2014) Organochlorine pesticides (OCPs) and polychlorinated biphenyls (PCBs) in sediments from the Gulf of Batabanó, Cuba. Chemosphere 94, 36-41.

Alonso-Hernández, C., Tolosa, I., Mesa-Albernas, M., Díaz-Asencio, M., Corcho-Alvarado, J., and Sánchez-Cabeza, J. (2015) Historical trends of organochlorine pesticides in a sediment core from the Gulf of Batabanó, Cuba. Chemosphere 137, 95-100.

Alonso-Hernández, C.M., Fanelli, E., Diaz-Asencio, M., Santamaría, J.M., and Morera-Gómez, Y. (2020) Carbon and nitrogen isotopes to distinguish sources of sedimentary organic matter in a Caribbean estuary. Isotopes in Environmental and Health Studies 56, 654-672.

Alonso-Hernández, C.M., Garcia-Moya, A., Tolosa, I., Diaz-Asencio, M., Corcho-Alvarado, J.A., Morera-Gomez, Y., and Fanelli, E. (2017) Tracing organic matter sources in a tropical lagoon of the Caribbean Sea. Continental shelf research 148, 53-63.

Andrási, N., Molnár, B., Dobos, B., Vasanits-Zsigrai, A., Záray, G., and Molnár-Perl, I. (2013) Determination of steroids in the dissolved and in the suspended phases of wastewater and Danube River samples by gas chromatography, tandem mass spectrometry. Talanta 115, 367-373.

Antizar-Ladislao, B. (2009) Polycyclic aromatic hydrocarbons, polychlorinated biphenyls, phthalates and organotins in northern Atlantic Spain's coastal marine sediments. Journal of Environmental Monitoring 11, 85-91.

Appleby, P.G. and Oldfieldz, F. (1983) The assessment of 210Pb data from sites with varying sediment accumulation rates. Hydrobiologia 103, 29-35.

Audry, S., Schäfer, J., Blanc, G., and Jouanneau, J.-M. (2004) Fifty-year sedimentary record of heavy metal pollution (Cd, Zn, Cu, Pb) in the Lot River reservoirs (France). Environmental Pollution 132, 413-426.

Baker, C.P. (2018) Cuba, 7th ed. Avalon Travel, Hachette Book Group, Berkeley, CA.

Baroudi, F., Al-Alam, J., Chimjarn, S., Delhomme, O., Fajloun, Z., and Millet, M. (2020) Conifers as environmental biomonitors: A multi-residue method for the concomitant quantification of pesticides, polycyclic aromatic hydrocarbons and polychlorinated biphenyls by LC-MS/MS and GC–MS/MS. Microchemical Journal 154, 104593.

Benfenati, E., Gini, G., Piclin, N., Roncaglioni, A. and Varì, M.R. (2003) Predicting logP of pesticides using different software. Chemosphere 53, 1155-1164.

Bianchi, T.S., Wysocki, L.A., Stewart, M., Filley, T.R., and McKee, B.A. (2007) Temporal variability in terrestrially-derived sources of particulate organic carbon in the lower Mississippi River and its upper tributaries. Geochimica et Cosmochimica Acta 71, 4425-4437.

Binford, M.W. (1990) Calculation and uncertainty analysis of 210Pb dates for PIRLA project lake sediment cores. Journal of Paleolimnology 3, 253-267.

Bolaños, P.P., Frenich, A.G., and Vidal, J.L.M. (2007) Application of gas chromatography-triple quadrupole mass spectrometry in the quantification-confirmation of pesticides and polychlorinated biphenyls in eggs at trace levels. Journal of Chromatography A 1167, 9-17.

Bravo-Linares, C., Ovando-Fuentealba, L., Mudge, S.M., Cerpa, J., and Loyola-Sepulveda, R. (2012) Source Allocation of Aliphatic and Polycyclic Aromatic Hydrocarbons in Particulate-Phase (PM10) in the City of Valdivia, Chile. Polycyclic Aromatic Compounds 32, 390-407.

Bray, E.E. and Evans, E.D. (1961) Distribution of n-paraffins as a clue to recognition of source beds. Geochimica et Cosmochimica Acta 22, 2-15.

Bronfman, A. (2010) History of Cuba. History of Antilles, vol 1. HAHR-Hisp. Am. Hist. Rev. 90, 701-702.

Brooks, G.R., Larson, R.A., Schwing, P.T., Romero, I., Moore, C., Reichart, G.-J., Jilbert, T., Chanton, J.P., Hastings, D.W., Overholt, W.A., Marks, K.P., Kostka, J.E., Holmes, C.W., and Hollander, D. (2015) Sedimentation Pulse in the NE Gulf of Mexico following the 2010 DWH Blowout. PLOS ONE 10, e0132341.

Burban, P.-Y., Lick, W., and Lick, J. (1989) The flocculation of fine-grained sediments in estuarine waters. Journal of Geophysical Research: Oceans 94, 8323-8330.

Burns, K.A. and Teal, J.M. (1979) The West Falmouth oil spill: Hydrocarbons in the salt marsh ecosystem. Estuarine and Coastal Marine Science 8, 349-360.

Camino-Sánchez, F., Zafra-Gómez, A., Ruiz-García, J., Bermúdez-Peinado, R., Ballesteros, O., Navalon, A., and Vílchez, J.L. (2011) UNE-EN ISO/IEC 17025: 2005 accredited method for the determination of 121 pesticide residues in fruits and vegetables by gas chromatography–tandem mass spectrometry. Journal of food Composition and Analysis 24, 427-440.

Canfield, D.E. (1994) Factors influencing organic carbon preservation in marine sediments. Chemical geology 114, 315-329.

Card, M.L., Gomez-Alvarez, V., Lee, W.-H., Lynch, D.G., Orentas, N.S., Lee, M.T., Wong, E.M., and Boethling, R.S. (2017) History of EPI Suite™ and future perspectives on chemical property estimation in US Toxic Substances Control Act new chemical risk assessments. Environmental Science: Processes & Impacts 19, 203-212.

Castellanos, L.P. and Alvarez, J. (1996) The transformation of the state extensive growth model in Cuba's sugarcane agriculture. Agriculture and Human Values 13, 59-68.

Chen, X., Bian, Z., Hou, H., Yang, F., Liu, S., Tang, G., and Hu, Q. (2013) Development and validation of a method for the determination of 159 pesticide residues in tobacco by gas chromatography–tandem mass spectrometry. Journal of agricultural and food chemistry 61, 5746-5757.

Chou, C.-C. and Liu, Y.-P. (2004) Determination of fecal sterols in the sediments of different wastewater outputs by GC-MS. International Journal of Environmental Analytical Chemistry 84, 379-388.

Coates, M., Connell, D.W., and Barron, D.M. (1985) Aqueous solubility and octan-1-ol-water partition coefficients of aliphatic hydrocarbons. Environmental science & technology 19, 628-632.

Coxon, T., Goldstein, L., and Odhiambo, B.K. (2019) Analysis of spatial distribution of trace metals, PCB, and PAH and their potential impact on human health in Virginian Counties and independent cities, USA. Environmental Geochemistry and Health 41, 783-801.

Craig, H. (1953) The geochemistry of the stable carbon isotopes. Geochimica et Cosmochimica Acta 3, 53-92.

Crawford, E., Crone, C., Horner, J., and Musselman, B. (2014) Food Packaging: Strategies for Rapid Phthalate Screening in Real Time by Ambient Ionization Tandem Mass Spectrometry, Chemistry of Food, Food Supplements, and Food Contact Materials: From Production to Plate. American Chemical Society, pp. 71-85.

Daly, K.L., Passow, U., Chanton, J., and Hollander, D. (2016) Assessing the impacts of oil-associated marine snow formation and sedimentation during and after the Deepwater Horizon oil spill. Anthropocene 13, 18-33.

Degens, E.T. (1969) Biogeochemistry of Stable Carbon Isotopes, in: Eglinton, G., Murphy, M.T.J. (Eds.), Organic Geochemistry: Methods and Results. Springer Berlin Heidelberg, Berlin, Heidelberg, pp. 304-329.

Díaz-Asencio, M., Alonso-Hernández, C., Bolanos-Álvarez, Y., Gómez-Batista, M., Pinto, V., Morabito, R., Hernández-Albernas, J., Eriksson, M., and Sanchez-Cabeza, J. (2009) One century sedimentary record of Hg and Pb pollution in the Sagua estuary (Cuba) derived from 210Pb and 137Cs chronology. Marine Pollution Bulletin 59, 108-115.

Díaz-Asencio, M., Alvarado, J.C., Alonso-Hernández, C., Quejido-Cabezas, A., Ruiz-Fernández, A., Sanchez-Sanchez, M., Gómez-Mancebo, M., Froidevaux, P., and Sanchez-Cabeza, J. (2011) Reconstruction of metal pollution and recent sedimentation processes in Havana Bay (Cuba): a tool for coastal ecosystem management. Journal of hazardous materials 196, 402-411.

Díaz-Asencio, M., Herguera, J.C., Schwing, P.T., Larson, R.A., Brooks, G.R., Southon, J., and Rafter, P. (2020) Sediment accumulation rates and vertical mixing of deep-sea sediments derived from14C and 210Pb in the southern Gulf of Mexico. Marine Geology 429, 106288.

Diercks, A.R., Romero, I.C., Larson, R.A., Schwing, P., Harris, A., Bosman, S., Chanton, J.P., and Brooks, G. (2021) Resuspension, Redistribution, and Deposition of Oil-Residues to Offshore Depocenters After the Deepwater Horizon Oil Spill. Frontiers in Marine Science 8.

Dierksmeier, G. (1996) Pesticide contamination in the Cuban agricultural environment. TrAC Trends in Analytical Chemistry 15, 154-159.

Dosal, P.J. (2006) Cuba libre: a brief history of Cuba. Harlan Davidson, Wheeling, Ill.

Dunnivant, F.M. and Elzerman, A.W. (1988) Aqueous solubility and Henry's law constant data for PCB congeners for evaluation of quantitative structure-property relationships (QSPRs). Chemosphere 17, 525-541.

El Nemr, A., El-Sadaawy, M.M., Khaled, A., and Draz, S.O. (2013) Aliphatic and polycyclic aromatic hydrocarbons in the surface sediments of the Mediterranean: assessment and source recognition of petroleum hydrocarbons. Environmental Monitoring and Assessment 185, 4571-4589.

Faroon, O.M., Keith, S., Jones, D., and De Rosa, C. (2001) Effects of polychlorinated biphenyls on development and reproduction. Toxicology and Industrial Health 17, 63-93.

Farrington, J.W. and Tripp, B.W. (1977) Hydrocarbons in western North Atlantic surface sediments. Geochimica et Cosmochimica Acta 41, 1627-1641.

Fernández-González, V., Muniategui-Lorenzo, S., López-Mahía, P., and Prada-Rodríguez, D. (2008) Development of a programmed temperature vaporization-gas chromatography–tandem mass spectrometry method for polycyclic aromatic hydrocarbons analysis in biota samples at ultratrace levels. Journal of Chromatography A 1207, 136-145.

Fernandez, A., Singh, A., and Jaffé, R. (2007) A literature review on trace metals and organic compounds of anthropogenic origin in the Wider Caribbean Region. Marine Pollution Bulletin 54, 1681-1691.

Frame, G.M., Cochran, J.W., and Bøwadt, S.S. (1996) Complete PCB congener distributions for 17 aroclor mixtures determined by 3 HRGC systems optimized for comprehensive, quantitative, congener-specific analysis. Journal of High Resolution Chromatography 19, 657-668.

Franco, M.A., Viñas, L., Soriano, J.A., de Armas, D., González, J.J., Beiras, R., Salas, N., Bayona, J.M., and Albaigés, J. (2006) Spatial distribution and ecotoxicity of petroleum hydrocarbons in sediments from the Galicia continental shelf (NW Spain) after the Prestige oil spill. Marine Pollution Bulletin 53, 260-271.

Franco, N.R., Giraldo, M.Á., López-Alvarez, D., Gallo-Franco, J.J., Dueñas, L.F., Puentes, V., and Castillo, A. (2021) Bacterial Composition and Diversity in Deep-Sea Sediments from the Southern Colombian Caribbean Sea. Diversity 13, 10.

Garrido Frenich, A., González-Rodríguez, M.J., Arrebola, F.J., and Martínez Vidal, J.L. (2005) Potentiality of Gas Chromatography−Triple Quadrupole Mass Spectrometry in Vanguard and Rearguard Methods of Pesticide Residues in Vegetables. Analytical Chemistry 77, 4640-4648.

Giri, A., Coutriade, M., Racaud, A., Okuda, K., Dane, J., Cody, R.B., and Focant, J.-F. (2017) Molecular Characterization of Volatiles and Petrochemical Base Oils by Photo-Ionization GC×GC-TOF-MS. Analytical Chemistry 89, 5395-5403.

Gleijeses, P. (2002) Conflicting Missions: Havana, Washington, and Africa, 1959-1976. Univ of North Carolina Press.

Gliessman, S.R. (1985) Multiple cropping systems: A basis for developing an alternative agriculture, US Congress Off ice of Technology Assessment. Innovative biological technologies for lesser developed countries: workshop proceedings. Congress of the USA. Washington, DC, USA, pp. 67-83.

Gómez-Gutiérrez, A., Garnacho, E., Bayona, J.M., and Albaigés, J. (2007) Screening ecological risk assessment of persistent organic pollutants in Mediterranean sea sediments. Environment International 33, 867-876.

Gorsuch, A.E. (2015) "Cuba, My Love": The Romance of Revolutionary Cuba in the Soviet Sixties. Am. Hist. Rev. 120, 497-526.

Gott, R. (2005) Cuba: a new history. Yale Nota Bene, Yale University Press, New Haven; London.

Guo, J., Wu, F., Luo, X., Liang, Z., Liao, H., Zhang, R., Li, W., Zhao, X., Chen, S., and Mai, B. (2010) Anthropogenic input of polycyclic aromatic hydrocarbons into five lakes in Western China. Environmental Pollution 158, 2175-2180.

Halek, F., Nabi, G., and Kavousi, A. (2008) Polycyclic aromatic hydrocarbons study and toxic equivalency factor (TEFs) in Tehran, IRAN. Environmental Monitoring and Assessment 143, 303-311.

Hansch, C., Leo, A., and Hoekman, D. (1995) Exploring QSAR: Hydrophobic, electronic, and steric constants, in: Hansch, C., Leo, A., Hoekman, D.H. (Eds.), ACS Professional Reference Book. American Chemical Society, Washington, DC.

Harrad, S.J., Sewart, A.P., Alcock, R., Boumphrey, R., Burnett, V., Duarte-Davidson, R., Halsall, C., Sanders, G., Waterhouse, K., Wild, S.R., and Jones, K.C. (1994) Polychlorinated biphenyls (PCBs) in the British environment: Sinks, sources and temporal trends. Environmental Pollution 85, 131-146.

He, W., Chen, Y., Yang, C., Liu, W., Kong, X., Qin, N., He, Q., and Xu, F. (2017) Optimized Multiresidue Analysis of Organic Contaminants of Priority Concern in a Daily Consumed Fish (Grass Carp). Journal of Analytical Methods in Chemistry 2017, 9294024.

Heemken, O.P., Theobald, N., and Wenclawiak, B.W. (1997) Comparison of ASE and SFE with Soxhlet, Sonication, and Methanolic Saponification Extractions for the Determination of Organic Micropollutants in Marine Particulate Matter. Analytical Chemistry 69, 2171-2180.

Heim, S. and Schwarzbauer, J. (2013) Pollution history revealed by sedimentary records: a review. Environmental Chemistry Letters 11, 255-270.

Herrera-Herrera, A.V., Leierer, L., Jambrina-Enríquez, M., Connolly, R., and Mallol, C. (2020) Evaluating different methods for calculating the Carbon Preference Index (CPI): Implications for palaeoecological and archaeological research. Organic Geochemistry 146, 104056.

Hilal, S.H., Karickhoff, S.W., and Carreira, L.A. (2003) Prediction of the Vapor Pressure Boiling Point, Heat of Vaporization and Diffusion Coefficient of Organic Compounds. QSAR & Combinatorial Science 22, 565-574.

Honda, M. and Suzuki, N. (2020) Toxicities of Polycyclic Aromatic Hydrocarbons for Aquatic Animals. International Journal of Environmental Research and Public Health 17, 1363.

Ingall, E.D. and Van Cappellen, P. (1990) Relation between sedimentation rate and burial of organic phosphorus and organic carbon in marine sediments. Geochimica et Cosmochimica Acta 54, 373-386.

Ishikawa, M., Ogawa, N.O., Ohkouchi, N., Husana, D.E.M., and Kase, T. (2017) Stable carbon isotope compositions of foot tissue, conchiolin opercula, and organic matrix within the shells of two marine gastropods from a seagrass meadow in the Philippines. Geochemical journal 51, 241-250.

Jacquot, F., Doumenq, P., Guiliano, M., Munoz, D., Guichard, J.R., and Mille, G. (1996) Biodegradation of the (aliphatic + aromatic) fraction of Oural crude oil. Biomarker identification using GC/MS SIM and GC/MS/MS. Talanta 43, 319-330.

Jafarabadi, A.R., Bakhtiari, A.R., Aliabadian, M., and Toosi, A.S. (2017) Spatial distribution and composition of aliphatic hydrocarbons, polycyclic aromatic hydrocarbons and hopanes in superficial sediments of the coral reefs of the Persian Gulf, Iran. Environmental Pollution 224, 195-223.

Jensen, T. (1994) Petroleum hydrocarbons: Compositional changes during biodegradation and transport in unsaturated soil. PhD thesis. National Environmental Research Institute, Roskilde, Denmark.

John, G.F., Yin, F., Mulabagal, V., Hayworth, J.S., and Clement, T.P. (2014) Development and application of an analytical method using gas chromatography/triple quadrupole mass spectrometry for characterizing alkylated chrysenes in crude oil samples. Rapid Communications in Mass Spectrometry 28, 948-956.

Jones, K.C. and De Voogt, P. (1999) Persistent organic pollutants (POPs): state of the science. Environmental pollution 100, 209-221.

Kalachova, K., Pulkrabova, J., Cajka, T., Drabova, L., Stupak, M., and Hajslova, J. (2013) Gas chromatography–triple quadrupole tandem mass spectrometry: a powerful tool for the (ultra)trace analysis of multiclass environmental contaminants in fish and fish feed. Analytical and Bioanalytical Chemistry 405, 7803-7815.

Kennedy, H., Gacia, E., Kennedy, D.P., Papadimitriou, S., and Duarte, C.M. (2004) Organic carbon sources to SE Asian coastal sediments. Estuarine, Coastal and Shelf Science 60, 59-68.

Kinross, A.D., Hageman, K.J., Doucette, W.J., and Foster, A.L. (2020) Comparison of Accelerated Solvent Extraction (ASE) and Energized Dispersive Guided Extraction (EDGE) for the analysis of pesticides in leaves. Journal of Chromatography A 1627, 461414.

Klotz, W.L., Schure, M.R., and Foley, J.P. (2001) Determination of octanol–water partition coefficients of pesticides by microemulsion electrokinetic chromatography. Journal of Chromatography A 930, 145-154.

Kochman, M., Gordin, A., Goldshlag, P., Lehotay, S.J., and Amirav, A. (2002) Fast, high-sensitivity, multipesticide analysis of complex mixtures with supersonic gas chromatography–mass spectrometry. Journal of Chromatography A 974, 185-212.

Koesukwiwat, U., Lehotay, S.J., and Leepipatpiboon, N. (2011) Fast, low-pressure gas chromatography triple quadrupole tandem mass spectrometry for analysis of 150 pesticide residues in fruits and vegetables. Journal of Chromatography A 1218, 7039-7050.

LaGrega, M., Buckingham, P., and Evans, J. (2001) Hazard waste management, 2nd edn. McGraw-Hall. Inc., New York.

Larson, R.A., Brooks, G.R., Schwing, P.T., Holmes, C.W., Carter, S.R., and Hollander, D.J. (2018) High-resolution investigation of event driven sedimentation: Northeastern Gulf of Mexico. Anthropocene 24, 40-50.

Laušević, M., Splendore, M., and March, R.E. (1996) Modulated Resonant Excitation of Selected Polychlorobiphenyl Molecular Ions in an Ion Trap Mass Spectrometer. Journal of Mass Spectrometry 31, 1244-1252.

Lee, J.E., Oh, H.B., Im, H., Han, S.B., and Kim, K.H. (2020) Multiresidue analysis of 85 persistent organic pollutants in small human serum samples by modified QuEChERS preparation with different ionization sources in mass spectrometry. Journal of Chromatography A 1623, 461170.

Lee, K.E., Schoenfuss, H.L., Jahns, N.D., Brown, G.K., and Barber, L.B. (2008) Alkylphenols, other endocrine-active chemicals, and fish responses in three streams in Minnesota-Study design and data, February-September 2007. Data Series 405, 44.

Lehotay, S.J., Son, K.A., Kwon, H., Koesukwiwat, U., Fu, W., Mastovska, K., Hoh, E., and Leepipatpiboon, N. (2010) Comparison of QuEChERS sample preparation methods for the analysis of pesticide residues in fruits and vegetables. Journal of Chromatography A 1217, 2548-2560.

Leo, A., Hansch, C., and Elkins, D. (1971) Partition coefficients and their uses. Chemical reviews 71, 525-616.

Lohmann, R., Breivik, K., Dachs, J., and Muir, D. (2007) Global fate of POPs: current and future research directions. Environmental pollution 150, 150-165.

Long, E.R., Macdonald, D.D., Smith, S.L., and Calder, F.D. (1995) Incidence of adverse biological effects within ranges of chemical concentrations in marine and estuarine sediments. Environmental management 19, 81-97.

Lundstedt, S., White, P.A., Lemieux, C.L., Lynes, K.D., Lambert, I.B., Öberg, L., Haglund, P., and Tysklind, M. (2007) Sources, fate, and toxic hazards of oxygenated polycyclic aromatic hydrocarbons (PAHs) at PAH-contaminated sites. AMBIO: A Journal of the Human Environment 36, 475-485.

MacDonald, I.R., Leifer, I., Sassen, R., Stine, P., Mitchell, R., and Guinasso Jr, N. (2002) Transfer of hydrocarbons from natural seeps to the water column and atmosphere. Geofluids 2, 95-107.

Marchand, C., Lallier-Vergès, E., Disnar, J.R., and Kéravis, D. (2008) Organic carbon sources and transformations in mangrove sediments: A Rock-Eval pyrolysis approach. Organic Geochemistry 39, 408-421.

Martins, C.C., Castellanos-Iglesias, S., Cabral, A.C., de Souza, A.C., Ferraz, M.A., and Alves, T.P. (2018) Hydrocarbon and sewage contamination near fringing reefs along the west coast of Havana, Cuba: A multiple sedimentary molecular marker approach. Marine pollution bulletin 136, 38-49.

McNutt, M.K., Camilli, R., Crone, T.J., Guthrie, G.D., Hsieh, P.A., Ryerson, T.B., Savas, O., and Shaffer, F. (2012) Review of flow rate estimates of the Deepwater Horizon oil spill. Proceedings of the National Academy of Sciences 109, 20260-20267.

Meylan, W.M. and Howard, P.H. (1995) Atom/fragment contribution method for estimating octanol–water partition coefficients. Journal of pharmaceutical sciences 84, 83-92.

Miller, M.M., Wasik, S.P., Huang, G.L., Shiu, W.Y. and Mackay, D. (1985) Relationships between octanol-water partition coefficient and aqueous solubility. Environmental science & technology 19, 522-529.

Mitra, S. and Bianchi, T.S. (2003) A preliminary assessment of polycyclic aromatic hydrocarbon distributions in the lower Mississippi River and Gulf of Mexico. Marine Chemistry 82, 273-288.

Moncreiff, C.A. and Sullivan, M.J. (2001) Trophic importance of epiphytic algae in subtropical seagrass beds: evidence from multiple stable isotope analyses. Marine ecology. Progress series (Halstenbek) 215, 93-106.

Niemi, G.J., Basak, S.C., Grunwald, G., and Veith, G.D. (1992) Prediction of octanol/water partition coefficient (KOW) with algorithmically derived variables. Environ. Toxicol. Chem. 11, 893-900.

Nikolaou, A., Kostopoulou, M., Petsas, A., Vagi, M., Lofrano, G., and Meric, S. (2009) Levels and toxicity of polycyclic aromatic hydrocarbons in marine sediments. TrAC Trends in Analytical Chemistry 28, 653-664.

Nowell, L.H. (2019) Pesticides in stream sediment and aquatic biota: distribution, trends, and governing factors. CRC Press.

Nowell, L.H., Norman, J.E., Moran, P.W., Martin, J.D., and Stone, W.W. (2014) Pesticide Toxicity Index—A tool for assessing potential toxicity of pesticide mixtures to freshwater aquatic organisms. Science of The Total Environment 476-477, 144-157.

Oberdörster, E., Cottam, D.M., Wilmot, F.A., Milner, M.J., and McLachlan, J.A. (1999) Interaction of PAHs and PCBs with ecdysone-dependent gene expression and cell proliferation. Toxicology and applied pharmacology 160, 101-108.

Oppenheim, S. (2001) Alternative agriculture in Cuba. American Entomologist 47, 216-227.

Overholt, W.A., Marks, K.P., Romero, I.C., Hollander, D.J., Snell, T.W., and Kostka, J.E. (2016) Hydrocarbon-degrading bacteria exhibit a species-specific response to dispersed oil while moderating ecotoxicity. Applied and Environmental Microbiology 82, 518-527.

Page, D.S., Boehm, P.D., Stubblefield, W.A., Parker, K.R., Gilfillan, E.S., Neff, J.M., and Maki, A.W. (2002) Hydrocarbon composition and toxicity of sediments following the Exxon valdez oil spill in Prince William Sound, Alaska, USA. Environ. Toxicol. Chem. 21, 1438-1450.

Pardo, G. (1975) Geology of Cuba, in: Nairn, A.E.M., Stehli, F.G. (Eds.), The Gulf of Mexico and the Caribbean. Springer US, Boston, MA, pp. 553-615.

Paschke, A., Neitzel, P.L., Walther, W., and Schüürmann, G. (2004) Octanol/Water Partition Coefficient of Selected Herbicides: Determination Using Shake-Flask Method and Reversed-Phase High-Performance Liquid Chromatography. Journal of Chemical & Engineering Data 49, 1639-1642.

Patil, G.S. (1994) Prediction of aqueous solubility and octanol—water partition coefficient for pesticides based on their molecular structure. Journal of Hazardous Materials 36, 34-43.

Pérez-Carrera, E., León, V.M.L., Parra, A.G., and González-Mazo, E. (2007) Simultaneous determination of pesticides, polycyclic aromatic hydrocarbons and polychlorinated biphenyls in seawater and interstitial marine water samples, using stir bar sorptive extraction–thermal desorption–gas chromatography–mass spectrometry. Journal of Chromatography A 1170, 82-90.

Pérez, L.A. (1983) Cuba between empires, 1878-1902. University of Pittsburgh Press.

Peterson, B.J. and Fry, B. (1987) Stable Isotopes in Ecosystem Studies. Annual Review of Ecology and Systematics 18, 293-320.

Powell, C.L. (2004) Commission for Assistance to a Free Cuba, Report to the President (May 2004), pp. 359-423.

Pruell, R.J. and Quinn, J.G. (1985) Geochemistry of organic contaminants in Narragansett Bay sediments. Estuarine, Coastal and Shelf Science 21, 295-312.

Ramdahl, T. (1983) Retene—a molecular marker of wood combustion in ambient air. Nature 306, 580-582.

Reddy, C.M., Eglinton, T.I., Palić, R., Benitez-Nelson, B.C., Stojanović, G., Palić, I., Djordjević, S., and Eglinton, G. (2000) Even carbon number predominance of plant wax n-alkanes: a correction. Organic Geochemistry 31, 331-336.

Reitsma, P.J., Adelman, D., and Lohmann, R. (2013) Challenges of Using Polyethylene Passive Samplers to Determine Dissolved Concentrations of Parent and Alkylated PAHs under Cold and Saline Conditions. Environmental Science & Technology 47, 10429-10437.

Resmi, P., Manju, M.N., Gireeshkumar, T.R., Ratheesh Kumar, C.S., and Chandramohanakumar, N. (2016) Source characterisation of Sedimentary organic matter in mangrove ecosystems of northern Kerala, India: Inferences from bulk characterisation and hydrocarbon biomarkers. Regional Studies in Marine Science 7, 43-54.

Richardson, S. (1998) Encyclopedia of environmental analysis and remediation. Hoboken, New Jersey: John Wiley & Sons, 1398.

Romero, I.C. (2018) A high-throughput method (ASE-GC/MS/MS/MRM) for quantification of multiple hydrocarbon compounds in marine environmental samples. Marine Technology Society Journal 52, 66-70.

Romero, I.C., Chanton, J.P., Brooks, G.R., Bosman, S., Larson, R.A., Harris, A., Schwing, P., and Diercks, A. (2021) Molecular Markers of Biogenic and Oil-Derived Hydrocarbons in Deep-Sea Sediments Following the Deepwater Horizon Spill. Frontiers in Marine Science 8.

Romero, I.C., Judkins, H., and Vecchione, M. (2020) Temporal Variability of Polycyclic Aromatic Hydrocarbons in Deep-Sea Cephalopods of the Northern Gulf of Mexico. Frontiers in Marine Science 7.

Romero, I.C., Özgökmen, T., Snyder, S., Schwing, P., O'Malley, B.J., Beron-Vera, F.J., Olascoaga, M.J., Zhu, P., Ryan, E., and Chen, S.S. (2016) Tracking the Hercules 265 marine gas well blowout in the Gulf of Mexico. Journal of Geophysical Research: Oceans 121, 706-724.

Romero, I.C., Schwing, P.T., Brooks, G.R., Larson, R.A., Hastings, D.W., Ellis, G., Goddard, E.A., and Hollander, D.J. (2015) Hydrocarbons in deep-sea sediments following the 2010 Deepwater Horizon blowout in the northeast Gulf of Mexico. PLoS One 10, e0128371.

Romero, I.C., Sutton, T., Carr, B., Quintana-Rizzo, E., Ross, S.W., Hollander, D.J., and Torres, J.J. (2018) Decadal Assessment of Polycyclic Aromatic Hydrocarbons in Mesopelagic Fishes from the Gulf of Mexico Reveals Exposure to Oil-Derived Sources. Environmental Science & Technology 52, 10985-10996.

Romero, I.C., Toro-Farmer, G., Diercks, A.-R., Schwing, P., Muller-Karger, F., Murawski, S., and Hollander, D.J. (2017) Large-scale deposition of weathered oil in the Gulf of Mexico following a deep-water oil spill. Environmental Pollution 228, 179-189.

Roulet, M., Lucotte, M., Canuel, R., Farella, N., Courcelles, M., Guimaraes, J.-R., Mergler, D., and Amorim, M. (2000) Increase in mercury contamination recorded in lacustrine sediments following deforestation in the central Amazon. Chemical Geology 165, 243-266.

Ruddy, B.A., Qadah, D.T., Aldstadt, J.H., and Bootsma, H.A. (2008) Improving analytical confidence in the determination of PCBs in complex matrices by a sequential GC-MS/MS approach. International Journal of Environmental Analytical Chemistry 88, 337-351.

Safe, S., and Hutzinger, O. (1984) Polychlorinated Biphenyls (PCBs) and Polybrominated Biphenyls (PBBs): Biochemistry, Toxicology, and Mechanism of Action. CRC Critical Reviews in Toxicology 13, 319-395.

Safe, S.H. (1994) Polychlorinated Biphenyls (PCBs): Environmental Impact, Biochemical and Toxic Responses, and Implications for Risk Assessment. Critical Reviews in Toxicology 24, 87-149.

Sanders, M., Sivertsen, S., and Scott, G. (2002) Origin and Distribution of Polycyclic Aromatic Hydrocarbons in Surficial Sediments from the Savannah River. Archives of Environmental Contamination and Toxicology 43, 0438-0448.

Sangster, J. (1989) Octanol-water partition coefficients of simple organic compounds. Journal of Physical and Chemical Reference Data 18, 1111-1229.

Sangster, J. (1997) Octanol-water partition coefficients: fundamentals and physical chemistry. John Wiley & Sons.

Saravanabhavan, G., Helleur, R., and Hellou, J. (2009) GC–MS/MS measurement of natural and synthetic estrogens in receiving waters and mussels close to a raw sewage ocean outfall. Chemosphere 76, 1156-1162.

Schwing, P.T., Brooks, G.R., Larson, R.A., Holmes, C.W., O'Malley, B.J., and Hollander, D.J. (2017) Constraining the Spatial Extent of Marine Oil Snow Sedimentation and Flocculent Accumulation Following the Deepwater Horizon Event Using an Excess 210Pb Flux Approach. Environmental Science & Technology 51, 5962-5968.

Schwing, P.T., Romero, I.C., Brooks, G.R., Hastings, D.W., Larson, R.A., and Hollander, D.J. (2015) A decline in benthic foraminifera following the Deepwater Horizon event in the northeastern Gulf of Mexico. PLoS One 10.

Schwing, P.T., Romero, I.C., Larson, R.A., O'Malley, B.J., Fridrik, E.E., Goddard, E.A., Brooks, G.R., Hastings, D.W., Rosenheim, B.E., and Hollander, D.J. (2016) Sediment core extrusion method at millimeter resolution using a calibrated, threaded-rod. JoVE (Journal of Visualized Experiments), e54363.

Sharp, Z. (2017) Principles of Stable Isotope Geochemistry, 2nd Edition ed.

Smith, A., Campbell, J., Keys, D., and Fisher, J. (2005) Rat tissue and blood partition coefficients for n-alkanes (C8 to C12). International journal of toxicology 24, 35-41.

Sørensen, L., Meier, S., and Mjøs, S.A. (2016) Application of gas chromatography/tandem mass spectrometry to determine a wide range of petrogenic alkylated polycyclic aromatic hydrocarbons in biotic samples. Rapid Communications in Mass Spectrometry 30, 2052-2058.

Sosa, D., Hilber, I., Faure, R., Bartolomé, N., Fonseca, O., Keller, A., Bucheli, T.D., and Escobar, A. (2019) Polycyclic aromatic hydrocarbons and polychlorinated biphenyls in urban and semi-urban soils of Havana, Cuba. Journal of Soils and Sediments 19, 1328-1341.

Staten, C.L. (2005) The history of Cuba. Palgrave Macmillan, New York,NY.

Stevens, D., Shi, Q., and Hsu, C.S. (2013) Novel Analytical Technique for Petroleum Biomarker Analysis. Energy & Fuels 27, 167-171.

Stout, S.A., Payne, J.R., Ricker, R.W., Baker, G., and Lewis, C. (2016) Macondo oil in deep-sea sediments: Part 2 — Distribution and distinction from background and natural oil seeps. Marine Pollution Bulletin 111, 381-401.

Su, M.-C., Christensen, E.R., and Karls, J.F. (1998) Determination of PAH sources in dated sediments from Green Bay, Wisconsin, by a chemical mass balance model. Environmental Pollution 99, 411-419.

Suárez, J.A., Beatón, P.A., Escalona, R.F., and Montero, O.P. (2012) Energy, environment and development in Cuba. Renewable and Sustainable Energy Reviews 16, 2724-2731.

Subedi, B., Mottaleb, M.A., Chambliss, C.K., and Usenko, S. (2011) Simultaneous analysis of select pharmaceuticals and personal care products in fish tissue using pressurized liquid extraction combined with silica gel cleanup. Journal of Chromatography A 1218, 6278-6284.

Summers, E.M. (1955) Pesticides in Sugar Cane, Pesticides in Tropical Agricultures. American Chemical Society, pp. 14-17.

Sun, S., Shi, W., Tang, Y., Han, Y., Du, X., Zhou, W., Zhang, W., Sun, C., and Liu, G. (2021) The toxic impacts of microplastics (MPs) and polycyclic aromatic hydrocarbons (PAHs) on haematic parameters in a marine bivalve species and their potential mechanisms of action. Science of The Total Environment 783, 147003.

Tolosa, I., Mesa-Albernas, M., and Alonso-Hernandez, C. (2009) Inputs and sources of hydrocarbons in sediments from Cienfuegos bay, Cuba. Marine Pollution Bulletin 58, 1624-1634.

Tolosa, I., Mesa-Albernas, M., and Alonso-Hernandez, C. (2010) Organochlorine contamination (PCBs, DDTs, HCB, HCHs) in sediments from Cienfuegos bay, Cuba. Marine Pollution Bulletin 60, 1619-1624.

Tolosa, I., Mesa, M., and Alonso-Hernandez, C. (2014) Steroid markers to assess sewage and other sources of organic contaminants in surface sediments of Cienfuegos Bay, Cuba. Marine pollution bulletin 86, 84-90.

Tomlin, C.D. (2009) The pesticide manual: A world compendium. British Crop Production Council.

Tsochatzis, E.D., Nebel, C., Danielsen, M., Sundekilde, U.K., and Kastrup Dalsgaard, T. (2021) Thermal degradation of metabolites in urine using multiple isotope-labelled internal standards for off-line GC metabolomics - effects of injector and oven temperatures. Journal of Chromatography B 1181, 122902.

Van den Berg, M., Birnbaum, L.S., Denison, M., De Vito, M., Farland, W., Feeley, M., Fiedler, H., Hakansson, H., Hanberg, A., Haws, L., Rose, M., Safe, S., Schrenk, D., Tohyama, C., Tritscher, A., Tuomisto, J., Tysklind, M., Walker, N., and Peterson, R.E. (2006) The 2005 World Health Organization Reevaluation of Human and Mammalian Toxic Equivalency Factors for Dioxins and Dioxin-Like Compounds. Toxicological Sciences 93, 223-241.

Venkatesan, M.I. (1988) Occurrence and possible sources of perylene in marine sediments-a review. Marine Chemistry 25, 1-27.

Volkman, J.K., Holdsworth, D.G., Neill, G.P., and Bavor Jr, H. (1992) Identification of natural, anthropogenic and petroleum hydrocarbons in aquatic sediments. Science of the Total Environment 112, 203-219.

Wang, G., Ma, P., Zhang, Q., Lewis, J., Lacey, M., Furukawa, Y., O'Reilly, S.E., Meaux, S., McLachlan, J., and Zhang, S. (2012) Endocrine disrupting chemicals in New Orleans surface waters and Mississippi Sound sediments. Journal of Environmental Monitoring 14, 1353-1364.

Wang, Z., Fingas, M., and Page, D.S. (1999) Oil spill identification. Journal of Chromatography A 843, 369-411.

Wang, Z.D., Stout, S.A., and Fingas, M. (2006) Forensic fingerprinting of biomarkers for oil spill characterization and source identification. Environ. Forensics 7, 105-146.

Williams, A.J., Grulke, C.M., Edwards, J., McEachran, A.D., Mansouri, K., Baker, N.C., Patlewicz, G., Shah, I., Wambaugh, J.F., and Judson, R.S. (2017) The CompTox Chemistry Dashboard: a community data resource for environmental chemistry. Journal of cheminformatics 9, 1-27.

Wise, S.A., Rodgers, R.P., Reddy, C.M., Nelson, R.K., Kujawinski, E.B., Wade, T.L., Campiglia, A.D., and Liu, Z. (2022) Advances in Chemical Analysis of Oil Spills Since the Deepwater Horizon Disaster. Critical Reviews in Analytical Chemistry, 1-60.

Withheld, N. (2008) Health consequences of Cuba's Special Period. Can. Med. Assoc. J. 179, 257-257.

Wolfe, N., Zepp, R., Schlotzhauer, P., and Sink, M. (1982) Transformation pathways of hexachlorocyclopentadiene in the aquatic environment. Chemosphere 11, 91-101.

Wong, J.W., Zhang, K., Tech, K., Hayward, D.G., Krynitsky, A.J., Cassias, I., Schenck, F.J., Banerjee, K., Dasgupta, S., and Brown, D. (2010) Multiresidue Pesticide Analysis of Ginseng Powders Using Acetonitrile- or Acetone-Based Extraction, Solid-Phase Extraction Cleanup, and Gas Chromatography−Mass Spectrometry/Selective Ion Monitoring (GC-MS/SIM) or −Tandem Mass Spectrometry (GC-MS/MS). Journal of Agricultural and Food Chemistry 58, 5884-5896.

Xing, L., Zhang, H., Yuan, Z., Sun, Y., and Zhao, M. (2011) Terrestrial and marine biomarker estimates of organic matter sources and distributions in surface sediments from the East China Sea shelf. Continental Shelf Research 31, 1106-1115.

Yan, Y., Zhao, B., Xie, L., and Zhu, Z. (2021) Trend reversal of soil n-alkane Carbon Preference Index (CPI) along the precipitation gradient and its paleoclimatic implication. Chemical Geology 581, 120402.

Yang, C., Wang, Z., Liu, Y., Yang, Z., Li, Y., Shah, K., Zhang, G., Landriault, M., Hollebone, B., and Brown, C. (2013) Aromatic steroids in crude oils and petroleum products and their applications in forensic oil spill identification. Environ. Forensics 14, 278-293.

Zamora, H.A., Nelson, S.M., Flessa, K.W., and Nomura, R. (2013) Post-dam sediment dynamics and processes in the Colorado River estuary: Implications for habitat restoration. Ecological engineering 59, 134-143.

Zhang, P., Song, J., Fang, J., Liu, Z., Li, X., and Yuan, H. (2009) One century record of contamination by polycyclic aromatic hydrocarbons and polychlorinated biphenyls in core sediments from the southern Yellow Sea. Journal of Environmental Sciences 21, 1080-1088.

Zhao, Z., Zhang, L., Wu, J., Fan, C., and Shang, J. (2010) Assessment of the potential mutagenicity of organochlorine pesticides (OCPs) in contaminated sediments from Taihu Lake, China. Mutation Research/Genetic Toxicology and Environmental Mutagenesis 696, 62-68.

APPENDIX A:

PHYSICAL PARAMETERS TABLES

Table A1: Properties for analyzed aliphatics, fecal sterols, and phthalates. MW: molecular weight (g/mol), Log K_{ow}: octanol-water partitioning coefficient.

Group	Abbreviation	Compound	CAS Number	MW	Formula	Log K_{OW}	References
Aliphatics	nC10	Decane	124-18-5	142	C10H22	5.01	1,2,4
	nC11	Undecane	1120-21-4	156	C11H24	5.74	2,4,5,6
	nC12	Dodecane	112-40-3	170	C12H26	6.10	1,2,4
	nC13	Tridecane	629-50-5	184	C13H28	6.37	2,4,5,6
	nC14	Tetradecane	629-59-4	198	C14H30	7.20	1,2,4
	nC15	Pentadecane	629-62-9	212	C15H32	7.71	2,4,5,6
	nC16	Hexadecane	544-76-3	226	C16H34	8.20	2,4,5,6
	nC17	Heptadecane	629-78-7	240	C17H36	8.69	2,4,5,6
	nC18	Octadecane	593-45-3	255	C18H38	9.18	3,4,5,6
	nC19	Nonadecane	629-92-5	269	C19H40	9.67	4,5,6
	nC20	Eicosane	112-95-8	283	C20H42	10.16	4,5,6
	nC21	Heneicosane	629-94-7	297	C21H44	10.65	4,5,6
	nC22	Docosane	629-97-0	311	C22H46	11.15	4,5,6
	nC23	Tricosane	638-67-5	325	C23H48	11.64	4,5,6
	nC24	Tetracosane	646-31-1	339	C24H50	12.13	4,5,6
	nC25	Pentacosane	629-99-2	353	C25H52	12.62	4,5,6
	nC26	Hexacosane	630-01-3	367	C26H54	13.11	5,6
	nC27	Heptacosane	593-49-7	381	C27H56	13.60	5,6
	nC28	Octacosane	630-02-4	395	C28H58	14.10	5,6
	nC29	Nonacosane	630-03-5	409	C29H60	14.60	5,6
	nC30	Triacontane	638-68-6	423	C30H62	15.07	5,6
	nC31	Hentriacontane	630-04-6	437	C31H64	15.57	5,6
	nC32	Dotriacontane	544-85-4	451	C32H66	16.06	5,6
	nC33	Tritriacontane	630-05-7	465	C33H68	16.55	5,6
	nC34	Tetratriacontane	14167-59-0	479	C34H70	17.04	5,6
	nC35	Pentatriacontane	630-07-9	493	C35H72	17.53	5,6
	nC36	Hexatriacontane	630-06-8	507	C36H74	18.02	5,6
	nC37	Heptatriacontane	7194-84-5	521	C37H76	18.51	5,6
	Pr	Pristane	1921-70-6	269	C19H40	9.38	5,6
	Phy	Phytane	638-36-8	283	C20H42	9.87	5,6
Fecal Sterols	CP/epi-CP	5β-cholestan-3β-ol, coprostanol/ 5β-cholestan-3α-ol, epi-coprostanol	360-68-9/ 516-92-7	388/ 388	C27H48O/ C27H48O	8.82/ 8.82	6,7,8,9,11 6,7,9,11
	CSA	5α-cholestan-3β-ol, cholestanol	80-97-7	388	C27H48O	8.82	6,7,10,11
	CSE	5-cholesten-3β-ol, cholesterol	57-88-5	386	C27H46O	8.74	6,7,8,11
Phthalates	DMP	Dimethyl phthalate	131-11-3	194	C10H10O4	1.60	12
	DEP	Diethyl phthalate	84-66-2	222	C12H14O4	2.42	12
	DBP	Di-n-butyl phthalate	84-74-2	278	C16H22O4	4.50	12
	BBP	Benzyl butyl phthalate	85-68-7	312	C19H20O4	4.73	12
	DEHP	Bis (2-ethylhexyl) phthalate	117-81-7	391	C24H38O4	7.27	12
	DnOP	Di-n-octyl phthalate	117-84-0	391	C24H38O4	8.10	12

1: Sangster 1989, 2: Smith et.al. 2005, 3: Jensen 1994, 4: Coates et. al. 1985, 5: Card et.al. 2017, 6: Meylan and Howard 1995, 7: Sangster 1997, 8: Lee et. al.2008, 9: Leo et.al. 1971, 10: Richardson 1998, 11: Chou and Liu 2004, 12: Williams et. al. 2017

Table A2: Properties for analyzed hopanes, steranes, and tri-aromatic steroids. MW: molecular weight (g/mol), Log K_{ow}: octanol-water partitioning coefficient.

Group	Abbreviation	Compound	CAS Number	MW	Formula	Log K_{OW}	References
Hopanes, Steranes, and Triaromatic Steroids	Tm	Trisnorhopane-17a	53584-59-1	371	C27H46	11.96	1
	Ts	Trisnorhopane-18a	55199-72-9	371	C27H46	11.96	1
	BNH	Bisnorhopane	65636-26-2	385	C28H48	8.5	1
	NH/NNH	Norneohopane/ Norhopane	53584-60-4/ 119613-71-7	398/ 398	C29H50/ C29H50	8.80/ n/a	1
	NM	Normoretane	3258-87-5	398	C29H50	12.98	1
	H	Hopane	13849-96-2	412	C30H52	13.33	1
	M	Moretane	1176-44-9	412	C30H52	13.33	1
	HH-S	22S-homohopane	60305-23-9	426	C31H54	9.5	1
	HH-R	22R-homohopane	60305-23-9	426	C31H54	9.5	1
	HM	Homomoretane	n/a	426	C31H54	n/a	
	BHH-S	22S-bishomohopane	67069-15-2	440	C32H56	n/a	
	BHH-R	22R-bishomohopane	67069-15-2	440	C32H56	n/a	
	THH-S	22S-trishomohopane	67069-16-3	454	C33H58	n/a	
	THH-R	22R-trishomohopane	67069-16-3	454	C33H58	n/a	
	TkHH-S	22S-tetrakishhomohopane	79897-70-4	468	C34H60	10.7	1
	TkHH-R	22R-tetrakishhomohopane	79897-70-4	468	C34H60	10.7	1
	PHH-S	22S-pentakishhomohopane	54370-82-0	482	C35H62	11.1	1
	PHH-R	22R-pentakishhomohopane	54370-82-0	482	C35H62	11.1	1
	DiaC27βα S	S-C27βα-diasterane	56975-84-9	372	C27H48	n/a	
	DiaC27βα R	R-C27βα-diasterane	56975-84-9	372	C27H48	n/a	
	C27ααα S	a,a,a 20S-cholestane	n/a	372	C27H48	n/a	
	C27ααα R	a,a,a 20R-cholestane	n/a	372	C27H48	n/a	
	C27αββ S	a,b,b 20S-cholestane	n/a	372	C27H48	n/a	
	C27αββ R	a,b,b 20R-cholestane	n/a	372	C27H48	n/a	
	DiaC28βα S	S-C28βα-diasterane	n/a	386	C28H50	n/a	
	DiaC28βα R	R-C28βα-diasterane	n/a	386	C28H50	n/a	
	C28ααα S	20S a,a,a-ergostane	n/a	386	C28H50	n/a	
	C28ααα R	20R a,a,a-ergostane	n/a	386	C28H50	n/a	
	C28αββ S	20S a,b,b-ergostane	n/a	386	C28H50	n/a	
	C28αββ R	20R a,b,b-ergostane	n/a	386	C28H50	n/a	
	DiaC29βα S	S-C29βα-diasterane	n/a	400	C29H52	n/a	
	DiaC29βα R	R-C29βα-diasterane	n/a	400	C29H52	n/a	
	C29ααα S	20S a,a,a-stigmastane	n/a	400	C29H52	n/a	
	C29ααα R	20R a,a,a-stigmastane	n/a	400	C29H52	n/a	
	C29αββ S	20S a,b,b-stigmastane	n/a	400	C29H52	n/a	
	C29αββ R	20R a,b,b-stigmastane	n/a	400	C29H52	n/a	
	C20 TAS	C20-triaromatic steroid	81943-50-21	260	C20H20	7.02	2,3,4
	C21 TAS	C21-triaromatic steroid	n/a	274	C21H22	7.36	2,4
	S-C26 TAS	C26-20S-triaromatic steroid	80382-29-2	345	C26H32	9.67	2
	R-C26/S-C7 TAS	C26-20R-triaromatic steroid/ C27-20S-triaromatic steroid	80382-29-2/ n/a	345/ 359	C26H32/ C27H34	9.67/ 9.87	2 2
	S-C28 TAS	C28-20S-triaromatic steroid	80382-33-8	373	C28H36	10.26	2,4
	R-C27 TAS	C27-20R-triaromatic steroid	n/a	359	C27H34	9.87	2
	R-C28 TAS	C28-20R-triaromatic steroid	80382-33-8	373	C28H36	10.26	2,4

1: Hilal et. al. 2003, 2:Aeppli et.al. 2014, 3: Yang et. al. 2013, 4: Wise et.al. 2022

Table A3: Properties for analyzed polycyclic aromatic hydrocarbons (PAHs). MW: molecular weight (g/mol), Log K_{ow}: octanol-water partitioning coefficient.

Group	Abbreviation	Compound	CAS Number	MW	Formula	Log K_{OW}	References
Polycyclic Aromatic Hydrocarbons	N	Naphthalene	91-20-3	128	C10H8	3.37	1, 2
	2-me-N	2 Methyl Naphthalene	91-57-6	142	C11H10	3.88	3
	1-me-N	1 Methyl Naphthalene	90-12-0	142	C11H10	3.87	3
	2,6-dme-N	2,6 Dimethyl Naphthalene	581-42-0	156	C12H12	4.36	4
	1,6-dme-N	1,6 dimethyl naphthalene	575-43-9	156	C12H12	4.35	4
	ACL	Acenaphthylene	208-96-8	152	C12H8	4.00	1
	1,2-dme-N	1,2 dimethyl naphthalene	573-98-8	156	C12H12	4.31	3
	ACE	Acenaphthene	83-32-9	154	C12H10	3.92	1,2
	F	Fluorene	86-73-7	166	C13H10	4.18	1,2
	D	Dibenzothiophene	132-65-0	184	C12H8S	4.38	3
	P	Phenanthrene	85-01-8	178	C14H10	4.57	1,2,8
	AN	Anthracene	120-12-7	178	C14H10	4.54	1,2
	4-me-D	4 methyl dibenzothiophene	7372-88-5	198	C13H10S	4.84	4
	2/3-me-D	2/3 methyl dibenzothiophene	20928-02-3	198	C13H10S	n/a	
	1-me-D	1 methyl dibenzothiophene	31317-07-4	198	C13H10S	n/a	
	1-me-P	1 methyl phenanathrene	832-69-9	192	C15H12	5.08	5
	2-me-P	2 methyl phenananthrene	2531-84-2	192	C15H12	4.86	5
	1-me-AN	1 methyl anthracene	610-48-0	192	C15H12	5.11	4
	3-me-P	3 methyl phenanthrene	832-71-3	192	C15H12	5.15	5
	9-me-P	9 methyl phenathrene	883-20-5	192	C15H12	4.30	4
	1,2-dme-P	1,2 dimethyl phenanthrene	20291-72-9	206	C16H14	5.46	4
	FL	Fluoranthene	206-44-0	202	C16H10	5.22	1,2
	PY	Pyrene	129-00-0	202	C16H10	5.18	1,2
	2-me-FL	2 methyl fluoranthene	33543-31-6	216	C17H12	5.70	4
	Re	Retene	483-65-8	234	C18H18	6.46	6
	1-me-PY	1 methyl pyrene	2381-21-7	216	C17H12	5.48	7
	4-me-PY	4 methyl pyrene	3353-12-6	216	C17H12	5.68	4
	BAA	Benz[a]anthracene	56-55-3	228	C18H12	5.91	1,7
	CHR	Chrysene	218-01-9	228	C18H12	5.56	7,8
	3-me-CHR	3 methyl chrysene	3351-31-3	242	C19H14	6.25	4
	6-me-CHR	6 methyl chrysene	1705-85-7	242	C19H14	5.90	4
	1-me-CHR	1 methyl chrysene	3351-28-8	242	C19H14	6.24	4
	BBFL	Benzo[b]fluoranthene	205-99-2	252	C20H12	5.80	1,7
	BKFL	Benzo[k]fluoranthene	207-08-9	252	C20H12	6.00	1,7
	BEPY	Benzo(e)pyrene	192-97-2	252	C20H12	6.44	3
	BAPY	Benzo[a]pyrene	50-32-8	252	C20H12	6.04	1
	Pe	Perylene	198-55-0	252	C20H12	6.50	2
	BGP	Benzo[g,h,i]perylene	191-24-2	276	C22H12	7.10	2
	ID	Indeno[1,2,3]pyrene	193-39-5	276	C22H12	7.66	1,7
	DA	Dibenz[a,h]anthracene	53-70-3	278	C22H14	6.75	1,7
	N1	C1 naphthalene	1321-94-4	143	C11H10	3.72	5
	N2	C2 naphthalene	n/a	156	C12H12	n/a	
	N3	C3 naphthalene	n/a	170	C13H14	n/a	
	N4	C4 naphthalene	n/a	184	C14H16	n/a	
	F1	C1 fluorene	n/a	180	C14H12	n/a	
	F2	C2 fluorene	n/a	194	C15H14	n/a	
	F3	C3 fluorene	n/a	208	C16H16	n/a	
	D1	C1 dibenzothiophene	30995-64-3	198	C13H10S	4.84	4
	D2	C2 dibenzothiophene	n/a	212	C14H12S	n/a	
	D3	C3 dibenzothiophene	n/a	226	C15H14S	n/a	
	D4	C4 dibenzothiophene	n/a	240	C16H16S	n/a	
	P/AN1	C1 phenanthrene-anthracene	n/a	192	C15H12	5.16	8
	P/AN2	C2 phenanthrene-anthracene	n/a	206	C16H14	5.54	8
	P/AN3	C3 phenanthrene-anthracene	n/a	220	C17H16	5.85	8
	P/AN4	C4 phenanthrene-anthracene	n/a	234	C18H18	n/a	
	FL/PY1	C1 fluoranthene-pyrene	n/a	216	C17H12	n/a	
	FL/PY2	C2 fluoranthene-pyrene	n/a	230	C18H14	n/a	
	FL/PY3	C3 fluoranthene-pyrene	n/a	244	C19H16	n/a	
	FL/PY4	C4 fluoranthene-pyrene	n/a	258	C20H18	n/a	
	BAA/CHR1	C1 benz[a]anthracene-chrysene	n/a	242	C19H14	6.24	8
	BAA/CHR2	C2 benz[a]anthracene-chrysene	n/a	256	C20H16	6.6	8
	BAA/CHR3	C3 benz[a]anthracene-chrysene	n/a	270	C21H18	7.01	8
	BAA/CHR4	C4 benz[a]anthracene-chrysene	n/a	284	C22H20	n/a	
	BP/PER1	C1 benzopyrene-perylene	n/a	266	C21H14	n/a	
	BP/PER2	C2 benzopyrene-perylene	n/a	280	C22H16	n/a	
	BP/PER3	C3 benzopyrene-perylene	n/a	294	C23H18	n/a	

1: LaGrega et.al. 2001, 2: Miller et.al. 1985, 3: Hansch et.al. 1995, 4: Hilal et.al. 2003, 5: Williams et.al. 2017, 6: Reitsma et.al. 2013, 7: Halek et.al. 2008, 8: Aeppli et.al. 2014

Table A4: Properties for analyzed oxidized-polycyclic aromatic hydrocarbons (oxid-PAHs). MW: molecular weight (g/mol), Log K_{ow}: octanol-water partitioning coefficient.

Group	Abbreviation	Compound	CAS Number	MW	Formula	Log K_{OW}	References
Oxidized PAHs	1,4-NQ	1,4-naphthoquinone	130-15-4	158	C10H6O2	1.71	1
	NQ	Naphthoquinones	n/a	158	C10H6O2	n/a	
	1-NH	1-naphthaldehyde	66-77-3	156	C11H8O	2.74	2
	2-NH	2-naphthaldehyde	66-99-9	156	C11H8O	2.74	2
	NH	Naphthaldehydes	n/a	156	C11H8O	n/a	
	1-HN	1-hydroxynaphthalene	90-15-3	144	C10H8O	2.85	1
	2-HN	2-hydroxynaphthalene	135-19-3	144	C10H8O	2.70	1
	HN	Hydroxynaphthalenes	n/a	144	C10H8O	n/a	
	1-NN	1-nitronaphthalene	86-57-7	173	C10H7NO2	3.19	1
	2-NN	2-nitronaphthalene	581-89-5	173	C10H7NO2	3.24	3
	NN	Nitronaphthalenes	n/a	173	C10H7NO2	n/a	
	9-FLO	9-fluorenone	486-25-9	180	C13H8O	3.58	1
	FLO	Fluorenones	n/a	180	C13H8O	n/a	
	9,10-ANT	9,10-anthrone	90-44-8	194	C14H10O	3.66	1
	ANT	Anthrones	n/a	194	C14H10O	n/a	
	2-NF	2-nitrofluorene	607-57-8	211	C13H9NO2	3.37	1
	NF	Nitrofluorenes	n/a	211	C13H9NO2	n/a	
	XA	Xanthones	n/a	196	C13H8O2	n/a	
	9-XA	9-xanthone	90-47-1	196	C13H8O2	3.39	1
	9-NAN	9-nitroanthracene	602-60-8	223	C14H9NO2	4.78	3
	9-NP	9-nitrophenanthrene	954-46-1	223	C14H9NO2	4.55	2
	NAN/NP	Nitroanthracene-Phenanthrenes	n/a	223	C14H9NO2	n/a	
	2,3-HP	2,3-hydroxyphenanthrene	n/a	210	C14H10O2	n/a	
	4,9-HP	4,9-hydroxyphenanthrene	n/a	210	C14H10O2		
	HP	Hydroxyphenanthrenes	n/a	210	C14H10O2	n/a	
	9,10-PQ	9,10-phenanthroquinone	84-11-7	208	C14H8O2	2.52	1
	PQ	Phenanthroquinones	n/a	208	C14H8O2	n/a	
	3-NFL	3-nitrofluoranthene	829-21-7	247	C16H9NO2	n/a	
	1-NPY	1-nitropyrene	5522-43-0	247	C16H9NO2	5.06	1
	NFL/NPY	Nitrofluoranthene-Pyrenes	n/a	247	C16H9NO2	n/a	
	6-NCHR	6-nitrochrysene	7496-02-8	273	C18H11NO2	5.34	4
	NCHR	Nitrochrysenes	n/a	273	C18H11NO2	n/a	
	6-NBAPY	6-nitrobenzo(a)pyrene	63041-90-7	297	C20H11NO2	5.44	5
	NBAPY	Nitrobenzopyrenes	n/a	297	C20H11NO2	n/a	

1: Hansch et.al. 1995, 2: Hilal et.al. 2003, 3: Williams et.al. 2017, 4: Card et.al. 2017, 5: Sangster 1997

Table A5: Properties for analyzed organochlorine pesticides and polychlorinated biphenyls. MW: molecular weight (g/mol), Log K_{ow}: octanol-water partitioning coefficient.

Group	Abbreviation	Compound	CAS Number	MW	Formula	Log K_{OW}	References
Organochlorinated Pesticides	ALA	Alachlor	15972-60-8	270	C14H20ClNO2	3.30	4,6
	ALD	Aldrin	309-00-2	365	C12H8Cl6	5.52	1,6
	DLD	Dieldrin	60-57-1	381	C12H8Cl6O	5.16	3,6
	END	Endrin	72-20-8	381	C12H8Cl6O	5.16	1,6
	END-AL	Endrin aldehyde	7421-93-4	381	C12H8Cl6O	6.44	5,6
	ATA	Atrazine	1912-24-9	216	C8H14ClN5	2.66	1,6
	a-HCH	Alpha-hexachlorocyclohexane	319-84-6	291	C6H6Cl6	3.70	3,6
	b-HCH	Beta-hexachlorocyclohexane	319-85-7	291	C6H6Cl6	3.70	3,6
	g-HCH	Gamma-hexachlorocyclohexane	58-89-9	291	C6H6Cl6	3.70	3,6
	d-HCH	Delta-hexachlorocyclohexane	319-86-8	291	C6H6Cl6	3.70	3,6
	CBL	Chlorobenzilate	510-15-6	325	C16H14Cl2O3	3.05	4,6
	CNB	Chloroneb	2675-77-6	207	C8H8Cl2O2	3.44	5,6
	CTN	Chlorothalonil	1897-45-6	266	C8Cl4N2	2.87	4,6
	g-CHL	g-Chlordane	5103-74-2	410	C10H6Cl8	6.00	1,6
	a-CHL	a-Chlordane	5103-71-9	410	C10H6Cl8	6.00	1,6
	CYA	Cyanazine	21725-46-2	241	C9H13ClN6	2.22	2,6
	DCPA	Dimethyl tetrachloroterephthalate	1861-32-1	332	C10H6Cl4O4	4.40	5,6
	DDE	p,p'-Dichlorodiphenyl dichloroethylene	72-55-9	318	C14H8Cl4	6.09	1,6
	DDD	p,p'-Dichlorodiphenyl dichloroethane	72-54-8	320	C14H10Cl4	6.22	1,6
	DDT	p,p'-Dichlorodiphenyl trichloroethane	50-29-3	354	C14H9Cl5	6.38	1,6
	EDS-I	Endosulfan I	959-98-8	407	C9H6Cl6O3S	3.83	5,6
	EDS-II	Endosulfan II	33213-65-9	407	C9H6Cl6O3S	3.83	5,6
	EDS-sul	Endosulfan sulfate	1031-07-8	423	C9H6Cl6O4S	6.01	5,6
	ETR	Etridiazole	2593-15-9	248	C5H5Cl3N2OS	3.37	5,6
	HEP	Heptachlor	76-44-8	373	C10H5Cl7	5.40	1,6
	HEP-epox	Heptachlor epoxide	1024-57-3	389	C10H5Cl7O	5.45	1,6
	BHC	Hexachlorobenzene	118-74-1	285	C6Cl6	5.47	1,6
	HCCPD	Hexachlorocyclopentadiene	77-47-4	273	C5Cl6	5.51	5,6,7
	MOXC	Methoxychlor	72-43-5	346	C16H15Cl3O2	5.08	3,6
	MOAC	Metolachlor	51218-45-2	284	C15H22ClNO2	3.11	4,6
	MEB	Metribuzin	21087-64-9	214	C8H14N4OS	1.70	1,6
	PPC	Propachlor	1918-16-7	212	C11H14ClNO	2.18	2,6
	SMZ	Simazine	122-34-9	202	C7H12ClN5	2.11	1,6
	cis-PERM	cis-Permethrin	61949-76-6	391	C21H20Cl2O3	6.60	1,6
	trans-PERM	trans-Permethrin	61949-77-7	391	C21H20Cl2O3	6.60	1,6
	TRI	Trifluralin	1582-09-8	335	C13H16F3N3O4	5.34	1,6
Polychlorinated Biphenyls	PCB 8	2,4'-Dichlorobiphenyl	34883-43-7	223	C12H8Cl2	5.07	10,11,12
	PCB 28	2,4,4'-Trichlorobiphenyl	7012-37-5	258	C12H7Cl3	5.67	8,10,11,12
	PCB 37	3,4,4'-Trichlorobiphenyl	38444-90-5	258	C12H7Cl3	5.83	10,11,12
	PCB 44	2,2',3,5'-Tetrachlorobiphenyl	41464-39-5	292	C12H6Cl4	5.75	10,11,12,13
	PCB 49	2,2',4,5'-Tetrachlorobiphenyl	41464-40-8	292	C12H6Cl4	5.85	10,11,12
	PCB 52	2,2',5,5'-Tetrachlorobiphenyl	35693-99-3	292	C12H6Cl4	5.84	8,10,11,12
	PCB 60	2,3,4,4'-Tetrachlorobiphenyl	33025-41-1	292	C12H6Cl4	6.11	10,11,12
	PCB 66	2,3',4,4'-Tetrachlorobiphenyl	32598-10-0	292	C12H6Cl4	6.20	10,11
	PCB 70	2,3',4',5-Tetrachlorobiphenyl	32598-11-1	292	C12H6Cl4	6.20	10,11
	PCB 74	2,4,4',5-Tetrachlorobiphenyl	32690-93-0	292	C12H6Cl4	6.20	10,11
	PCB 77	3,3',4,4'-Tetrachlorobiphenyl	32598-13-3	292	C12H6Cl4	6.36	9,10,11
	PCB 82	2,2',3,3',4-Pentachlorobiphenyl	52663-62-4	326	C12H5Cl5	6.20	10,11
	PCB 87	2,2',3,4,5'-Pentachlorobiphenyl	38380-02-8	326	C12H5Cl5	6.29	10,11
	PCB 99	2,2',4,4',5-Pentachlorobiphenyl	38380-01-7	326	C12H5Cl5	6.39	10,11
	PCB 101	2,2',4,5,5'-Pentachlorobiphenyl	37680-73-2	326	C12H5Cl5	6.38	8,10,11
	PCB 105	2,3,3',4,4'-Pentachlorobiphenyl	32598-14-4	326	C12H5Cl5	6.65	9,10,11
	PCB 114	2,3,4,4',5-Pentachlorobiphenyl	74472-37-0	326	C12H5Cl5	6.65	9,10,11
	PCB 118	2,3',4,4',5-Pentachlorobiphenyl	31508-00-6	326	C12H5Cl5	6.74	9,10,11
	PCB 126	3,3',4,4',5-Pentachlorobiphenyl	57465-28-8	326	C12H5Cl5	6.89	9,10,11
	PCB 128	2,2',3,3',4,4'-Hexachlorobiphenyl	38380-07-3	361	C12H4Cl6	6.74	10,11
	PCB 138	2,2',3,4,4',5'-Hexachlorobiphenyl	35065-28-2	361	C12H4Cl6	6.83	8,10,11
	PCB 153	2,2',4,4',5,5'-Hexachlorobiphenyl	35065-27-1	361	C12H4Cl6	6.92	8,10,11
	PCB 156	2,3,3',4,4',5-Hexachlorobiphenyl	38380-08-4	361	C12H4Cl6	7.18	9,10,11
	PCB 158	2,3,3',4,4',6-Hexachlorobiphenyl	74472-42-7	361	C12H4Cl6	7.02	10,11
	PCB 166	2,3,4,4',5,6-Hexachlorobiphenyl	41411-63-6	361	C12H4Cl6	6.93	10,11
	PCB 169	3,3',4,4',5,5'-Hexachlorobiphenyl	32774-16-6	361	C12H4Cl6	7.42	9,10,11
	PCB 170	2,2',3,3',4,4',5-Heptachlorobiphenyl	35065-30-6	395	C12H3Cl7	7.27	10,11
	PCB 179	2,2',3,3',5,6,6'-Heptachlorobiphenyl	52663-64-6	395	C12H3Cl7	6.73	10,11
	PCB 180	2,2',3,4,4',5,5'-Heptachlorobiphenyl	35065-29-3	395	C12H3Cl7	7.36	8,10,11
	PCB 183	2,2',3,4,4',5',6-Heptachlorobiphenyl	52663-69-1	395	C12H3Cl7	7.20	10,11
	PCB 187	2,2',3,4',5,5',6-Heptachlorobiphenyl	52663-68-0	395	C12H3Cl7	7.17	10,11
	PCB 189	2,3,3',4,4',5,5'-Heptachlorobiphenyl	39635-31-9	395	C12H3Cl7	7.71	9,10,11

1: Klotz et.al. 2001, 2: Paschke et.al. 2004, 3: Patil 1994, 4: Benfenati et.al. 2003, 5: Niemi et.al. 1992, 6: Tomlin 2009, 7: Wolfe et.al. 1982, 8: Harrad et.al. 1994, 9: Van den Berg et.al. 2006, 10: Frame et.al. 1996, 11: Dunnivant and Elzerman 1988, 12: Safe and Hutsinger 2008, 13: Faroon et.al. 2001

APPENDIX B:

SELECTION OF MASS SPECTRA

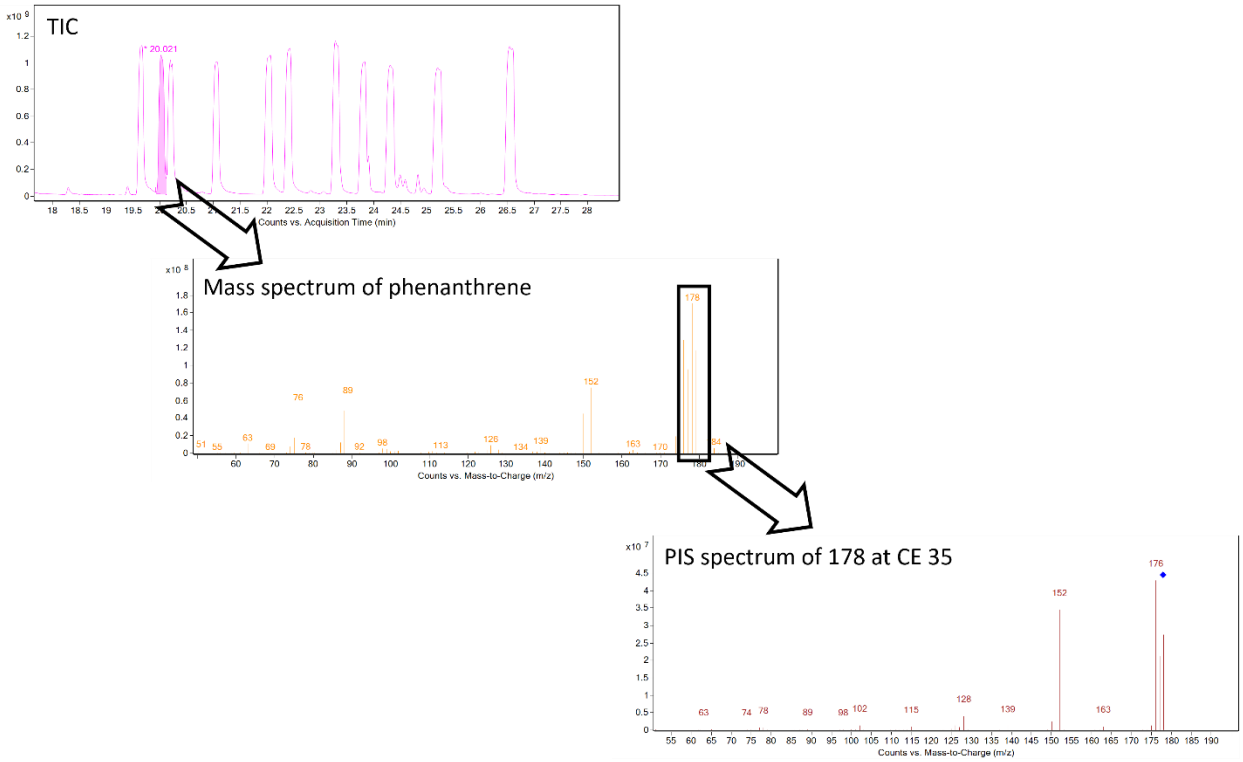

Figure B1: The typical process of SRM creation. This example is of phenanthrene, beginning with total ion chromatogram (TIC) and entire mass spectrum, the largest ion present for phenanthrene is 178 in the TIC spectrum, which is then used as the precursor ion used to select for the appropriate product ion; 176 for phenanthrene.

APPENDIX C:

RECOVERY, LIMIT OF DETECTION, AND LIMIT OF QUANTITATION TABLES

Table C1: Empirically determined correlation coefficients (R^2), percentage recovery, and limits of detection (LOD) and limits of quantitation (LOQ) in ng/g for analyzed aliphatics, fecal sterols, and phthalates. R^2 values are based on 5-point calibration series and n=10 for LOD and LOQ determination.

Group	Compound	R^2	%Recovery	LOD (ng/g)	LOQ (ng/g)
Aliphatics	nC10	0.982	85.9	0.26	0.85
	nC11	0.980	76.1	0.64	2.14
	nC12	0.963	94.8	0.47	1.56
	nC13	0.934	107.9	0.20	0.68
	nC14	0.939	111.7	0.14	0.46
	nC15	0.926	121.9	0.22	0.74
	nC16	0.929	126.4	0.11	0.38
	nC17	0.945	122.2	0.11	0.37
	Pr	0.957	114.1	0.06	0.19
	nC18	0.952	120.4	0.15	0.50
	Phy	0.986	121.1	0.10	0.34
	nC19	0.966	122.6	0.20	0.68
	nC20	0.976	99.6	0.07	0.23
	nC21	0.988	104.7	0.03	0.10
	nC22	0.994	105.9	0.03	0.11
	nC23	0.995	102.7	0.04	0.14
	nC24	0.995	110.4	0.09	0.30
	nC25	0.997	122.1	0.03	0.11
	nC26	0.994	125.6	0.05	0.18
	nC27	0.996	122.3	0.15	0.51
	nC28	0.994	92.3	0.04	0.12
	nC29	0.993	111.7	0.18	0.60
	nC30	0.990	111.6	0.13	0.43
	nC31	0.988	132.4	0.06	0.21
	nC32	0.985	107.3	0.08	0.25
	nC33	0.977	125.4	0.05	0.17
	nC34	0.980	121.0	0.05	0.17
	nC35	0.975	115.6	0.06	0.20
	nC36	0.971	111.8	0.14	0.48
	nC37	0.946	122.5	0.03	0.11
Fecal Sterols	CP+epi-CP	0.927	90.1	0.26	0.85
	CSE	0.894	90.7	0.51	1.70
	CSA	0.887	88.4	0.26	0.87
Phthalates	DMP	0.938	68.9	0.02	0.07
	DEP	0.940	80.0	0.09	0.30
	DBP	0.956	77.4	0.69	2.29
	BBP	0.950	72.1	0.14	0.48
	DEHP	0.956	99.4	0.08	0.27
	DnOP	0.951	80.1	0.20	0.67

Table C2: Empirically determined correlation coefficients (R^2), percentage recovery, and limits of detection (LOD) and limits of quantitation (LOQ) in ng/g for analyzed hopanes, steranes, and tri-aromatic steroids. R^2 values are based on 5-point calibration series and n=10 for LOD and LOQ determination.

Group	Compound	R^2	%Recovery	LOD (ng/g)	LOQ (ng/g)
Hopanes, Steranes, and Triaromatic Steroids	DiaC27βα S	0.994	74.6	0.219	0.732
	DiaC27βα R	0.996	78.5	0.670	2.233
	C27ααα S	0.986	105.9	1.654	5.514
	C27αββ R	0.992	95.3	0.182	0.607
	C27αββ S	0.979	97.4	0.186	0.621
	C27ααα R	0.991	80.9	0.843	2.809
	DiaC28βα S	0.992	70.6	0.069	0.230
	DiaC28βα R	0.987	79.2	0.158	0.527
	C28ααα S	0.982	95.5	0.368	1.228
	C28αββ R	0.971	88.0	0.246	0.821
	C28αββ S	0.989	81.6	0.353	1.177
	C28ααα R	0.986	111.4	0.629	2.096
	DiaC29βα S	0.996	83.3	0.097	0.322
	DiaC29βα R	0.979	90.8	0.027	0.090
	C29ααα S	0.991	91.5	0.425	1.417
	C29αββ R	0.990	104.9	0.277	0.923
	C29αββ S	0.993	92.0	0.435	1.450
	C29ααα R	0.986	102.1	0.262	0.874
	Ts	0.995	73.1	0.091	0.304
	Tm	0.996	79.2	0.106	0.354
	BNH	0.962	76.2	0.194	0.647
	NH + NNH	0.996	91.0	0.120	0.399
	NM	0.984	123.3	0.203	0.678
	H	0.994	94.2	0.242	0.806
	M	0.990	116.6	0.111	0.370
	HH-S	0.992	96.6	0.161	0.538
	HH-R	0.989	99.4	0.204	0.681
	HM	0.974	n/a	0.184	0.613
	BHH-S	0.993	108.0	0.137	0.457
	BHH-R	0.993	116.7	0.267	0.889
	THH-S	0.992	127.1	0.356	1.186
	THH-R	0.975	124.0	0.247	0.824
	TkHH-S	0.975	123.3	0.148	0.493
	TkHH-R	0.985	121.6	0.320	1.067
	PHH-S	0.978	117.5	0.136	0.455
	PHH-R	0.986	123.4	0.126	0.420
	C20 TAS	0.985	74.0	0.019	0.065
	C21 TAS	0.993	72.7	0.017	0.058
	S-C26 TAS	0.986	82.1	0.035	0.117
	R-C26 + S-C7 TAS	0.989	81.1	0.074	0.248
	S-C28 TAS	0.986	98.7	0.051	0.169
	R-C27 TAS	0.988	102.5	0.039	0.130
	R-C28 TAS	0.984	129.9	0.055	0.182

Table C3: Empirically determined correlation coefficients (R^2), percentage recovery, and limits of detection (LOD) and limits of quantitation (LOQ) in ng/g for analyzed polycyclic aromatic hydrocarbons. R^2 values are based on 5-point calibration series and n=10 for LOD and LOQ determination.

Group	Compound	R^2	%Recovery	LOD (ng/g)	LOQ (ng/g)
Polycyclic Aromatic Hydrocarbons	N	0.997	92.0	0.022	0.072
	N1	0.996	100.0	1.085	3.617
	2-me-N	0.997	100.9	0.005	0.018
	1-me-N	0.991	95.4	0.016	0.053
	N2	0.996	103.9	0.484	1.612
	2,6-dme-N	0.992	n/a	0.024	0.079
	1,6-dme-N	0.996	102.1	0.016	0.052
	1,2-dme-N	0.991	107.8	0.005	0.017
	N3	0.998	108.3	0.808	2.692
	N4	0.998	113.1	0.241	0.804
	ACL	0.995	110.2	0.002	0.007
	ACE	0.997	115.5	0.022	0.072
	F	0.999	123.4	0.032	0.105
	F1	0.998	120.4	0.367	1.224
	F2	0.995	126.6	0.664	2.212
	F3	0.998	127.3	0.286	0.953
	D	0.998	78.8	0.062	0.207
	D1	0.997	77.7	0.070	0.233
	4-me-D	0.997	n/a	0.027	0.089
	2/3-me-D	0.997	n/a	0.061	0.203
	1-me-D	0.999	n/a	0.035	0.118
	D2	0.997	76.6	0.122	0.406
	D3	0.997	76.3	0.078	0.260
	D4	0.998	68.7	0.318	1.060
	P	0.998	119.5	0.155	0.516
	AN	0.904	126.6	0.005	0.015
	P/AN1	0.997	123.2	0.339	1.131
	1-me-P	0.993	111.4	0.023	0.076
	2-me-P	0.992	121.8	0.025	0.083
	1-me-AN	0.899	n/a	0.039	0.129
	3-me-P	0.998	116.1	0.021	0.070
	9-me-P	0.993	113.5	0.078	0.260
	P/AN2	0.999	125.4	0.446	1.486
	1,2-dme-P	0.996	105.4	0.042	0.141
	P/AN3	0.998	127.5	0.313	1.042
	P/AN4	0.999	124.7	0.578	1.928

Group	Compound	R^2	%Recovery	LOD (ng/g)	LOQ (ng/g)
Polycyclic Aromatic Hydrocarbons	Re	0.997	n/a	0.214	0.714
	FL	0.989	117.7	0.205	0.683
	PY	0.989	126.4	0.153	0.511
	FL/PY1	0.998	121.4	1.967	6.557
	2-me-FL	0.974	n/a	0.119	0.395
	1-me-PY	0.994	123.0	0.049	0.164
	4-me-PY	0.992	127.5	0.109	0.363
	FL/PY2	0.997	124.1	1.006	3.353
	FL/PY3	0.996	126.3	0.536	1.788
	FL/PY4	0.993	120.6	0.123	0.410
	BAA	0.941	121.4	0.178	0.595
	CHR	0.986	128.0	0.047	0.156
	BAA/CHR1	0.993	119.9	0.230	0.768
	3-me-CHR	0.984	n/a	0.055	0.182
	6-me-CHR	0.997	109.6	0.059	0.196
	1-me-CHR	0.970	n/a	0.086	0.286
	BAA/CHR2	0.991	119.1	0.716	2.387
	BAA/CHR3	0.988	108.1	0.563	1.878
	BAA/CHR4	0.985	124.7	0.966	3.221
	BBFL	0.973	128.2	0.041	0.136
	BKFL	0.916	125.2	0.305	1.017
	BEPY	0.977	120.1	0.367	1.222
	BAPY	0.988	128.3	0.321	1.069
	Pe	0.957	129.3	0.106	0.354
	BP/PER1	0.996	n/a	0.905	3.018
	BP/PER2	0.989	n/a	1.057	3.524
	BP/PER3	0.986	n/a	0.998	3.327
	DA	0.941	59.6	0.331	1.102
	ID	0.923	116.2	0.323	1.078
	BGP	0.889	100.1	0.241	0.804

Table C4: Empirically determined correlation coefficients (R^2), percentage recovery, and limits of detection (LOD) and limits of quantitation (LOQ) in ng/g for analyzed oxidized-polycyclic aromatic hydrocarbons. R^2 values are based on 5-point calibration series and n=10 for LOD and LOQ determination.

Group	Compound	R^2	%Recovery	LOD (ng/g)	LOQ (ng/g)
Oxidized PAHs	1,4-NQ	n/a	69.8	0.071	0.235
	NQ	0.608	n/a	3.547	11.823
	1-NH	0.996	72.4	0.037	0.124
	2-NH	n/a	82.5	0.021	0.069
	NH	0.998	n/a	4.110	13.699
	1-HN	0.816	71.3	1.014	3.382
	2-HN	0.795	63.0	1.102	3.673
	HN	0.693	n/a	7.352	24.508
	1-NN	0.968	108.5	0.073	0.243
	2-NN	n/a	97.0	0.226	0.754
	NN	0.651	n/a	1.339	4.464
	9-FLO	0.882	71.9	0.338	1.127
	FLO	0.924	n/a	4.798	15.994
	9,10-ANT	0.976	69.1	0.104	0.345
	ANT	0.981	n/a	4.276	14.254
	2-NF	n/a	114.4	0.023	0.077
	NF	0.872	n/a	0.239	0.798
	XA	0.567	n/a	1.901	6.336
	9-XA	0.715	80.5	0.111	0.369
	9-NAN	0.992	84.6	0.211	0.702
	9-NP	0.958	113.3	0.025	0.082
	NAN/NP	0.860	n/a	0.233	0.777
	2,3-HP	0.964	n/a	5.080	16.932
	4,9-HP	0.966	82.8	1.431	4.772
	HP	0.948	n/a	7.241	24.138
	9,10-PQ	0.839	84.2	0.052	0.172
	PQ	n/a	n/a	n/a	n/a
	3-NFL	0.906	71.8	0.047	0.156
	1-NPY	0.954	78.6	0.011	0.036
	NFL/NPY	0.950	n/a	0.121	0.404
	6-NCHR	0.820	120.7	0.027	0.090
	NCHR	0.388	n/a	0.149	0.497
	6-NBAPY	0.614	79.2	0.009	0.031
	NBAPY	0.769	n/a	0.041	0.136

Table C5: Empirically determined correlation coefficients (R^2), percentage recovery, and limits of detection (LOD) and limits of quantitation (LOQ) in ng/g for analyzed organochlorinated pesticides. R^2 values are based on 5-point calibration series and n=10 for LOD and LOQ determination.

Group	Compound	R^2	%Recovery	LOD (ng/g)	LOQ (ng/g)
Organochlorinated Pesticides	ALA	0.995	86.3*	0.139	0.465
	ALD	0.993	93.4	0.029	0.097
	DLD	0.996	98.9	0.049	0.163
	END	0.983	97.8	0.194	0.648
	END-AL	0.991	92.1	0.553	1.844
	ATA	0.993	79.2*	0.013	0.044
	a-HCH	0.994	107.3	0.017	0.055
	b-HCH	0.992	110.9	0.032	0.105
	g-HCH	0.996	113.0	0.026	0.086
	d-HCH	0.997	100.4	0.084	0.281
	CBL	0.964	88.3	0.029	0.095
	CNB	0.996	100.8	0.011	0.038
	CTN	0.992	98.3	0.710	2.367
	g-CHL	0.998	117.2	0.022	0.075
	a-CHL	0.996	123.7	0.028	0.095
	DCPA	0.995	68.0	0.002	0.007
	DDE	0.994	97.3	0.004	0.015
	DDD	0.989	97.0	0.010	0.032
	DDT	0.987	127.5	0.014	0.048
	EDS-I	0.975	127.1	0.036	0.120
	EDS-II	0.989	85.7	0.088	0.292
	EDS-sul	0.986	75.3	0.498	1.659
	ETR	0.985	101.5	0.021	0.069
	HEP	0.996	118.4	0.011	0.037
	HEP-epox	0.998	123.1	0.033	0.111
	BHC	0.994	97.4	0.007	0.022
	HCCPD	0.983	89.0	0.078	0.261
	MOXC	0.950	117.7	0.126	0.419
	MOAC	0.989	77.3*	0.002	0.006
	PPC	0.990	124.9*	0.046	0.152
	cis-PERM	0.862	68.3	0.971	3.237
	trans-PERM	0.881	51.0	0.695	2.315
	TRI	0.988	97.2	0.408	1.361

* indicates compounds that required secondary extraction with 100% DCM

Table C6: Empirically determined correlation coefficients (R^2), percentage recovery, and limits of detection (LOD) and limits of quantitation (LOQ) in ng/g for analyzed polychlorinated biphenyls. R^2 values are based on 5-point calibration series and n=10 for LOD and LOQ determination.

Group	Compound	R^2	%Recovery	LOD (ng/g)	LOQ (ng/g)
Polychlorinated Biphenyls	PCB 8	0.990	111.7	0.0134	0.0446
	PCB 28	0.987	92.9	0.0074	0.0248
	PCB 37	0.959	86.5	0.0132	0.0441
	PCB 44	0.989	104.0	0.0110	0.0366
	PCB 49	0.994	87.5	0.0114	0.0379
	PCB 52	0.993	93.9	0.0385	0.1285
	PCB 60	0.919	89.5	0.0952	0.3172
	PCB 66	0.987	95.5	0.0179	0.0597
	PCB 70	0.991	118.5	0.0199	0.0664
	PCB 74	0.980	84.9	0.0251	0.0836
	PCB 77	0.983	90.7	0.0197	0.0656
	PCB 82	0.969	118.5	0.0209	0.0695
	PCB 87	0.994	110.6	0.0297	0.0991
	PCB 99	0.990	113.0	0.0358	0.1192
	PCB 101	0.988	114.6	0.0378	0.1259
	PCB 105	0.855	118.3	0.1481	0.4937
	PCB 114	0.979	113.9	0.0215	0.0717
	PCB 118	0.983	118.9	0.0128	0.0427
	PCB 126	0.991	98.4	0.0558	0.1859
	PCB 128	0.965	100.4	0.0310	0.1034
	PCB 138	0.964	109.2	0.0153	0.0511
	PCB 153	0.991	109.1	0.0255	0.0849
	PCB 156	0.989	115.7	0.0268	0.0894
	PCB 158	0.982	108.4	0.0269	0.0897
	PCB 166	0.889	102.8	0.1383	0.4609
	PCB 169	0.985	102.8	0.0213	0.0710
	PCB 170	0.974	117.2	0.0226	0.0753
	PCB 179	0.990	103.3	0.0397	0.1324
	PCB 180	0.990	107.7	0.0210	0.0699
	PCB 183	0.990	110.0	0.0171	0.0570
	PCB 187	0.958	116.2	0.0190	0.0633
	PCB 189	0.945	125.0	0.0586	0.1955

APPENDIX D:

METHOD VALIDATION SAMPLES

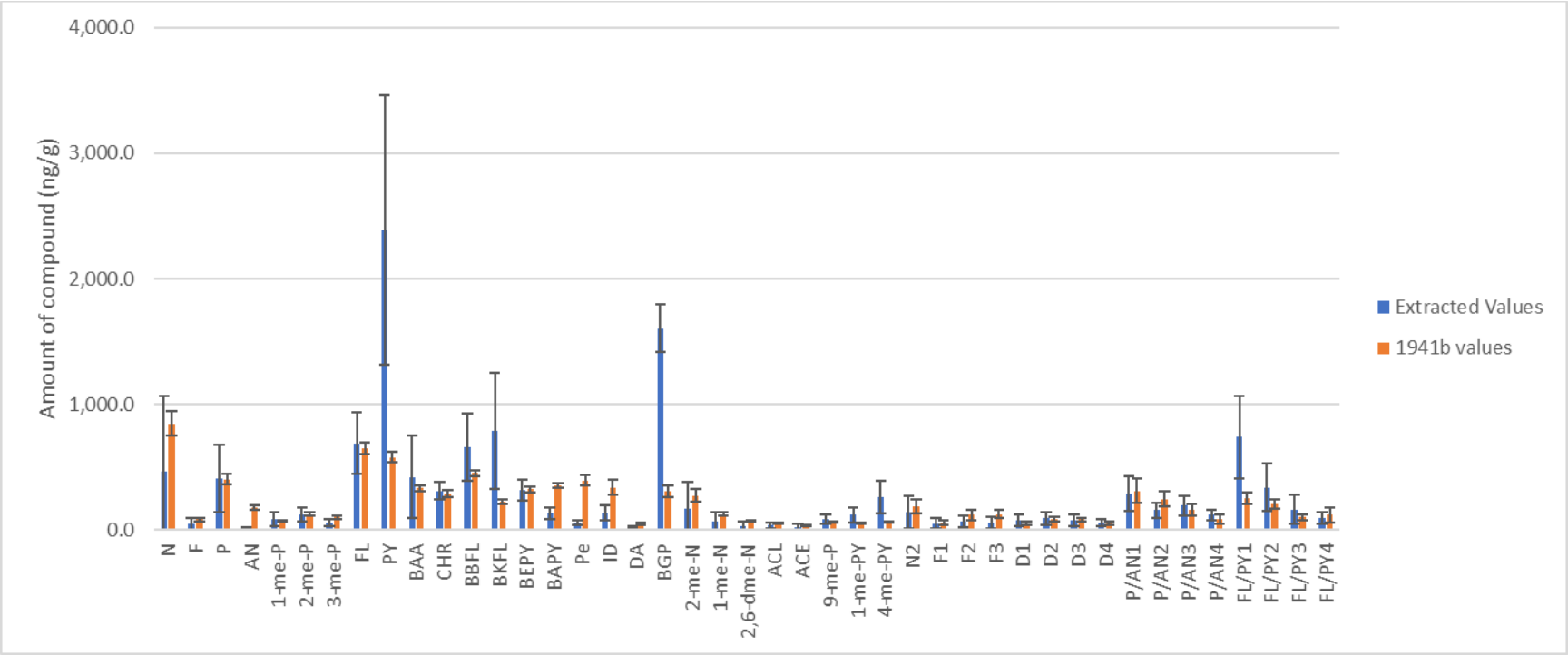

Figure D1: Comparison of PAH concentrations in extracts and reported values for NIST 1941b. Blue bars represent average calculated concentrations via the optimized method described in Chapter 2 and orange bars represent the certified concentrations reported by NIST for 1941b. Error bars are the 95% confidence intervals about the mean with a coverage factor of 2.

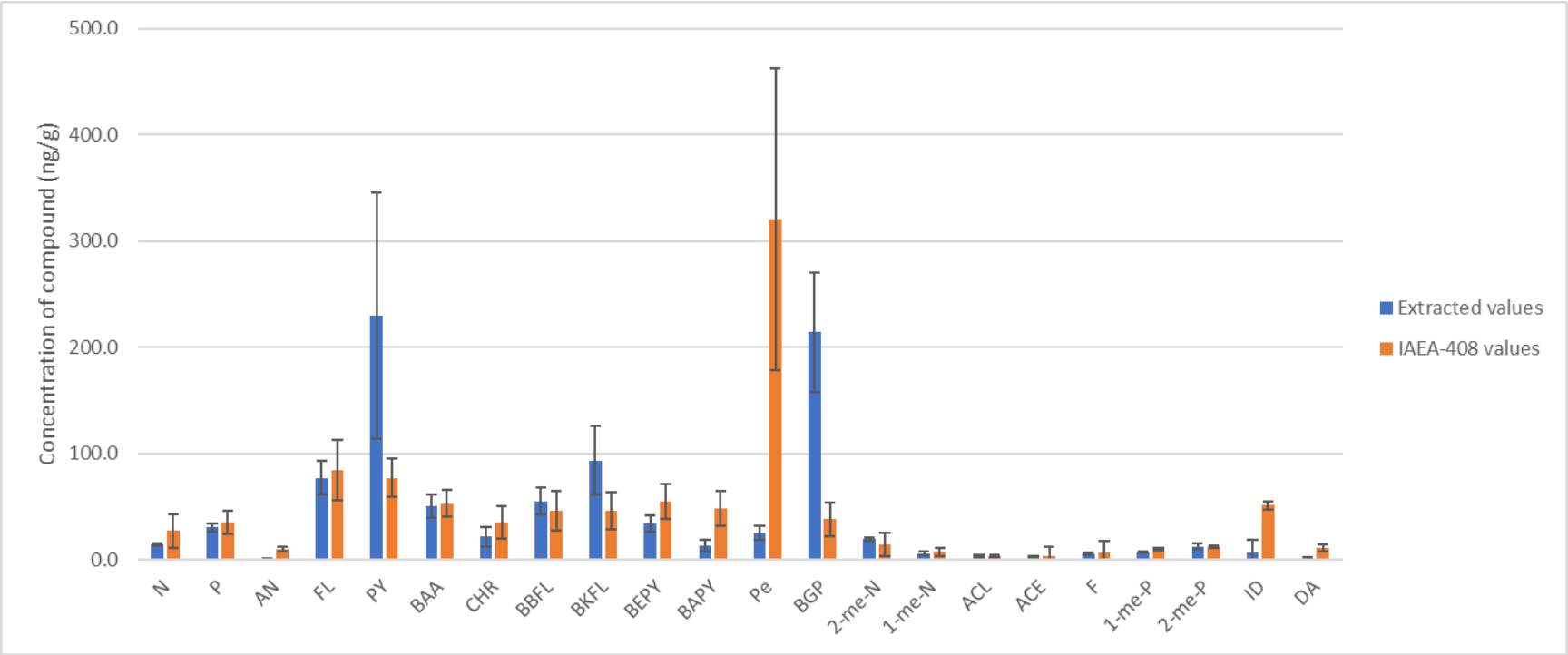

Figure D2: Comparison of PAH concentrations in extracts and reported values for IAEA-408. Blue bars represent median calculated concentrations via the optimized method described in Chapter 2 and orange bars represent the certified concentrations reported by IAEA for IAEA-408. Error bars are the 95% confidence intervals about the median.

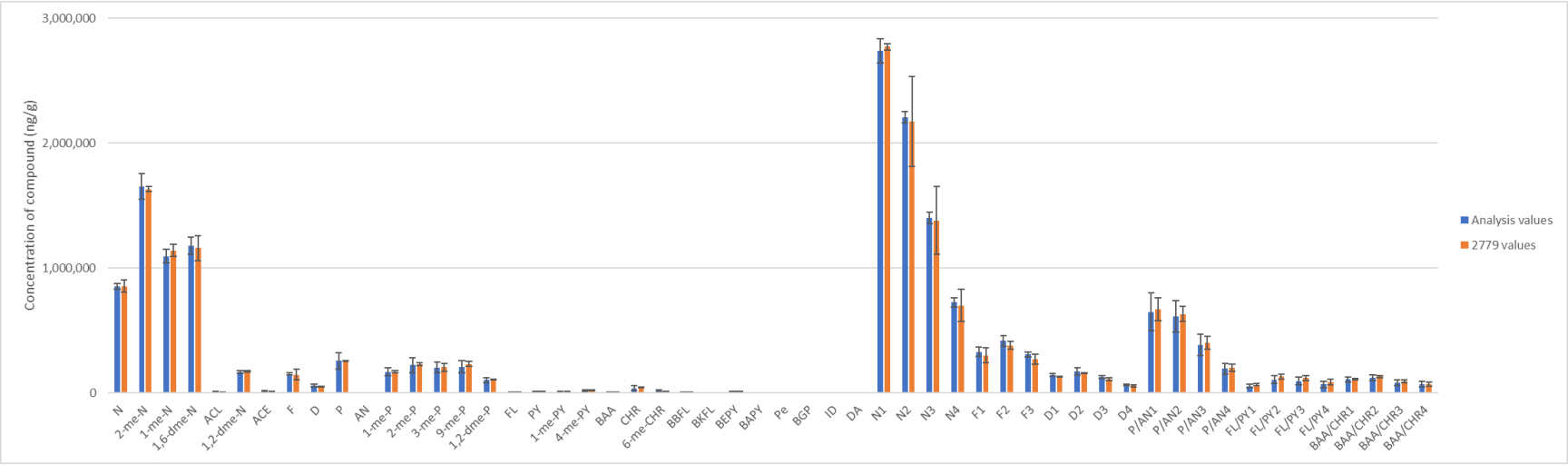

Figure D3: Comparison of calculated PAH concentrations in analysis and reported values for NIST 2779. Blue bars represent mean calculated concentrations via the optimized method described in Chapter 2 and orange bars represent the certified concentrations reported by NIST for NIST 2779. Error bars for values from this study are 1σ. Error bars for certified values are the expaned uncertainty about the mean with a coverage factor of 2, which was calculated by combining the within-method variences and between-method variances following the ISO guide.

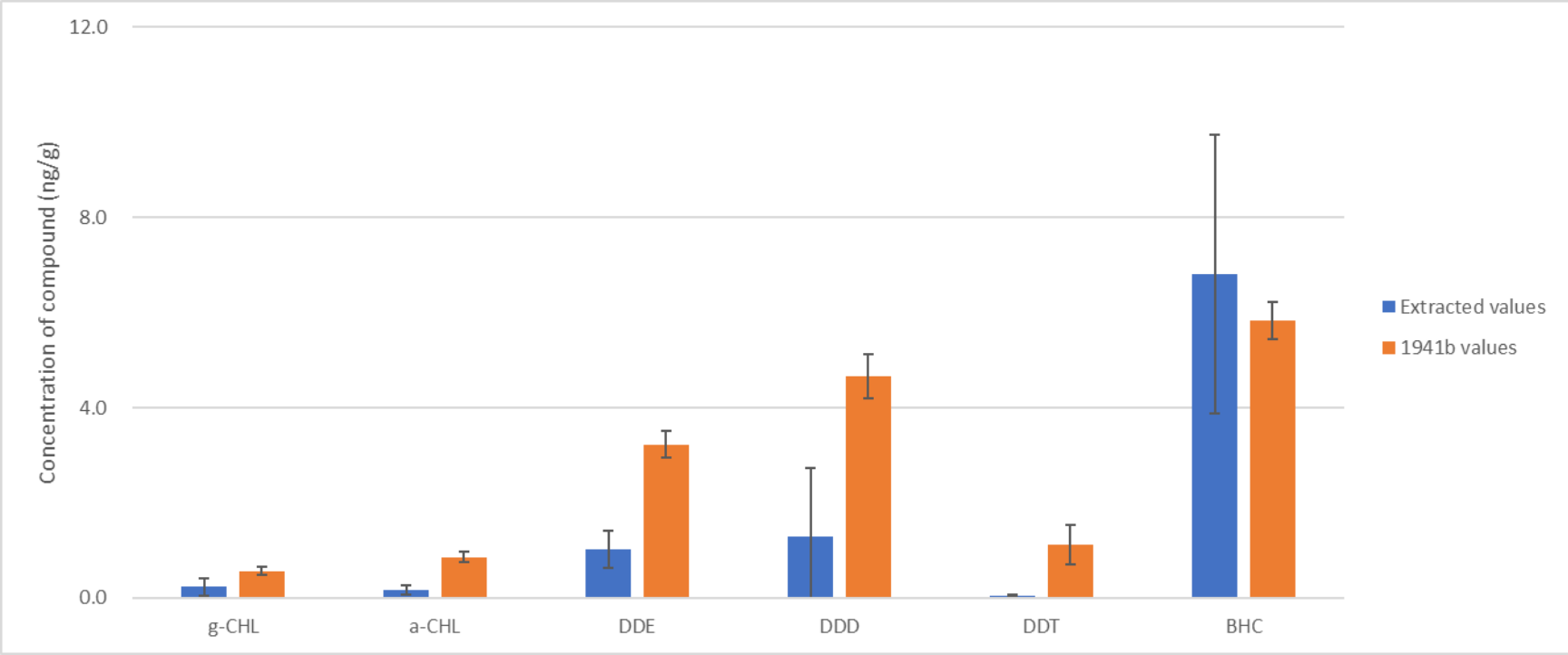

Figure D4: Comparison of OCP concentrations in extracts and reported values for NIST 1941b. Blue bars represent average calculated concentrations via the optimized method described in Chapter 2 and orange bars represent the certified concentrations reported by NIST for 1941b. Error bars are the 95% confidence intervals about the mean with a coverage factor of 2.

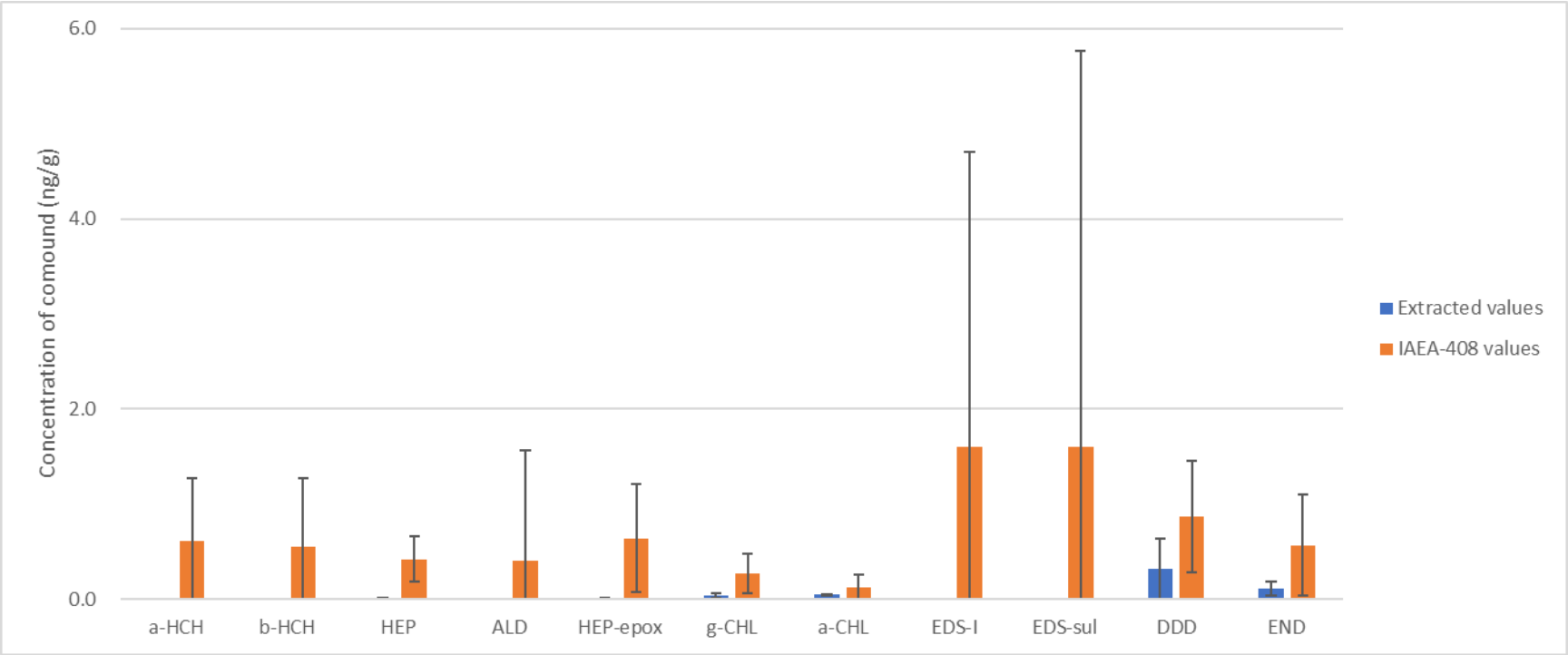

Figure D5: Comparison of OCP concentrations in extracts and reported values for IAEA-408. Blue bars represent median calculated concentrations via the optimized method described in Chapter 2 and orange bars represent the certified concentrations reported by IAEA for IAEA-408. Error bars are the 95% confidence intervals about the median.

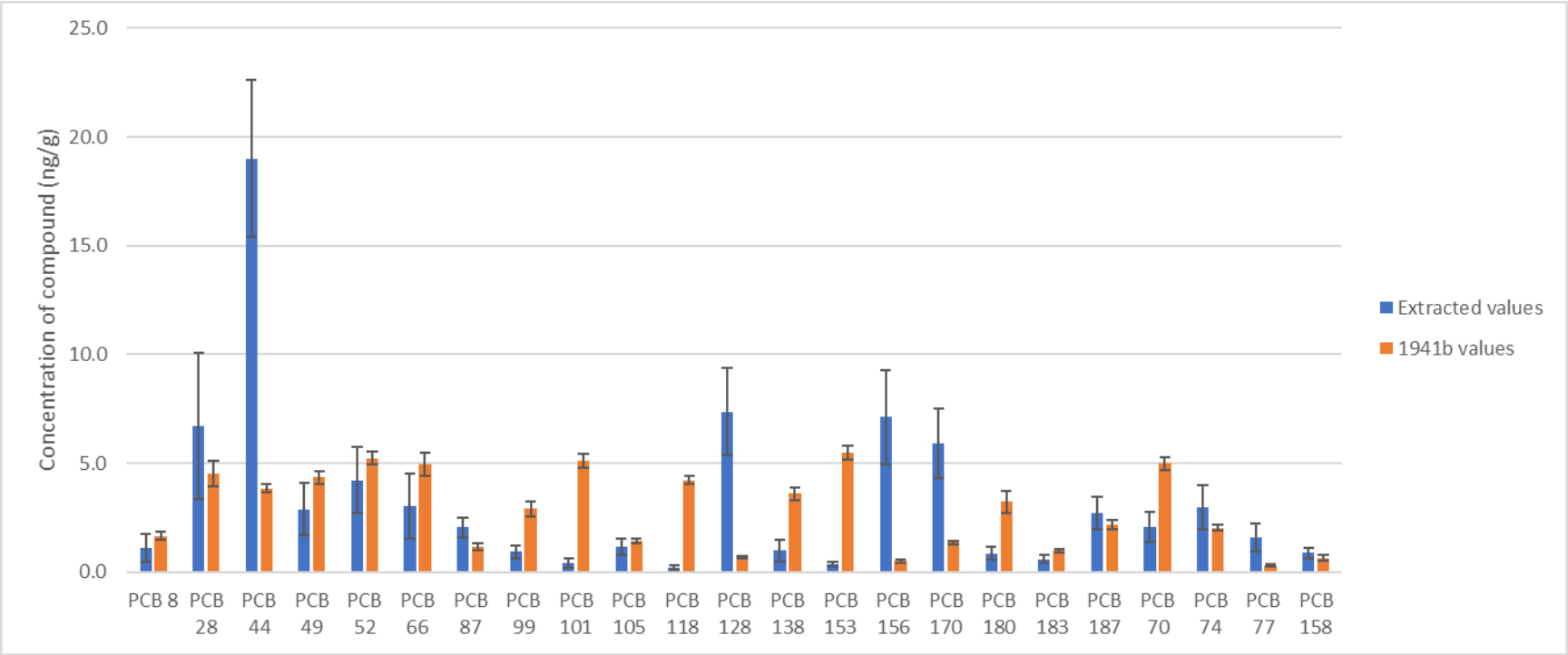

Figure D6: Comparison of PCB concentrations in extracts and reported values for NIST 1941b. Blue bars represent average calculated concentrations via the optimized method described in Chapter 2 and orange bars represent the certified concentrations reported by NIST for 1941b. Error bars are the 95% confidence intervals about the mean with a coverage factor of 2.

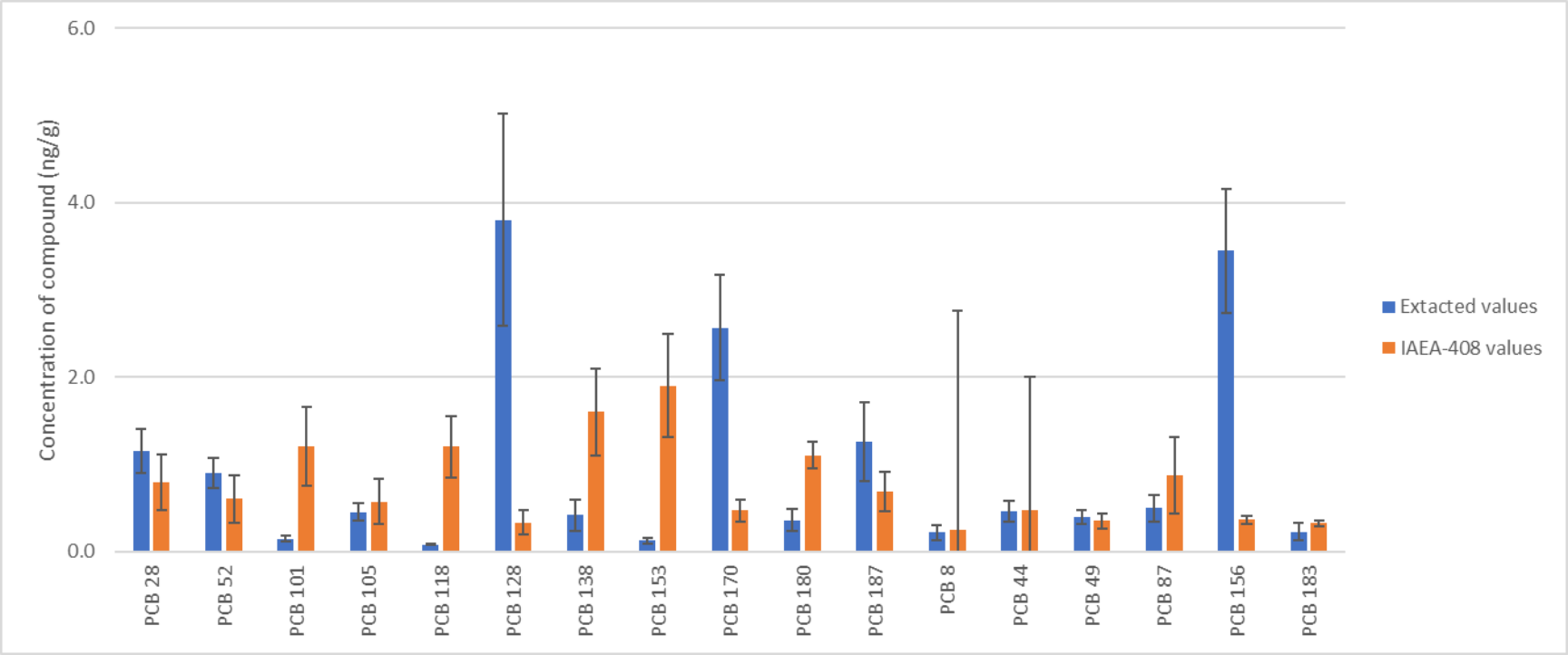

Figure D7: Comparison of PCB concentrations in extracts and reported values for IAEA-408. Blue bars represent median calculated concentrations via the optimized method described in Chapter 2 and orange bars represent the certified concentrations reported by IAEA for IAEA-408. Error bars are the 95% confidence intervals about the median.

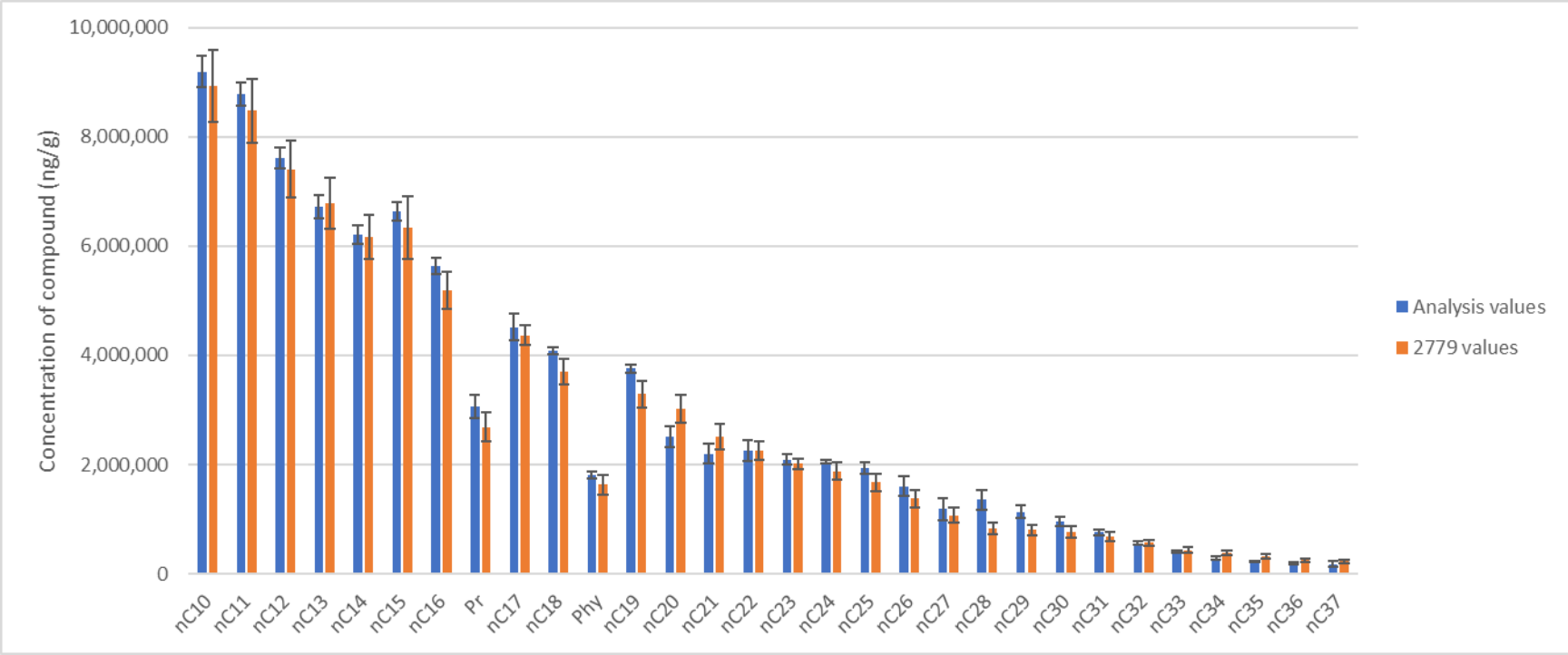

Figure D8: Comparison of calculated aliphatic hydrocarbon concentrations in analysis and reported values for NIST 2779. Blue bars represent mean calculated concentrations via the optimized method described in Chapter 2 and orange bars represent the certified concentrations reported by NIST for NIST 2779. Error bars for values from this study are 1σ. Error bars for certified values are the expaned uncertainty about the mean with a coverage factor of 2, which was calculated by combining the within-method variences and between-method variances following the ISO guide.

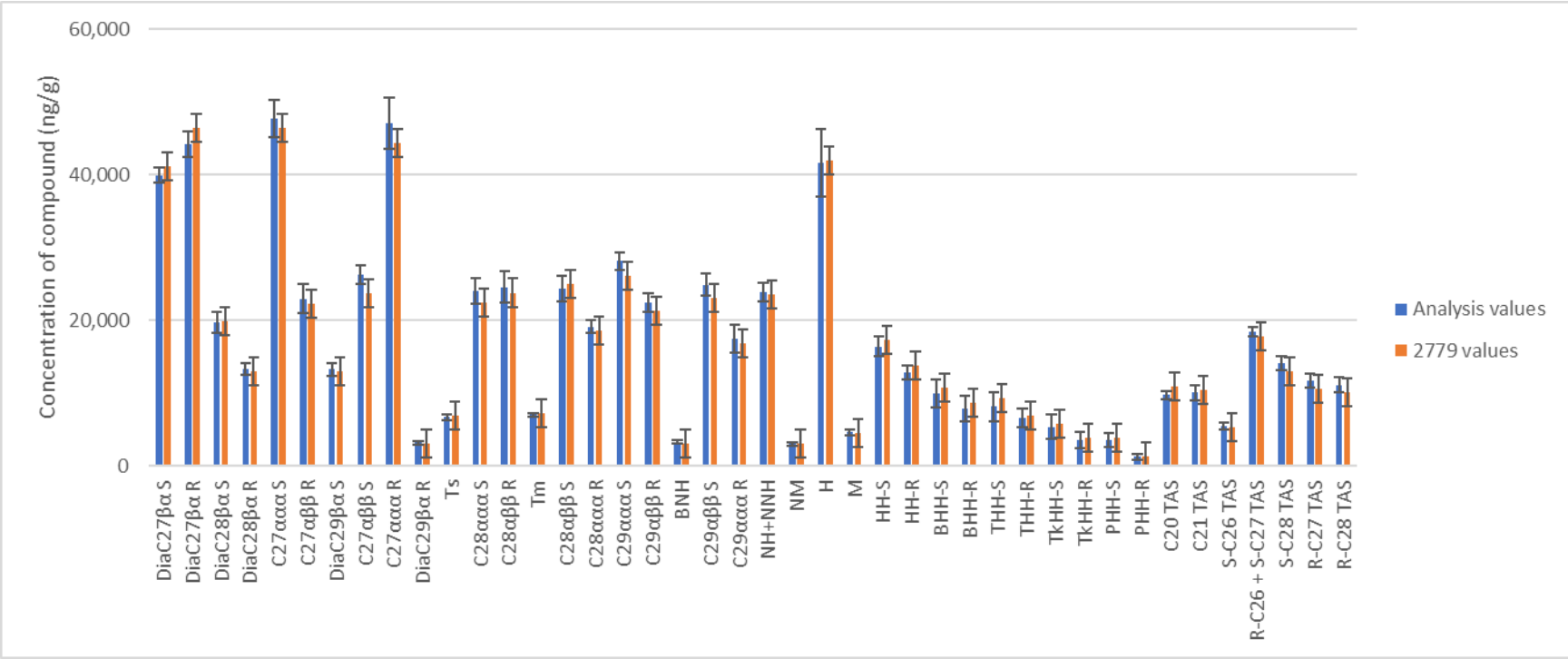

Figure D9: Comparison of calculated hopane, sterane, and tri-aromatic steroid concentrations in analysis and reported values for NIST 2779. Blue bars represent mean calculated concentrations via the optimized method described in Chapter 2 and orange bars represent the certified concentrations reported by NIST for NIST 2779. Error bars for values from this study are 1σ. Error bars for certified values are the expaned uncertainty about the mean with a coverage factor of 2, which was calculated by combining the within-method variences and between-method variances following the ISO guide.